Faculty of Science and Engineering

Western Australian School of Mines

Dynamic Testing of Mesh and Rock Bolt Support Systems

Agampodi Ushan De Zoysa

This thesis is presented for the degree
Master of Philosophy (Mining Engineering)
of
Curtin University

July 2015

DECLARATION

To the best of my knowledge and belief this thesis contains no material previously published by any other person except where due acknowledgment has been made. This thesis contains no material which has been accepted for the award of any other degree or diploma in any university.

Signature: ……

Date: ……....

ACKNOWLEDGEMENTS

Foremost, I would like to thank my supervisor Professor Ernesto Villaescusa for giving me this opportunity to pursue my higher studies under his Excellent supervision and for his guidance, patience, encouragement, motivation and help throughout the project.

I would also like to thank my co-supervisor Dr Alan Thompson for his support during the whole period of the study and for developing the in-house data analysis software.

I would like to acknowledge the major sponsors of the project: the Mineral and Energy Research Institute of Western Australia (MERIWA), Western Australia School of Mines (WASM), BHP Nickel West, Geobrugg, CODELCO EI Teniente, Lighting Nickel, Newcrest and Kalgoorlie Consolidated Gold Mines (KCGM).

Special thanks to Dr John Player for introducing me to the WASM Dynamic Test Facility. Also thank you for your dedication and support throughout the project.

The Rock Mechanics group members including Mr Nixon Saw, Mr Chris Windsor, Mr Pat Hogan and Mr Lance Fraser for their time spent, effort and support in theoretical and technical issues are highly acknowledged.

Finally I would like to thank my family, specially my father and my lovely wife for their support, patience and helping me to be on track during my studies.

ABSTRACT

Reinforcement and support systems are very important with respect to underground excavation stability and safety. With increased mining depth, underground openings in rock are subjected to higher stresses. This leads to failure of the rock masses. Different types of reinforcement and support systems are available to the mining industry to resist instability in underground excavations.

Understanding of reinforcement and support systems (ground support) responses to static and dynamic loads is important in designing the most suitable ground support scheme. Behaviour of rock reinforcement and support systems under static load conditions are widely researched and analysed. However, due to their complexity, rock support schemes subjected to dynamic load conditions are not well understood to date.

This study examines and analyses combined reinforcement and support systems subjected to dynamic loading conditions. Tests were conducted at the WASM Dynamic Test Facility located in Kalgoorlie, WA. The test facility was modified and enhanced during the project to allow ground support systems to be tested. Another major aspect of this study is to document the test procedure of combined schemes for future reference and to enhance the WASM dynamic test database.

The testing program included chain link and weld mesh in conjunction with fully coupled and decoupled threaded bar rock bolts. The first test program comprised with 5.6mm thick weld mesh and 4mm thick chain link mesh. The second test program consisted with 4mm and 5mm thick Codelco mesh and 4mm thick Geobrugg mesh (G-80). The combined systems were subjected to impact velocities ranged from 5.4m/s to 6.8m/s with respective total input energies ranged from 27kJ to 53.2kJ in the first test program while in the second test program velocities ranged from 7m/s to 7.3m/s with respective input energies from 52.8kJ to 57.5kJ. Decoupling and fully rupture modes of behaviour were observed with regards to the rock bolts.

Test results were characterised using force - displacement and energy dissipated - deformation charts. These charts were used to clearly identify the performance and energy dissipated by each of the components of the combined system. The highest

energy of 38.8kJ was dissipated by the test #199 combined schemes while the minimum energy of 16kJ was dissipated by the test sample #197 in the first test program. The maximum energy input of 57.5kJ was applied to the sample #235 of the second test program while the minimum energy input of 52.8kJ was applied to sample #236.

TABLE OF CONTENTS

LIST OF FIGURES

LIST OF TABLES

CHAPTER 1

INTRODUCTION

Excavation stability is one of the most important and critical aspects of underground development. The ratio of rock mass strength to induced stress determines the degree of stability of underground mines. With increasing depth the rock mass is subjected to higher levels of in situ and induced stresses and conditions become more precarious and complicated. Over past decades many fatal accidents have occurred due to failure of rock and its support. Improved underground support systems have been developed to extend the lifespan of the excavations and the safety of workers.

Reinforcement systems and supporting systems (areal restraint) are the major means of ground supporting systems in practice to improve the degree of stability of underground openings (Windsor and Thompson, 2012). Rock bolts, wire mesh and shotcrete are the most popular ground support systems and they have been used in mining applications for many decades.

A reinforcement scheme is a combination of an element or elements fixed into a drill hole in rock mass and a plate on the rock surface to restrain surface support (Windsor and Thompson, 2012). A support system can be mesh alone, a sprayed layer such as shotcrete or a combination of a sprayed layer with mesh. When mesh is used, it is restrained by reinforcement. The purpose of surface support is to resist surface rock movement.

Due to the larger scale and depth of production, the openings are getting wider and at depth rock surrounding the opening is subjected to higher stresses. Therefore, typically a pattern of reinforcement or combination of both reinforcement and support systems is often used to support large blocks and prevent deterioration. A combination of a reinforcement system and a support system is defined as a support scheme.

The capacity of rock support systems is important in designing the adequate and most economic rock support scheme. A large amount of research has been conducted to understand the behaviour of reinforcement and support systems subjected to static

and dynamic loads. The Western Australian School of Mines (WASM) Dynamic and Static Test Facilities, the drop test facility described by Ortlepp (1997) and the CANMET-MMSL test rig (Canada) are some of the facilities developed to determine the static and dynamic capacities of support systems.

It is understood that most of the research on rock support systems do not simulate the actual conditions. This includes incorrect reinforcement configuration and incorrect loading of the reinforcement system (Player, 2012). The WASM Dynamic Test Facility was constructed and developed to test reinforcement and support systems under dynamic load conditions. It is identified as the best test facility among all the available test facilities (Player, 2012).

The WASM Rock Mechanics Group has conducted a series of static and dynamic test programs to analyse the performance and to enhance the quality of rock support systems. The static and dynamic responses of support systems are different and it is important to understand this in order to design an effective ground support scheme. Additionally, dynamic test procedures and analyses are more complicated compared with static tests due to the complexity and the nature of dynamic loads.

To date most of the research has been to characterise individual reinforcement and support systems. The performances of combined reinforcement and support systems (ground support scheme) under dynamic load conditions have not been widely understood. This required studies and developments on combined reinforcement and support system test configurations.

As part of this new effort, the project “M417- Dynamic testing of surface support systems” was granted by MERIWA (The Mineral and Energy Research Institute of Western Australia) in cooperation with many leading mining companies and hardware suppliers. This thesis details the testing, data acquisition, analyses and interpretation of the performance of combined systems. Some of the devices used to monitor tests include accelerometers, load cells, potentiometers, laser distance measurers and high- speed digital cameras.

Analysis of the data is one of the most difficult and important roles of the entire research. The analysis used here included a combination of processes involving data acquisition software such as MiDAS ProAnalyst and also WASM in-house software.

Chapter two is an introduction to the reinforcement and support systems. This chapter presents the role of rock support systems in resisting rock failure and to stabilize the underground openings. The mechanisms of reinforcement and support systems are discussed and reinforcement systems are categorized according to their stabilizing mechanism.

The chapter also includes a brief introduction to WASM static test facility for reinforcement and support systems. Components of the large area static test facility and test setup for mesh and shotcrete are also described in this chapter.

Moreover, in this chapter, the WASM static and dynamic test results for threaded bar and mesh are presented.

Chapter three is the literature review of previous research conducted to study the performance of reinforcement and mesh under dynamic and static load conditions. The literature review includes static and dynamic test facilities and related results of the reinforcement and support systems. The CANMET-MMSL test rig, the CSIR Impact drop test facility for reinforcement, the CSIR drop test facility for ground support scheme ,the GRC support element test facility and Walenstadt test site for combined reinforcement and support are reviewed.

Chapter four describes the WASM dynamic test facilities in detail. The major components of the test facility include the drop-beam, the load mass, instrumentation, mesh frame, high speed camera and the buffers. The limitations of the WASM Dynamic Test Facility are discussed in this section. The momentum transfer concept is explained and illustrated to understand the energy balance of the system.

Moreover, the sensors and data acquisition used in the WASM Dynamic Test Facility are fully described.

Chapter five presents the bolt and mesh samples preparation and testing procedure in detail. The sample preparation is explained in steps. Furthermore, this chapter describes installation of instrumentation on to the test setup.

Chapter six presents the data collection and analysis. Data analysis was divided into two sections as video data analysis and sensor data analysis. Moreover this chapter

describes the data acquisition software which includes ProAnalyst (Extract, Analyse and report motion from video), MiDAS (Video capture and data acquisition system) and the WASM in-house software (developed by Dr. Alan Thompson).

The chapter also explains the entire test data collecting process (this includes pre-test and post-test data). The sensor data analysis process starts with data monitoring and it is followed by data filtering, data analysis, data processing and presenting a flow of results.

Chapter seven presents the test results together with an assessment of performance. This includes comparison charts and energy calculations. The energy dissipated by each component of the combined system is calculated and presented in this section.

This chapter summarises the overall performance of two bolt and mesh combined test programs. Overall photos of reinforcement and support systems are illustrated and the failure mechanisms are explained. Moreover, the dissection analyses of reinforcement systems are also described.

Chapter eight is summarises the study and its outcomes and implications for future ground support applications for excavations formed in highly stressed rock.

CHAPTER 2

BACKGROUND TO GROUND SUPPORT

2.1 ROCK MASS DEMAND

For underground openings, the surrounding rock mass initially moves towards the free faces due to lack of confinement. In addition, high stresses may cause compressive rock failure, propagation of fractures on pre-existing discontinuities or the creation of new discontinuities. Ground support systems are implemented around underground openings to resist movements that cause rock mass failure. They are required to match the rock mass demand to stabilise the underground openings to maintain safe working environments.

In most of the cases, the rock mass demand is very complicated to quantify. Basically, the rock mass demand changes with time and rock properties. “A stiff response may be required in the short term to minimize rock mass loosening, while in the longer term, the rock support systems may be required to absorb large displacements as the block size reduces and the rock mass creeps” (Villaescusa E 2014, p. 344). Therefore, the rock support system for this type of rock mass demand is more complicated to implement.

Force and displacement capacities are the quantitative means which characterise the performance of rock support systems. For example, a loose fragmented rock mass requires a higher demand for displacement near the opening face while a massive rock mass block requires a higher demand for the force capacity of the rock support system.

Moreover, massive rock or a rock mass with widely spaced joints may turn into a highly fractured rock mass due to overstressing. In these cases, a rock support system designed for static loading conditions may be inadequate to match the rock mass demand.

2.2 ROCK MASS FAILURE MODES

Hudson (1989) divided the rock mass instability and failure modes near underground openings into two groups as block failure (structurally controlled failure) and failures

induced by overstressing. Palmstrom and Stille (2007) added a third group to cover the influence of ground water in to the classification.

2.2.1 Block Failure (Structurally Related Failure)

Structurally related failure modes include loosening, ravelling, and block failure.

Definition of terms according to the New Australian Tunnelling Methods (NATM):

Loosening: Elastic behaviour of the rock mass, with small deformations which quickly decline. Small quickly declining deformations. No relief features after scaling. The rock masses are stable in the long term.

Ravelling: Far- reaching elastic behaviour of the rock mass with small deformations that quickly decrease. Jointing causes reduced rock mass strength, as well as limited stand-up time and active span. This results in relief and loosening along joints and weakness planes, mainly in the roof and upper part of walls.

Block failure is the most common type of rock failure method at relatively shallow depth, which is also known as wedge failure. This type of failures occur as a result of releasing of pre-existing blocks in the roof and on side walls. Joints, faults, and bedding planes are the major types of discontinuities present in rock.

Joints are the dominant and generally the most geotechnical influential discontinuities in rock. Joints are breaks on the rock and commonly associated with a group of parallel or sub parallel joints which are defined as joint sets. A rock mass can contain several joint sets. Blocks are formed by the intersection of three or more discontinuities. The structural arrangement, the orientation of the joint sets with respect to the intersecting angle to the axis of the underground opening is important towards the degree of stability.

The importance of the orientation of joints relative to the faces of an underground opening was explained by Bieniawski in 1984 as illustrated in Table 1.

Table 1: Characterization of discontinuity orientation related to an underground excavation (Bieniawski, 1984).

STRIKE	Dip = 0 - 20°	Dip = 20 - 45°	Dip = 45 - 90°
Strike across tunnel axis	fair	favourable* unfavourable**	very favourable* fair**
Strike parallel to tunnel axis	fair	fair	very unfavourable

* for drive with dip, ** for drive against dip

2.2.2 Failure Induced by Overstressing and Seismicity

Rock mass failure modes induced by overstressing include squeezing, spalling, rock burst and slabbing. Aydan et al. (1993) has proposed three possible forms of squeezing failure on surrounding rock in underground opening as shown in Figure 1.

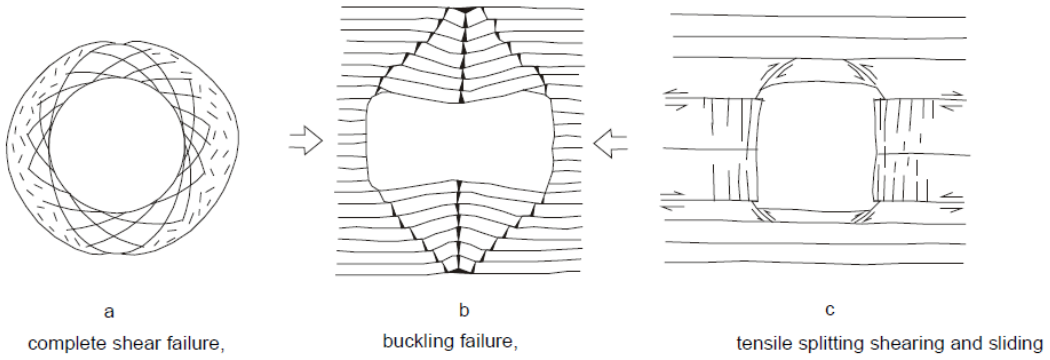

Figure 1: Types of failure mode in squeezing ground (Aydan et al., 1993).

These three forms may be described as:

Complete shear failure: This involves the complete process of shearing of the medium in comparison with the rock-bursting, in which the initiation by shearing process is followed by splitting and sudden detachment of the surrounding rock mass.

Buckling failure: This type of failure is generally observed in metamorphic rocks or thinly bedded rocks.

Tensile splitting, shearing and sliding failure: It is observed in relatively thickly bedded sedimentary rocks and it involves sliding along bedding planes and shearing of intact rock.

2.3 REINFORCEMENT SYSTEMS, SUPPORT SYSTEMS AND COMBINED SCHEMES

Ground support systems are categorized under two major categories such as reinforcement systems and support systems according to their mechanism of interaction with the rock surrounding an underground opening. Different types of reinforcement and support systems have been developed and adopted by the mining industry to match the rock mass demand. The following sections describe reinforcement systems, support systems and combinations of reinforcement and support systems used to satisfy the demands of challenging underground conditions caused by high stresses.

2.3.1 Introduction to Reinforcement and Support Systems

According to the mechanism of stabilising the unsupported rock mass, the ground support systems are categorized as reinforcement systems and support systems (Windsor and Thompson, 1993). A reinforcement system includes all the devices installed in a borehole. All the other surface fixtures such as wire mesh, shotcrete, steel straps and props are some of the widely used support systems in mining practices.

Reinforcement systems attempt to maintain the stability of an overall rock mass while support systems aim to improve the stability at the face of an excavation. Windsor and Thompson (1993) illustrated the distinction between reinforcement and support as shown in Figure 2.

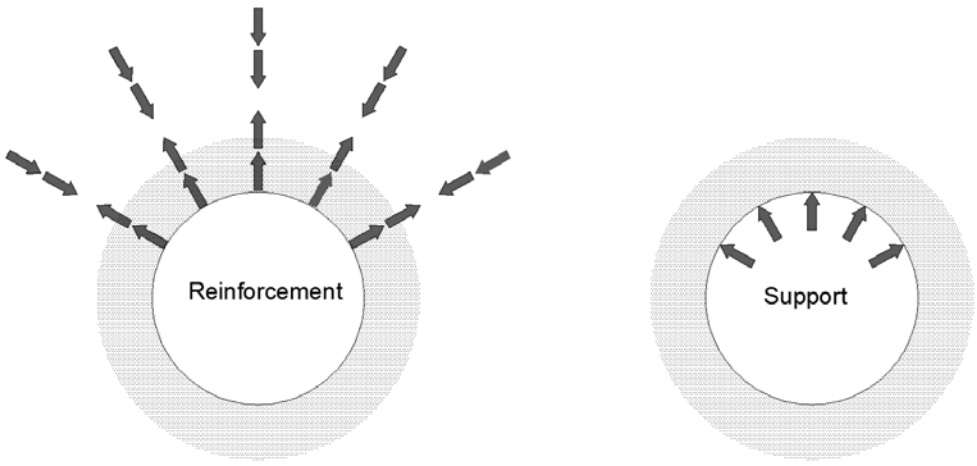

Figure 2: Reinforcement and support action (Windsor and Thompson, 1993).

A ground support scheme is a combination of reinforcement and support systems. According to the rock mass demand and many other factors, engineers select the most appropriate ground support scheme. A large variety of reinforcement systems and support systems are available for application to different underground requirements.

2.3.2 Reinforcement Systems

2.3.2.1 Load Transfer Mechanism of a Reinforcement System

Windsor and Thompson (1993) defined the reinforcement load transfer mechanism across a distinct interface or zone between a stable and an unstable rock. Figure 3 is an adaptation by Thompson and Villaescusa (2013) of this concept which is used to understand the behaviour of a reinforcement system.

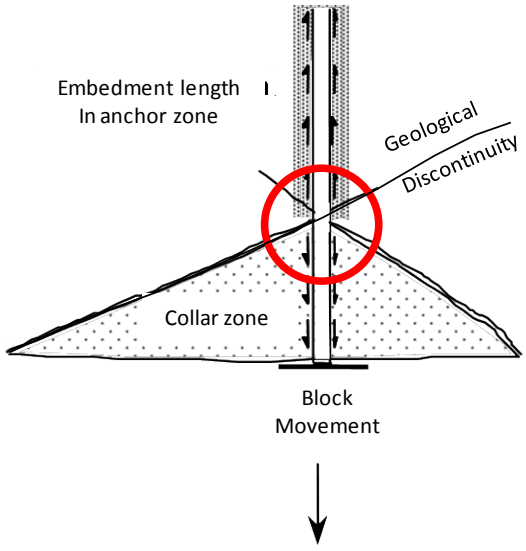

Figure 3: Load transfer and embedment length concept (e.g. Thompson and Villaescusa, 2013).

Windsor and Thompson (1993) explained the load transfer concept as three basic actions:

- Rock movement at the excavation boundary, which causes load transfer from the unstable rock, wedge, or slab to the reinforcing element.
- Transfer of load via the reinforcing element from the unstable portion to a stable interior region within the rock mass.
- Transfer of the reinforcing element load to the rock mass in the stable zone.

Failure of the supported rock block can occur during load transfer of any one of the three components due to insufficient steel capacity (rupture of the reinforcement element) or inadequate load transfer (slippage).

2.3.2.2 Components of a Reinforcement System

The main components of a reinforcement system are important in understanding the behaviour of the system. A generic reinforcement system comprises four main components as shown in Figure 4 (Windsor and Thompson 1993).

0. The rock.
1. The element.
2. The internal fixture.
3. The external fixture.

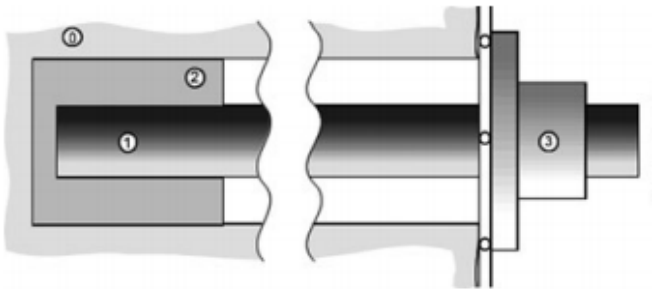

Figure 4: A schematic of a generic reinforcement system and its components (Windsor and Thompson 1993).

Each component interacts with two other components in load transfer:

- The rock interacts with the internal fixture and the external fixture.
- The element interacts with internal fixture and the external fixture.
- The internal fixture interacts with the rock and the element.
- The external fixture interacts with the rock and the element.

Figure 4 represents the basic components and may vary depending on different types of reinforcements. For example, friction stabilisers have no physical internal fixture and transfer load at the interface between the rock and the element.

2.3.2.3 Types of Reinforcement Systems

Reinforcement systems have been developed over many decades to improve their performance in increasingly difficult mining environments. According to the load transfer mechanism, Windsor and Thompson (1993) have described a classification for reinforcement systems under three categories.

- Continuous Mechanically Coupled (CMC) systems.
- Continuous Frictionally Coupled (CFC) systems.
- Discrete Mechanically or Frictionally Coupled (DMFC) systems.

2.3.2.3.1 Continuous Mechanically Coupled (CMC) Systems

Resin or cement based grouts are used to fill the annulus between the element and the borehole to transfer load along the entire length in a CMC system. Therefore, the strength and the correct installation of the grout without porosity to maintain continuous load transfer play a vital role in the performance of the overall system.

The reinforcing elements are often designed to have varying cross-sections to enhance the load transfer between the grout and the element.

2.3.2.3.2 Continuous Frictionally Coupled (CFC) Systems

In CFC systems, the reinforcing elements are directly in contact with the borehole wall. The performance of a CFC system relies on the frictional strength at the interface between the reinforcing element and the borehole wall. Radial pre-stressing during the installation controls the load transfer between the reinforcing element and the rock mass wall.

The frictional strength on the intact area between the reinforcing element and the borehole wall depends on the borehole diameter, the reinforcing element diameter and any geometrical irregularity of the bore hole (Windsor and Thompson, 1993).

Installation of a reinforcing element of this type is achieved by expanding an undersized element into an oversized borehole (e.g. Atlas Copco Swellex bolt and its derivatives) or contracting an oversized element into an undersized borehole (e.g. Ingersoll Rand Split Set and its derivatives).

2.3.2.3.3 Discrete Mechanically or Frictionally Coupled (DMFC) systems

DMFC systems transfer load at two discrete points; namely, at the collar and near the toe end. This type of a reinforcement system transfers the load between the reinforcing element and the rock at the anchoring point either mechanically or frictionally depending on the design. In a discrete frictionally coupled system, an expansion shell is used to anchor the reinforcement element with the borehole wall. This type of element is a suitable system for hard rock openings.

A discrete mechanically coupled system is suitable for soft rock applications as the device have a lower unit load transfer on the anchoring point compared with a discrete frictionally coupled system (Thompson and Windsor 1993). An example is a resin grouted anchor that can be used to transfer the load between the bolt, grout and the rock.

The force distributions for the three generic types of reinforcement systems are shown in Figure 5. It is important to note that the maximum force developed in the element may be quite different from that measured at the collar.

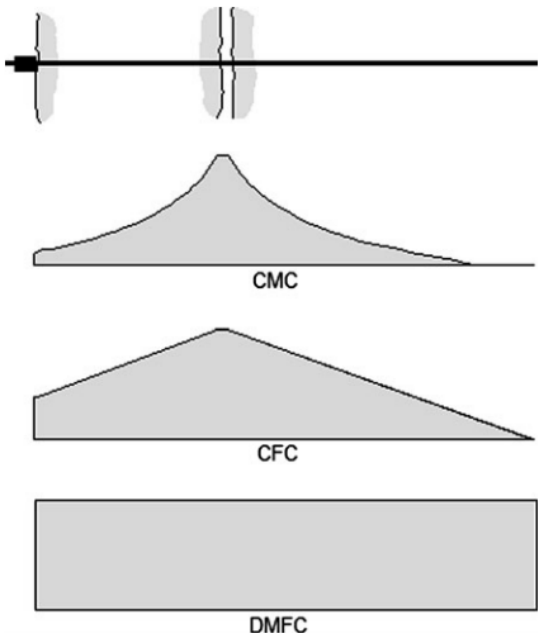

Figure 5: Force distribution for CMC, CFC and DMFC reinforcement systems (Thompson and Windsor 1993).

2.3.3 Support systems

2.3.3.1 Load Transfer Concept for Support Systems

Thompson et al. (2012) illustrated the concept of load transfer by surface support systems as shown in Figure 6 and Figure 7. Those are described as the force transferred to the points of restraints (rock bolts, cable bolts etc.) or as adhesion between the rock and the support system (zones of restraints).

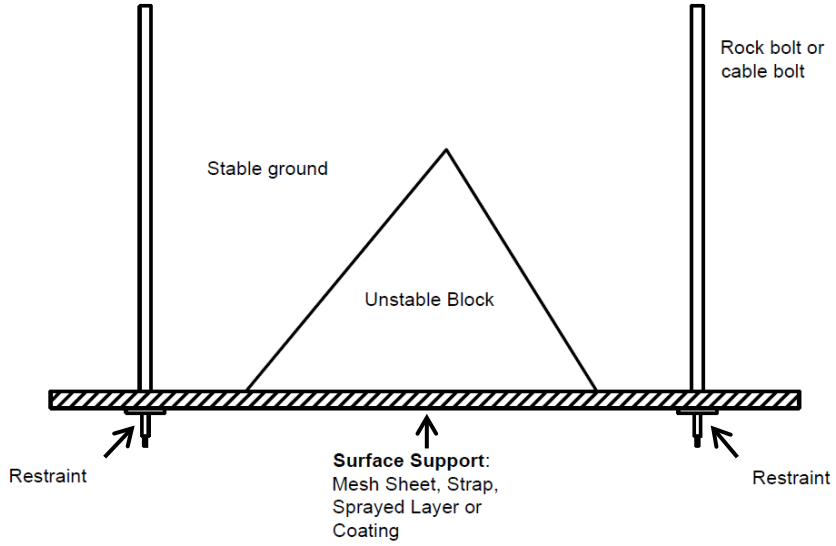

Figure 6: Load transferring from surface support to the points of restraints (rock bolts) (Thompson et al. 2012).

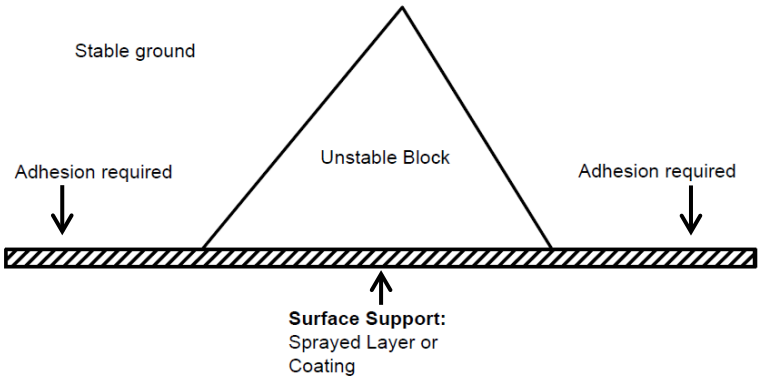

Figure 7 Load transferring between the surface support and the rock surface (Thompson et al. 2012).

2.3.3.2 Types of Support Systems

Support systems are also known as passive rock supports. They are mainly installed externally onto the rock surface to support the face of an underground excavation. Support systems are involved only in supporting of progressive movement of loosened rock mass on the opening face (Windsor and Thompson, 1993).

Different elements have their own advantages and disadvantages. Straps are used in slabby ground conditions, but are not suitable to support small pieces of loose rock or broken rock from falling. Meshes are used to support loose rock conditions, but some products cannot withstand high loads.

In this study, welded wire mesh and chain link mesh were used as the support systems. Those types of mesh have been used in the mining industry since the 1950s. Among those, the welded wire mesh is the most common type used in Australian mining industry. Welded wire mesh was firstly introduced to the building and construction industry as reinforcement for concrete slabs (Windsor and Thompson, 1993).

The welded wire mesh is typically designed in 100mm × 100mm grid with longitudinal wires and transverses wires welded at the intersections. Weld mesh with a 5.6mm wire diameter is the most common type. The chain link mesh is designed with zigzag shaped wire woven with another and joined at the ends. The strength of mesh depends on both the wire diameter and grade of the steel used to form the wires. The welded mesh wires used in the test programs have a tensile strength of about 600MPa while the Geobrugg chain link mesh has wire strengths of approximately 1700MPa.

2.3.3.3 Failure Modes in Mesh

Failure mechanisms are an indication of the quality of a mesh. Three modes of failure can be observed in welded wire mesh. These failure mechanisms can be described as shear failure at the weld points, failure at the heat affected zone (HAZ) and tensile failure of the wire as shown in Figure 8 (Morton, 2009).

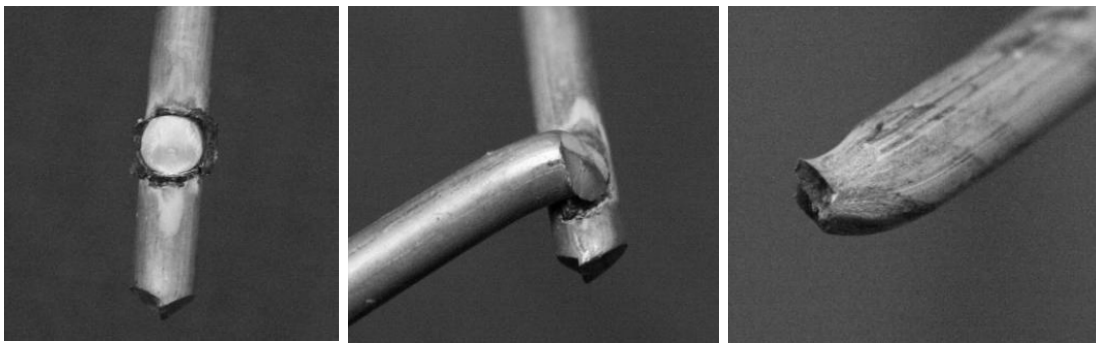

Figure 8: Welded wire mesh failure mechanisms: L-R weld failure, failure through heat affected zone (HAZ) and tensile wire failure. (From Morton 2009)

The weld failure (shear failure at the weld point) occurs due to poor welding processes and the failure at the heat affected zone occurs due to the excessive heat generated in the welding process. Both types of failures can be improved by the weld technology. Tensile strength of the wire depends on the wire manufacturing process, wire diameter and properties of the wire metal.

Tensile failure is the only mode of failure in chain link mesh as the wires are not welded to each other. “The mesh fails on the edge of the loading area either as a result of the loading weight cutting through the wires or as a result of wires cutting each other at a link” (Villaescusa, 2014).

2.3.4 Combined Scheme of Reinforcement and Support Systems

A combined scheme is basically a combination of reinforcement and support systems. Combined schemes such as bolt and mesh, bolt and shotcrete and also bolt, mesh and shotcrete all together are used to match the rock mass demand. This includes the combined scheme to withstand the loads and displacements during the life span of the underground opening.

This thesis is focused on understanding the performance of combined bolt and mesh systems subjected to dynamic loading.

2.4 Testing Requirements and Set of Criteria for Test Facilities

It is important to understand the response of each system within a combined scheme in order to design ground support appropriate to the rock mass demand. Laboratory testing cannot hope to simulate the actual loading conditions caused by rock mass failure around an underground excavation. Some of the reasons for this are

associated with the shape of excavation surfaces being convex or concave locally and the limited extent of the boundaries imposed in laboratory tests. Mostly tests are conducted on flat panels of shotcrete and mesh. However, the use of the same boundary conditions for different support systems combined with different types of reinforcement does enable a comparison to be made regarding their relative performance.

A facility for testing of ground support schemes should ideally enable measurement of the individual force-displacement responses for both the reinforcement and support systems from which the force and displacement capacities and dissipated energy can be determined.

In the following Chapter 3, a review is presented of selected dynamic test facilities. The facilities are described and assessed in relation to a number of criteria:

- The ability to use commercially available reinforcement and support systems.
- The ability to simulate reinforcement and/or support according to the mechanics of their load transfer.
- The method of applying dynamic loading and the magnitude of energy input.
- The ability to fail schemes in one loading event.
- The monitoring system and ability to quantify force-displacement responses and energy dissipation.

In Chapter 4, the WASM Dynamic Test Facility will be reviewed and described in detail. In particular, it will be demonstrated that the facility is the most sophisticated and satisfies the criteria given above. Professor Ted Brown, an internationally recognised authority in rock mechanics stated in his 2004 keynote presentation at the international ground support conference held in Perth that:

"The most advanced dynamic testing system known to the author is that developed recently at the Western Australian School of Mines (WASM) Kalgoorlie"

Since that time, many enhancements have been made to extend the capabilities of the facility in terms of testing combined reinforcement and support systems and the analysis of data.

CHAPTER 3

REVIEW OF DYNAMIC TEST FACILITIES

3.1 DYNAMIC TEST FACILITIES FOR ROCK SUPPORT IN MINING APPLICATIONS

Dynamic test facilities were developed in past decades to evaluate the performance of reinforcement and support systems under dynamic loading conditions. It was identified that some of the test facilities were unable to evaluate and present the results precisely due to lack of knowledge in energy balance (Player, 2012).

A number of test facilities have been selected for review in this chapter; namely:

- CSIR Terratek (hydraulic loading) facility [sourced from the research publication: An Examination of Dynamic Test Facilities by Player et al. (2005)]
- CSIR Impact drop test facility for reinforcement (Stacey and Ortlepp, 1998)
- CANMET-MMSL test rig. (Plouffe et al., 2007)
- GRC support element test facility (Kaiser et al., 1996)
- CSIR drop test facility for ground support scheme; sourced from the GAP221 report (Ortlepp and Stacey, 1997).
- Geobrugg Walenstadt test site (Bucher et al., 2013).

As mentioned previously, the WASM Dynamic Test Facility will be reviewed in Chapter 4. It is worth noting that the facilities were mainly developed to test either reinforcement systems or support systems. The last listed facility and the WASM Dynamic Test Facility both enable dynamic loading of combined reinforcement and support systems.

3.1.1 Dynamic Test Facilities for Reinforcement Systems

3.1.1.1 The CSIR Terratek Hydraulic Dynamic Test Facility

The CSIR Terratek hydraulic facility (Figure 9) was built in 1978 and this test facility is no longer being used. Two mechanisms were used in applying energy to the reinforcement test specimen.

- Hydraulic system to pull the collar of a shortened bolt.
- Push the top end of the test sample at a predetermined velocity.

Reinforcement systems were dynamically tested under tension, shear and props under compression with this test facility

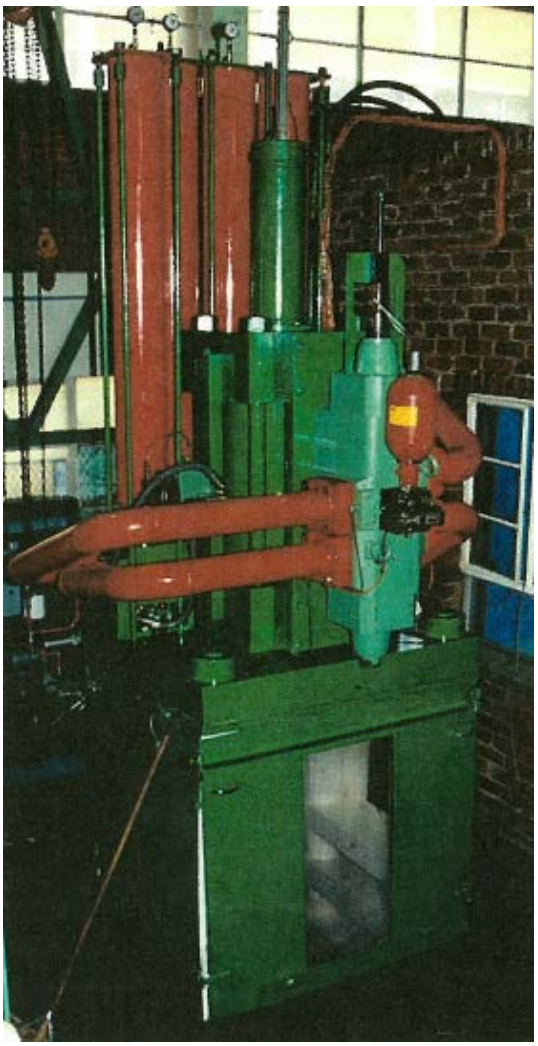

Figure 9: Terratek hydraulic dynamic test facility (provided by CSIR).

Surface hardware is an important component in a reinforcement system and should be considered in evaluating the performance of reinforcement system. But it was identified that the installation of surface hardware was not applicable in this test facility.

The facility had a capacity of a rapid displacement of 200mm at a velocity of 1.2m/s to 3m/s. Moreover, the dynamic tests were conducted in conjunction with slow displacement pulling tests of bolts at rates of 30mm/min or 15mm/min.

Test sample specifications (bolt sample lengths) for the Terratek hydraulic test facility are given in Figure 10. In general, these lengths are less than would be used in ground support practice and the loading is at the collar and not across a discontinuity.

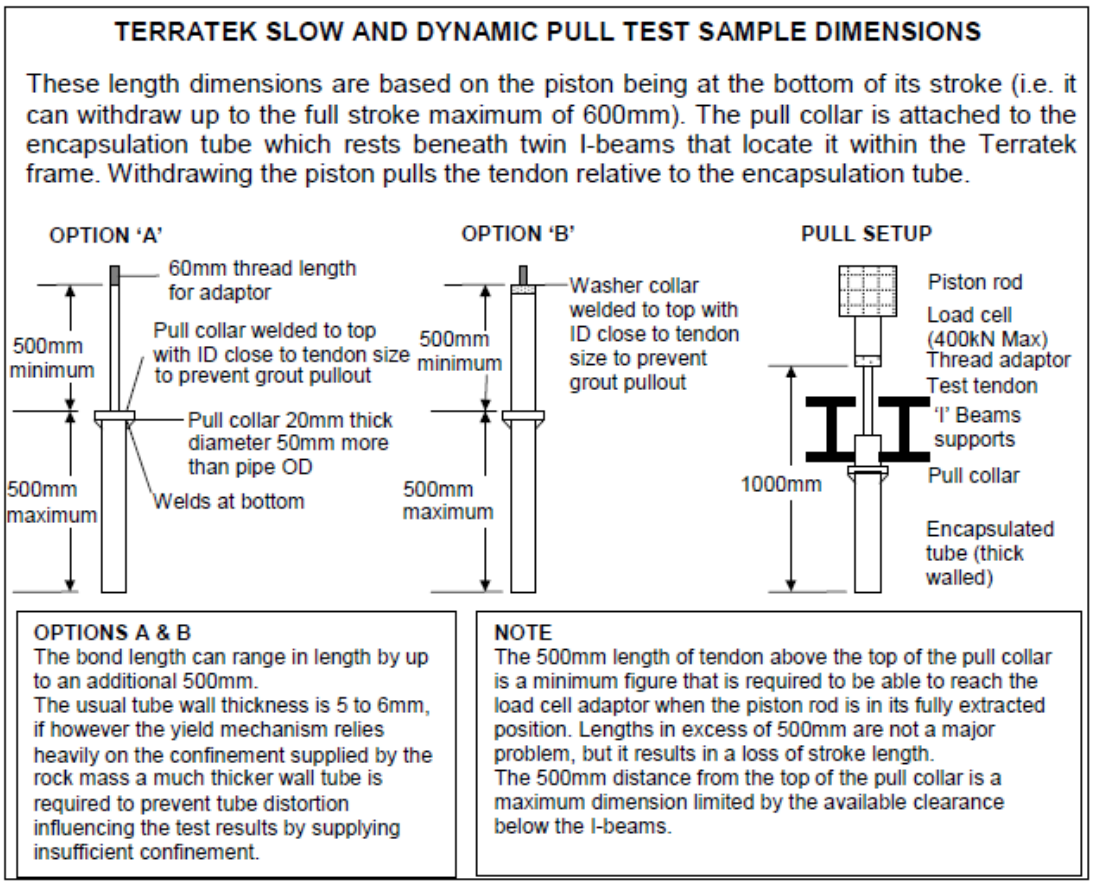

Figure 10: Terratek bolt sample lengths (provided by CSIR without adjustment).

Cheap test costs and a simple configuration which was able to test nearly fifteen tests a day were significant advantages of this test facility.

The force applied to a test specimen was not related to the energy input from the hydraulics of the facility. The force - time responses were not clear enough to identify the key loadings due to the lack of data filtering. A load cell was installed onto the pulling collar to measure the force response which is quite similar to the collar load cell of the WASM Dynamic Test Facility. The Terratek test rig could not accommodate a combined support scheme.

3.1.1.2 The CSIR Drop Test Facility for Reinforcing Element

The CSIR drop test facility for reinforcement was the second drop test facility developed by Steffan Robertson and Kirsten Consultants in 1998. The test facility is shown in Figure 11 and all the information is sourced from the GAP report 423 (Ortlepp and Stacey 1998).

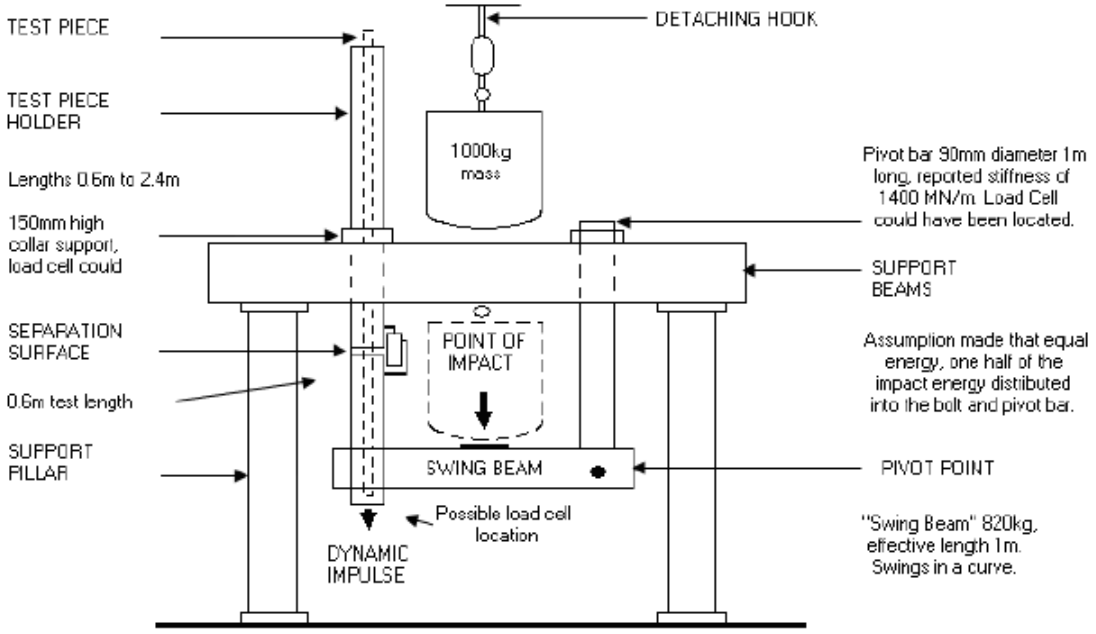

Figure 11: CSIR drop test facility for reinforcement systems (Stacey and Ortlepp ,1999).

Testing was initiated by releasing a 1000kg mass on to a swing beam as shown in Figure 11. The energy is transferred to the end of the swing beam and to the pipe wall (which simulates a borehole) where the reinforcement head is fixed. It was identified that the surface hardware was not installed in every test. Twelve of the fifty eight bolts tested failed on the first drop as reported in GAP Report 423 (Ortlepp and Staacey, 1998).

The facility simulated loading across a discontinuity. A low level of instrumentation and analysis methodology were used to calculate the energy dissipation capacity which could have been enhanced by installing load cells. A combined support scheme could not be tested with this facility.

3.1.1.3 The CANMET-MMSL Test Rig

Plouffe et al. (2008) described the CANMET-MMSL (Canada Centre for Mineral and Energy Technology- Mining and Mineral Science Laboratories) impact test facility (Figure 12) and summarized test results up to the date. Static and dynamic tests were conducted for Modified Cone Bolts (MCB) under different parameters.

Figure 12: CANMET-MMSL test rig (Plouffe et al., 2008).

This is an existing facility, where a concrete tube is used to simulate the rock mass, in a way which is similar to what is done at the WASM Dynamic Test Facility. A mass is dropped on to the support tendons installed in the simulated borehole in a selected distance. The mass can reach up to a maximum height of 2.1m and the available maximum velocity and energy are 6.5 m/s and 62kJ, respectively.

Line scan cameras are used to track the displacement of the simulated borehole by tracking a black and white target (Figure 13) fixed on the end of the plate nut or to the bolt end which is a much similar method as at the WASM Dynamic Test Facility to track the displacement.

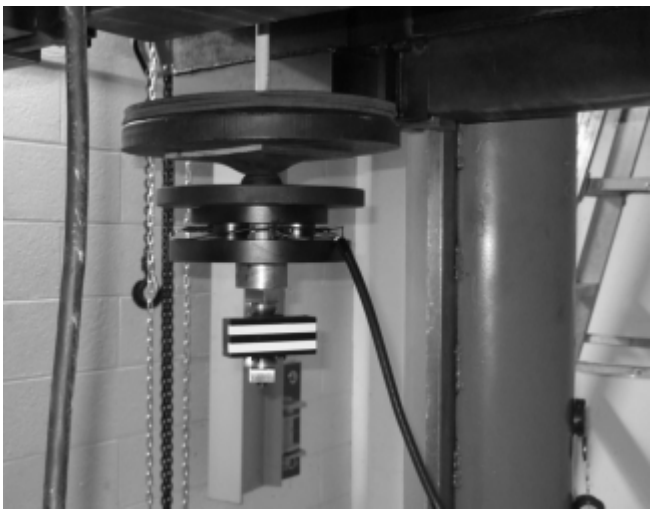

Figure 13: View of the displacement target and the load cells at the plate (Plouffe et al., 2008).

Repeated impacts method in the CANMET is a significant difference from other dynamic testing facilities protocols (Plouffe et al., 2008). Installation of the surface hardware to the reinforcement system is applicable in the CANMET test facility. This facility is unable to test a combined system.

3.1.2 Dynamic Test Facilities for Support Systems

3.1.2.1 GRC Support Element Test Facility

A drop test facility for support systems constructed at Creighton mine is shown schematically in Figure 14. This section is sourced from chapter four in the Canadian Rock Burst Support Handbook (Kaiser et al., 1996).

A cylindrical mass of 565kg is dropped freely on to the support test specimen (shotcrete, fibrecrete or mesh plus shotcrete). Load cells were installed under the support plates.

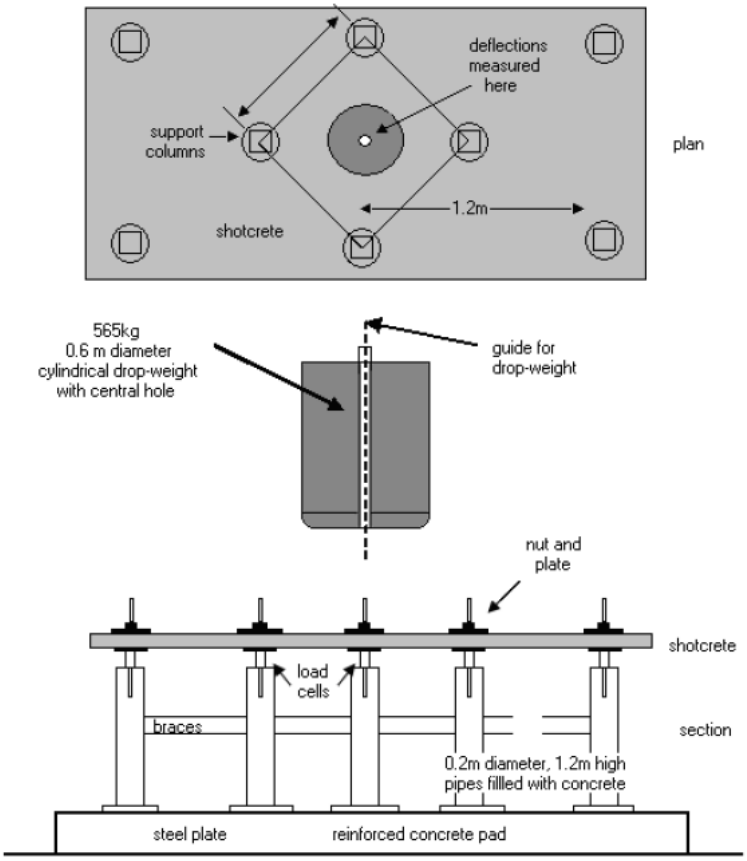

Figure 14: GRC test facility (Kaiser et al., 1996).

The reported maximum drop height, maximum velocity and the maximum energy were respectively 4m, 7.7m/s and 23kJ which are controversial because the reported energy of 23kJ requires 9m/s of impact velocity.

The GRC test facility had a well organised instrumentation system compared with other test facilities. A quick set up time of a sample is an advantage in this facility.

This test rig was not capable of testing ground support schemes.

3.1.3 Dynamic Test Facilities for Ground Support Schemes

3.1.3.1 The CSIR Drop Test Facility for Ground Support Scheme

Steffan Robertson and Kirsten Consultants developed a dynamic test facility (Figure 15) to test support systems under dynamic load condition in 1997. A sample size of 1.6m × 1.6m was fixed in to a flexible steel frame restrained with tensioned wire ropes in four corners and in middle of each side. Concrete and steel blocks were pre-loaded on top of the sample to simulate the rock mass.

A 10 tonne mass was dropped freely on to the collapsible roof and the impact was distributed through the pyramid of blocks supported by a steel plate. The maximum drop height of the facility is 3m with an impact velocity of 7.7 m/s to deliver maximum energy of 300kJ.

The test facility was designed to test multiple experiments on the one surface beam.

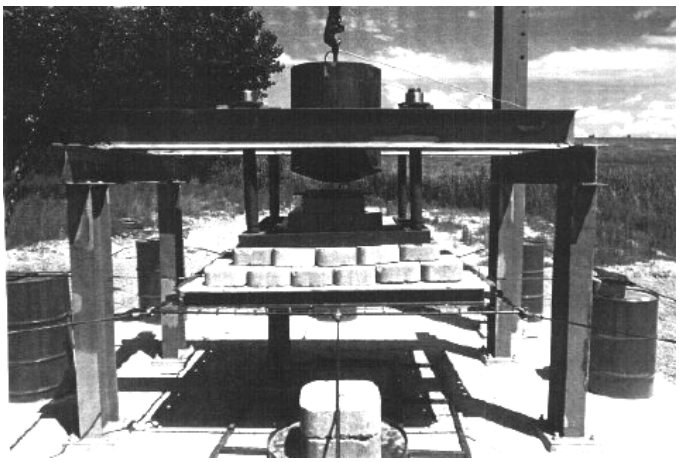

Figure 15: CSIR drop test facility for support scheme. (Ortlepp and Stacey 1997)

Stacey, T.R. & Ortlepp, W.D. (2001) described a drop testing facility to test support systems for use in tabular mining stopes. The most significant component of this facility is the collapsible roof, which simulates the hanging wall of a stope. All the components of the test facility are illustrated in Figure 16.

The collapsible roof is constructed with three cracked beams (12 high strength concrete slabs) to simulate a fractured hanging wall. The concrete slabs were packed into beams. The collapsible roof was supported with four concrete pillars at the corners.

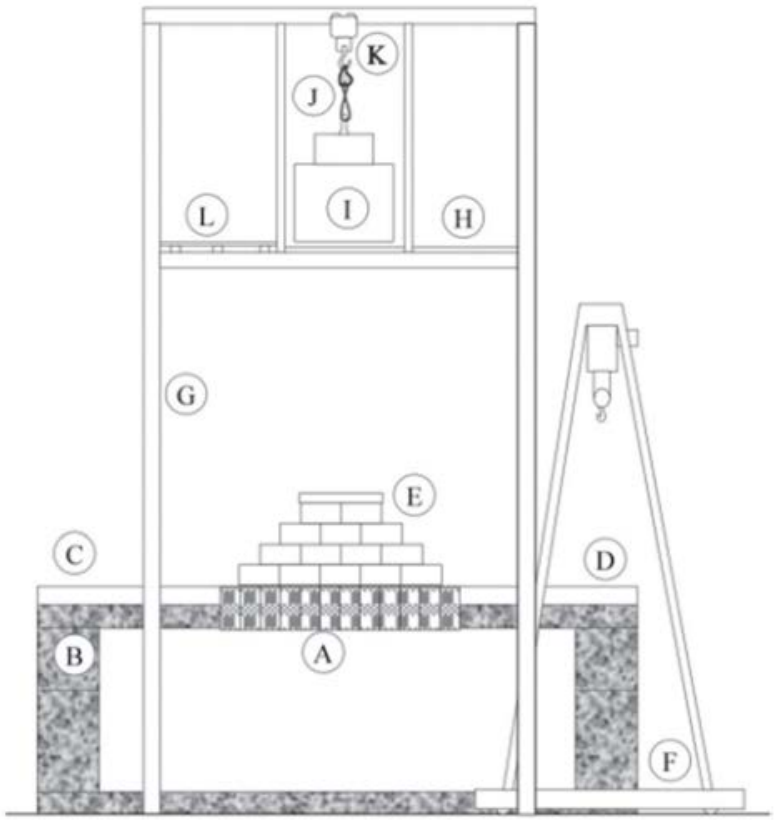

Figure 16: Section through the large-scale drop weight testing facility (Stacey, T.R. and Ortlepp, W.D. (2001).

The authors in describing this test facility concluded that the results should only be used as s relative ranking system for support systems.

The calculation of energy dissipated by a support system was not attempted. Force – time response of the support system was not available due to inadequate instrumentation. Moreover, this facility was not capable of testing a combined support scheme.

3.1.3.2 Geobrugg Walenstadt Test Site

Bucher et al. (2013) conducted a test series for rock bolts in combination with high-tensile wire mesh using a special large scale dynamic test facility shown in Figure

17. High tensile chain link mesh was fixed to a steel frame by lacing wire rope and was also restrained by four rock bolts.

A concrete block (6,280 kg) was lifted and dropped on to the impact platform. The lift height of the test block was limited to approximately 3.25m.

This test rig can facilitate combined scheme tests under dynamic loading conditions. Two load cells were installed on the upper (anchor) and the lower (collar) of one of the rock bolts. The anchor load cell measured the total force on the anchor which is similar to the WASM Dynamic Test Facility. In this test facility, the collar load cell was installed between the mesh and the reinforcement system to measure the vertical load taken by the mesh. In the WASM test facility, the collar load cell was installed between the dome plate and the nut to evaluate the performance of the surface hardware. High speed cameras and accelerometers were also used to measure behaviour during testing.

Research has been conducted with stiffer and softer test configurations to understand the energy distribution among reinforcement, mesh and the test setup. Layers of concrete, rocks and gravel were used to simulate a fractured rock mass. Tests were conducted under different setups by varying the thickness of the concrete slab and more or less interlock gravel on the assembly configuration.

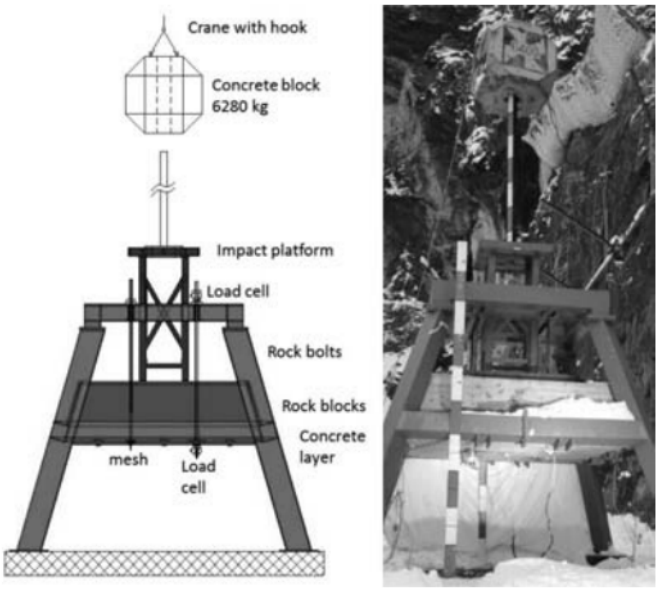

Figure 17: The Walenstadt test setup (Bucher et al., 2013).

For the *stiffer test setup*, the measured maximum force on the bolts was about 240kN (upper cell) and the measured maximum force on the mesh was about 65kN (lower cell). For the *softer test setup*, measured maximum forces on the bolts and on the mesh were about 165kN (upper cell) and 50kN (lower cell), repsectively.

The energy dissipated by the bolts within the *stiffer setup* was 32kJ in total (average of 8kJ per bolt) while the mesh dissipated 10kJ of energy. Therefore the support system dissipated a total of 42kJ of energy where the bolts contributed with 75% and the mesh contributed with 25%.

The energy dissipated by the bolts in the *softer setup* was 10kJ (average of 2.5kJ per bolt) while the mesh dissipated about 26kJ of energy. Total energy of 36kJ was distributed as 30% on the rock bolts and 70% on the mesh. The energy calculation was based on the test program conducted at WASM (Thompson et al., 2012).

CHAPTER 4

THE WASM DYNAMIC TEST FACILITY

4.1 INTRODUCTION TO THE WASM DYNAMIC TESTING FACILITY

The WASM Dynamic Test Facility is located at Kalgoorlie Consolidated Gold Mines (KCGM) mine lease, Kalgoorlie, Western Australia. The construction and commissioning project stages of the facility development were funded by the Minerals and Energy Research Institute of Western Australia (MERIWA) in projects M349 (Villaescusa et al., 2005) and M349A (Villaescusa et al., 2010).

The main purpose of the WASM Dynamic Test Facility is to test reinforcement systems, support systems and ground support schemes (combination systems) under dynamic load conditions. The test facility was designed to simulate the dynamic load conditions that may occur due to increased high stresses in underground excavations.

The WASM Dynamic Test Facility applies the momentum transfer concept to create dynamic loadings. The momentum transfer concept conceived by Professor Ernesto Villaescusa in the early 2000s is discussed in this chapter. A prototype unit (Figure 18) of the facility was designed and built to understand the momentum transfer concept on a combined ground support scheme prior to the construction of the test facility.

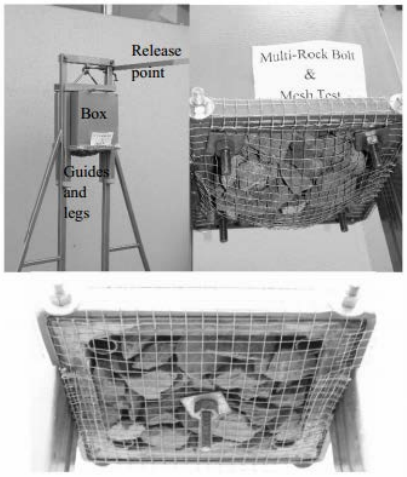

Figure 18: WASM Prototype dynamic loading of ground control scheme (Player et al., 2004).

The WASM Dynamic Test Facility shown in Figure 19 consists of a drop beam, a loading mass, a simulated reinforcement system and a simulated support system. The reinforcement system is installed in a simulated borehole which is formed in concrete contained within a steel pipe. The simulated borehole is anchored onto the beam while the support system is fixed onto a steel frame which is bolted to the beam. A slot is created in the steel pipe to simulate the rock mass discontinuity. All the components of the WASM Dynamic Test Facility are discussed in detail in the following sections.

Advanced monitoring include a high speed digital camera, accelerometers, load cells, and potentiometers. A computer with high speed data logger and software system are used to acquire and store data. The data are analysed using Pro Analyst, Midas, WASM in-house software developed by Dr Alan Thompson and Windows Excel. The data analysis process is described in detail in Chapter 6.

4.2 COMPONENTS OF THE WASM DYNAMIC TEST FACILITY

Thompson et al. (2004) described the WASM Dynamic Test Facility for reinforcement testing as having three major components;

- The Reinforcement System.
- The Collar Zone.
- The Anchor Zone.

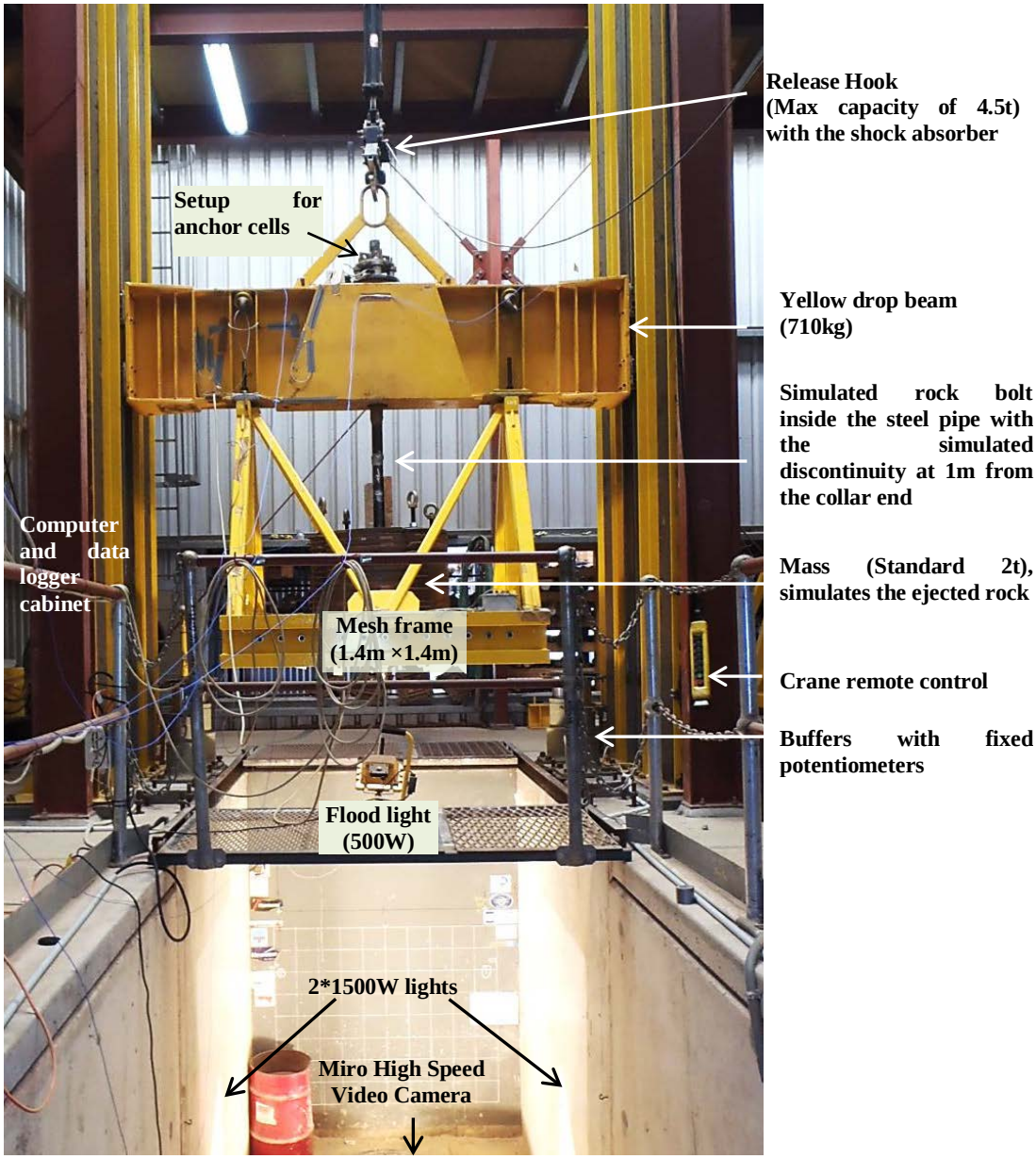

Figure 19: WASM Dynamic Test Facility for combined systems.

For combined systems, a support system forms part of the collar zone used to complement the reinforcement action in providing resistance to dynamic loading. The support system investigated is mesh attached on to a steel frame and bolted to a drop beam as shown in Figure 20.

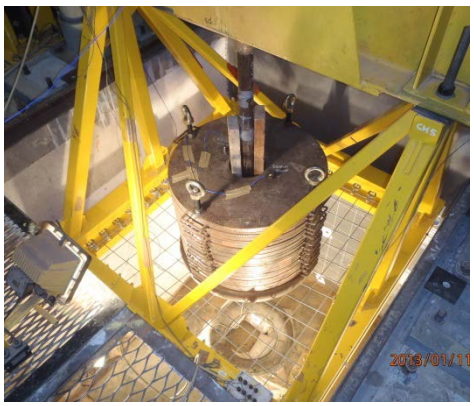

Figure 20: Support system configuration.

The reinforcement system is basically a rock bolt embedded in cement grout contained within a steel pipe which is divided into two lengths; one in the anchor zone and the other in the collar zone.

The collar zone comprises of the collar pipe section with a welded flange, a loading mass and an external fixture (surface hardware). The collar load cell is fixed by a nut to the reinforcement system. The collar zone simulates the ejected rock mass in an underground excavation.

The anchor zone comprises of the drop beam and the anchored simulated pipe section. Four anchor cells placed between the drop beam and a flange welded to the anchor pipe are used to monitor the force response in the reinforcement system during the test. The anchor zone simulates the surrounding (stable) rock near the anchor zone of the reinforcement system. The beam rests against buffers after the impact and allows the collar zone to move and dynamic loading to be resisted by the combined system of reinforcement and mesh.

4.2.1 The Drop Beam

The drop beam was designed to fall under gravity and its movement resisted by the buffers. A crane with a 5 tonne capacity is used to move the drop beam (710kg) inside the dynamic laboratory. The simulated sample is bolted with the four anchor cells onto the drop beam as shown in Figure 21. Accelerometers are installed on the beam.

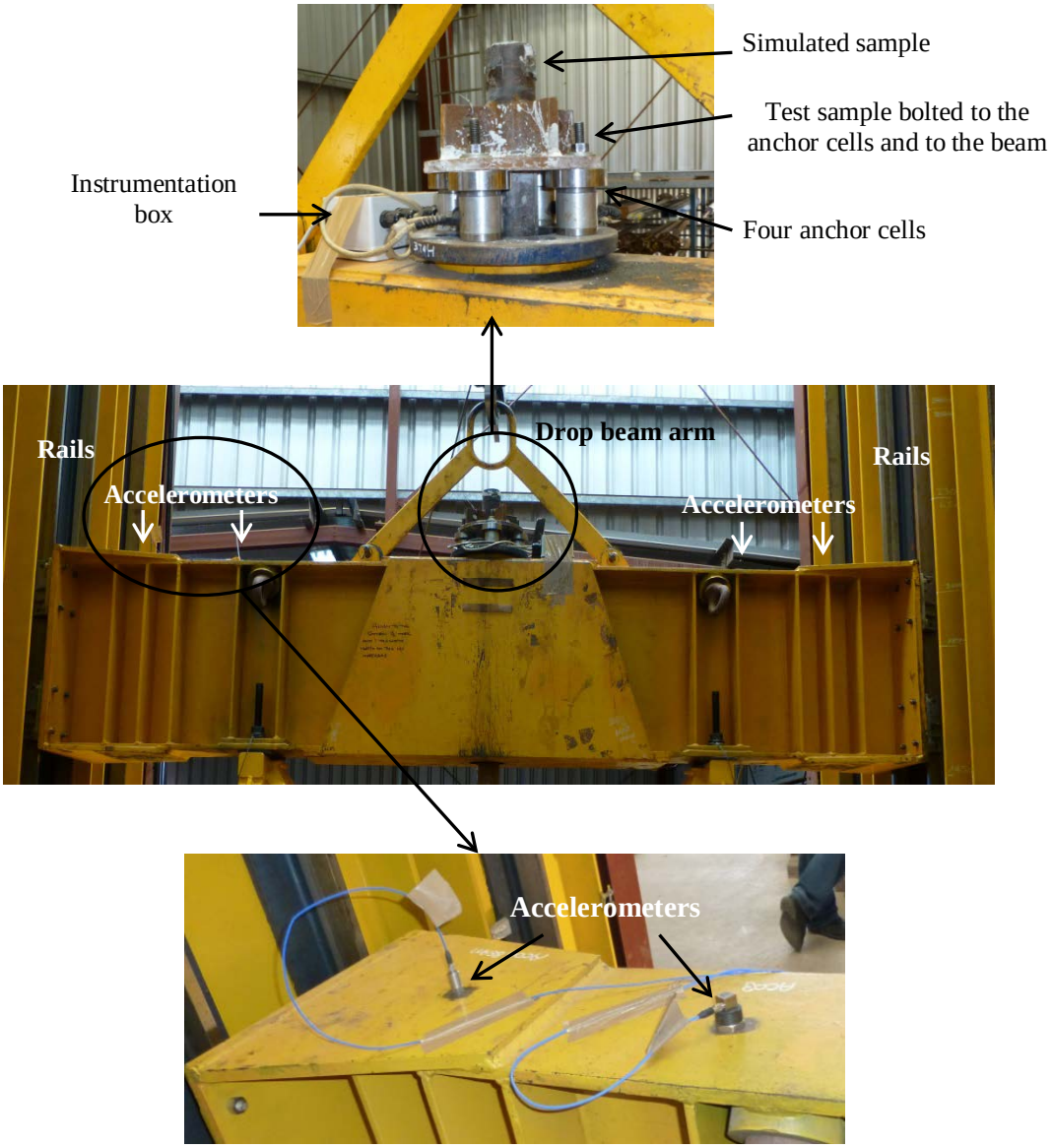

Figure 21: The instrumentation and configurations used for the drop beam.

4.2.2 The Mesh Frame

The mesh frame shown in Figure 22 is an attachment where the mesh is fixed prior to testing. The frame is designed to accommodate 1.4m × 1.4m welded mesh and chain link mesh samples. For slightly smaller mesh sizes, extra metal strips are used for adjustment. The mesh is fixed to the shackles and the shackles to the eye bolts (Figure 23) on the frame boundary.

Load cells were used to monitor load in a number of eye bolts (Figure 24)

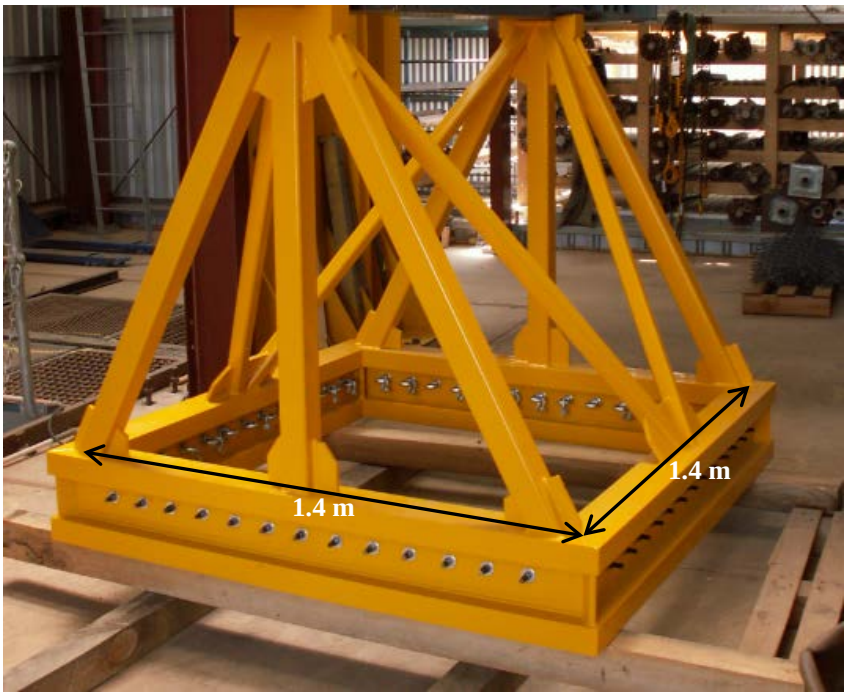

Figure 22: The mesh frame.

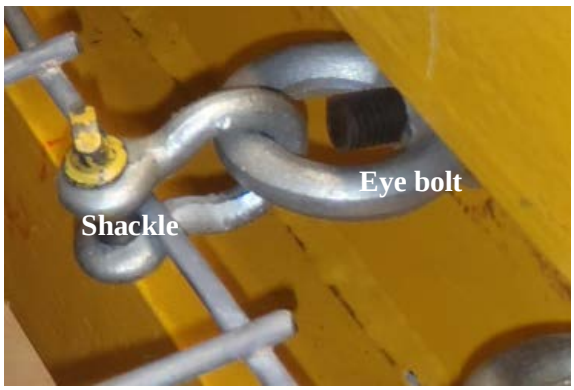

Figure 23: Eye bolt and the shackle arrangement.

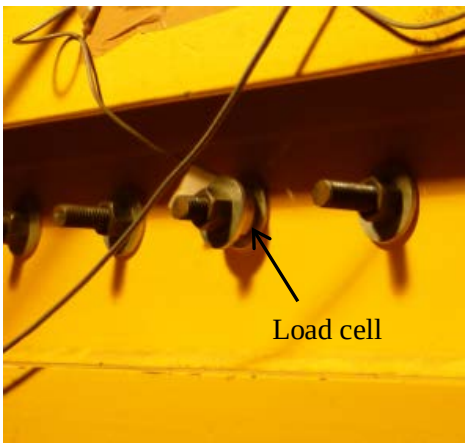

Figure 24: Load cell on the centre of the front side of mesh frame.

The mesh frame is bolted onto the drop beam. Four load cells were installed between the drop beam and the frame bolts. Another set of load cells were installed onto the centre of front, left, and right sides bolts of the frame (Figure 25).

Figure 25: Load cell between the drop beam and mesh frame attachment.

4.2.3 The Release Hook and the Shock Absorber

A capacity of 4536kg (1000lbs) helicopter hook (model 10K-001, Canam Aerospace) with a shock absorber was used to release the beam to let the system drop. During the test, noise was prevented by a shock absorber. The release hook and the shock absorber are shown in Figure 26.

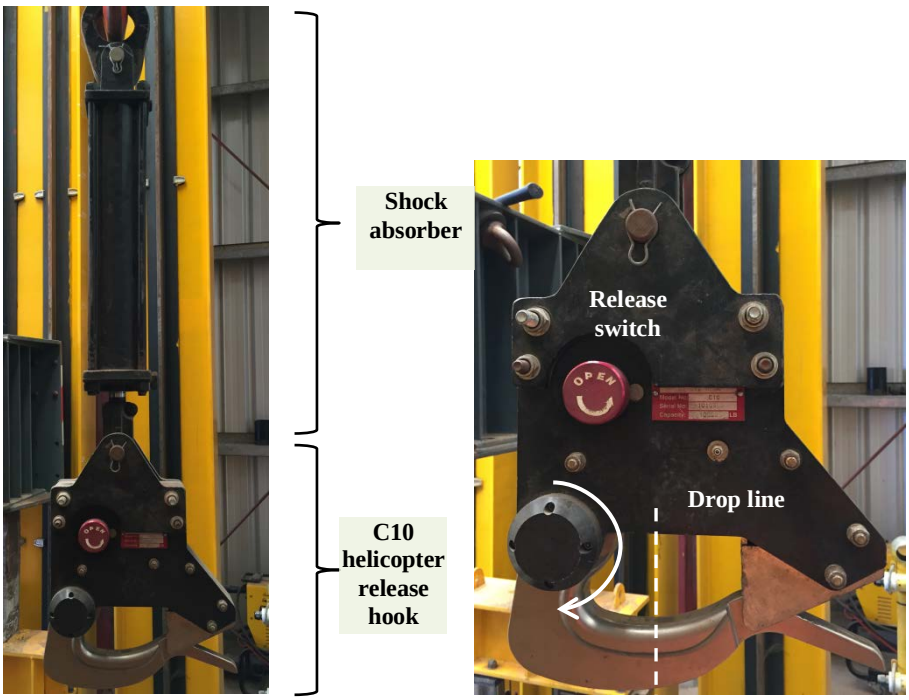

Figure 26: The helicopter release hook with the shock absorber.

4.2.4 The Overhead Crane

A 5 tonne crane is fixed onto a beam (Figure 27) through the release hook and is used to lift and move heavy items. This includes the drop beam, the simulated rock mass, the mesh frame and the simulated reinforcement systems.

Figure 27: The overhead crane arrangement.

4.2.5 High Speed Camera

A Phantom Miro eX4 high speed camera was used to record the reinforcement collar and the mesh movement. The camera was positioned in front of the drop plane on a tripod. The aperture and focusing were set prior to each test. Video data were recorded at a rate of a thousand frames per second.

4.2.6 The Reinforcement System

A steel pipe (60.0mm outer diameter and 49.5mm inner diameter) was used to simulate the surrounding rock mass in an underground excavation (Figure 28). The rock bolts were centralised onto the steel pipe and fixed with cement grout (0.4 W/C ratio). The grouting process is described in detail in Chapter 5.

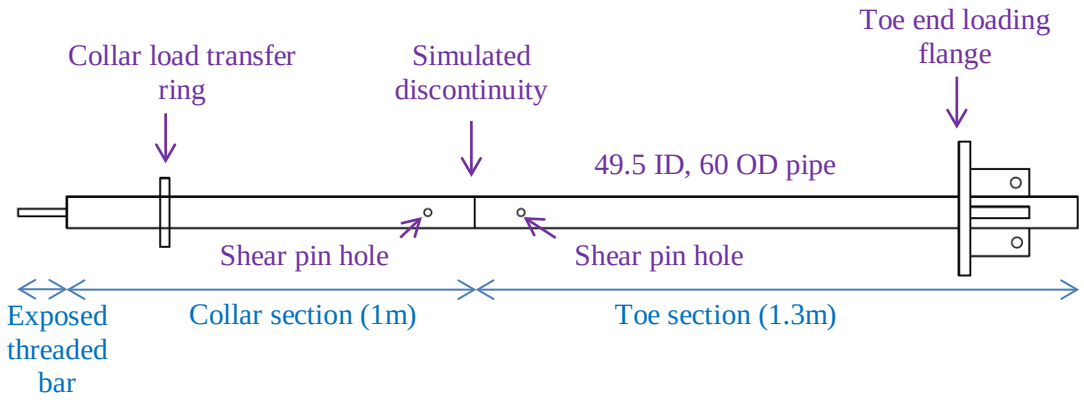

Figure 28: Reinforcement system configuration.

Four shear pin holes are drilled and welded to prevent grout sliding within the steel pipe. A cut through the circumference of the steel pipe at 1m distance from the collar end of the steel pipe was used to simulate a discontinuity in a rock mass.

The collar load transfer ring was used to integrate the collar section of the reinforcement system with the loading mass. The exposed threaded bar length was made adequate to install the surface hardware and the collar load cell.

4.2.7 The Loading Mass

The load mass of the WASM Dynamic Test Facility simulates the ejected rock mass in an underground excavation. Basically, the mass is a number (up to 35) of steel plates which weigh around 50.8 kg each. An extra curved steel plate (380kg) was

used in this combined test program at the bottom of the load mass. Therefore the total weight of the load mass may be up to 2158 kg (35×50.8kg + 380kg). The load transfer ring on the collar pipe was used to transfer the load from the load mass to the reinforcement system as shown in Figure 29. Two accelerometers were installed on the load mass to record the mass deceleration due to the resistance of the reinforcement and mesh. The accelerometer data were used in the analysis process for prediction of the net force on the loading mass.

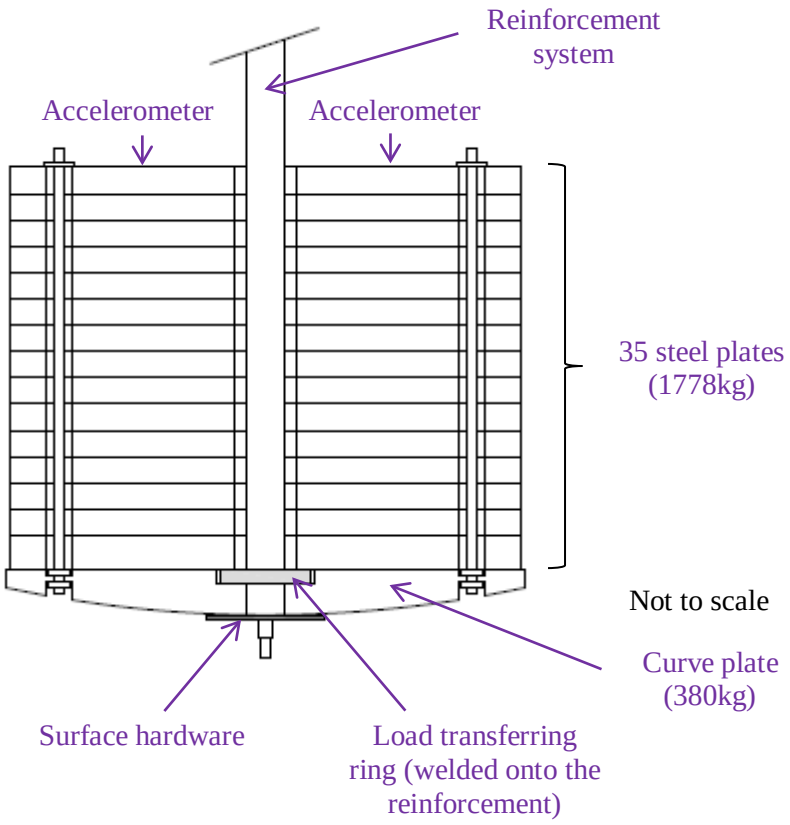

Figure 29: Configuration of the load mass.

Surface hardware was installed with the collar load cells on to the reinforcement system as shown in Figure 30. The nut was hand tensioned using a wrench.

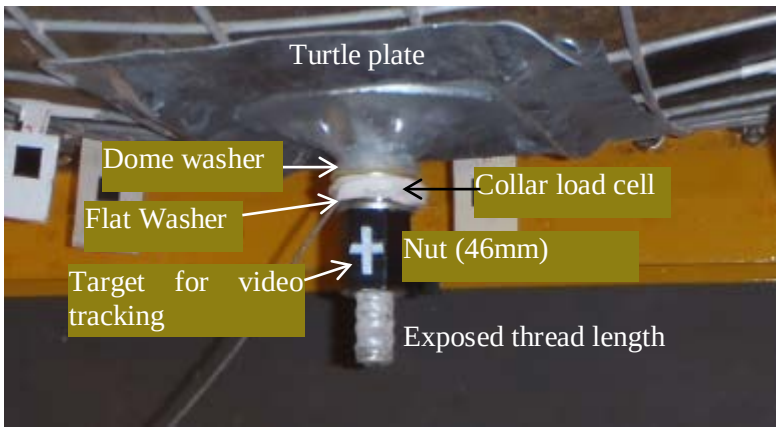

Figure 30: Set-up of the surface hardware and load cell.

4.2.8 Buffers

The drop beam falls freely under gravity and impacts on the buffers after which the beam is decelerated rapidly. The Oleo buffers (Figure 31 (a)) are used in the WASM dynamic facility due to their ability to endure repeated impact loadings. The impact energy on the buffers is dissipated by a turbulent flow and heating of oil inside the buffers. Figure 31 (b) illustrates a section of an Oleo buffer.

Rubber pads were placed on top of the buffers to reduce the noise generated in metal to metal contact. Potentiometers were installed on the buffers as shown in (Figure 31 (a) to measure their linear movement.

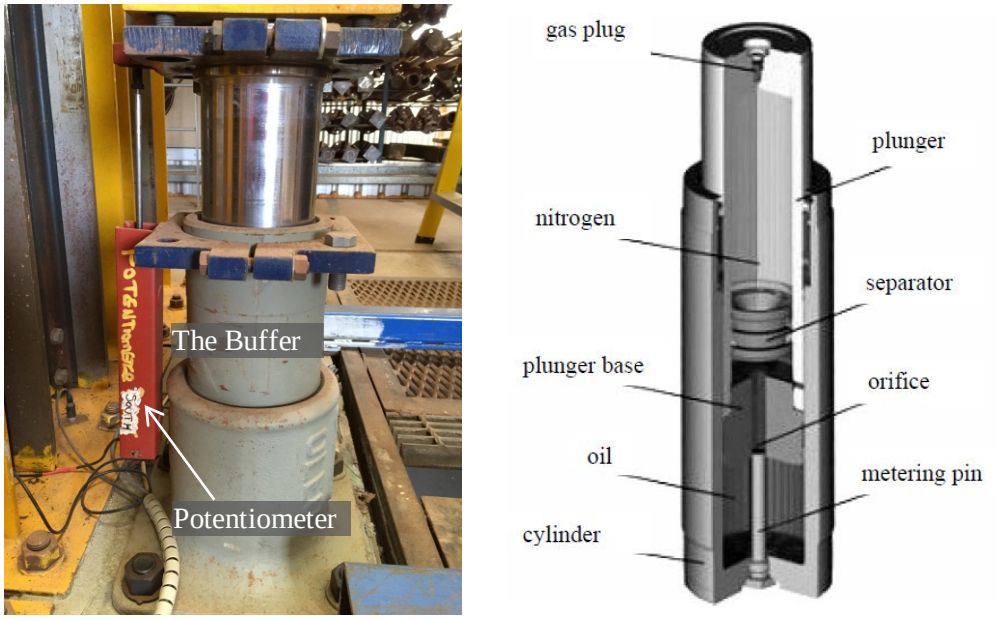

(a) (b)

Figure 31: (a) The buffer (b) Section of an Oleo buffer (Player et al., 2004).

4.2.9 Engineering calculations for bolt and mesh combined schemes

The WASM dynamic testing facility incorporates many advanced instruments. The load transfer concept and relevant forces of the WASM Dynamic Test Facility for a reinforcement system alone and a support system alone were described by Thompson et al. (2004) and Thompson et al. (2013), respectively. The load transfer and relevant forces of the WASM Dynamic Test Facility for a combination of reinforcement and mesh are shown in Figure 32. The symbols used in this figure and the corresponding dynamic equilibrium equations are as follows.

M_{DB} - mass of beam.
M_{PA} - mass of anchor pipe.
M_C - loading mass (including collar pipe).
M_B - mass of buffer piston.
M_M - mass of mesh panel.
M_{FM} - mass of mesh frame.
F_{AB} - buffer reaction force on beam.
F_{PJ} - pipe force transfer at the interface between the anchor and collar regions.
F_M - edge resistant force on mesh panel.
F_{SL} - force transfer between the mesh and loading mass.
F_{RJ} - element force at the interface between anchor and collar zone.

F_{PS} - force between reinforcement plate and surface support or loading mass.
T_C - load transfer between element and wall of pipe (or borehole) in collar region.
P_A - force transfer between the reinforcement anchor pipe and beam.
P_F - force transfer between the frame and beam.
P_B - internal buffer force.
U_B - displacement of the buffer.
U_A - displacement of beam.
U_{PA} - displacement of anchor pipe.
U_{FM} - displacement of mesh frame.
U_C - displacement of mesh sheet.

The dynamic equilibrium equations for the various components of a test on combination of reinforcement and mesh are as follows:

Buffer Mass:

$$M_B \ddot{u}_B = M_B g + F_{AB} - P_B \qquad \text{Eq 01}$$

Beam Mass:

$$M_{DB} \ddot{u}_A = M_{DB} g + P_F + P_A - N_B F_{AB} \qquad \text{Eq 02}$$

Upper pipe:

$$M_{PA} \ddot{u}_{PA} = M_{PA} g + F_{RJ} - F_{PJ} - P_A \qquad \text{Eq 03}$$

Frame:

$$M_{FM} \ddot{u}_{FM} = M_{FM} g + F_M - P_F \qquad \text{Eq 04}$$

Mesh sheet:

$$M_M \ddot{u}_C = M_M g + F_{SL} + F_M - F_{PS} \qquad \text{Eq 05}$$

Note that: $F_{SL} = F_{PS} + F_M$ Eq 06

Note that: $F_{SL} = F_{PS}$ prior to starting the test

Combined Lower Pipe and Loading Mass:

$$M_C \ddot{u}_C = M_C g - F_{SL} - T_C \qquad \text{Eq 07}$$

Which is the same as

$$M_C \ddot{u}_C = M_C g + F_{PJ} - F_{RJ} - F_M \qquad \text{Eq 08}$$

To eliminate $F_{AB,}$ multiply equation (1) by N_B and then add to equation (2) to obtain

$$M_{DM} \ddot{u}_A + N_B M_B \ddot{u}_B = M_{DB} g + N_B M_B g + P_F + P_A - N_B P_B \qquad \text{Eq 09}$$

This equation (Eq 09) may be used to estimate the average buffer reaction force P_B from the measured accelerations, frame force P_F and anchor force $P_{A.}$

The force in the mesh F_M can be estimated from the total force estimated to be causing mass declearation less the reinforcement force measured by the load cells and corrected for inertial of the anchor zone pipe.

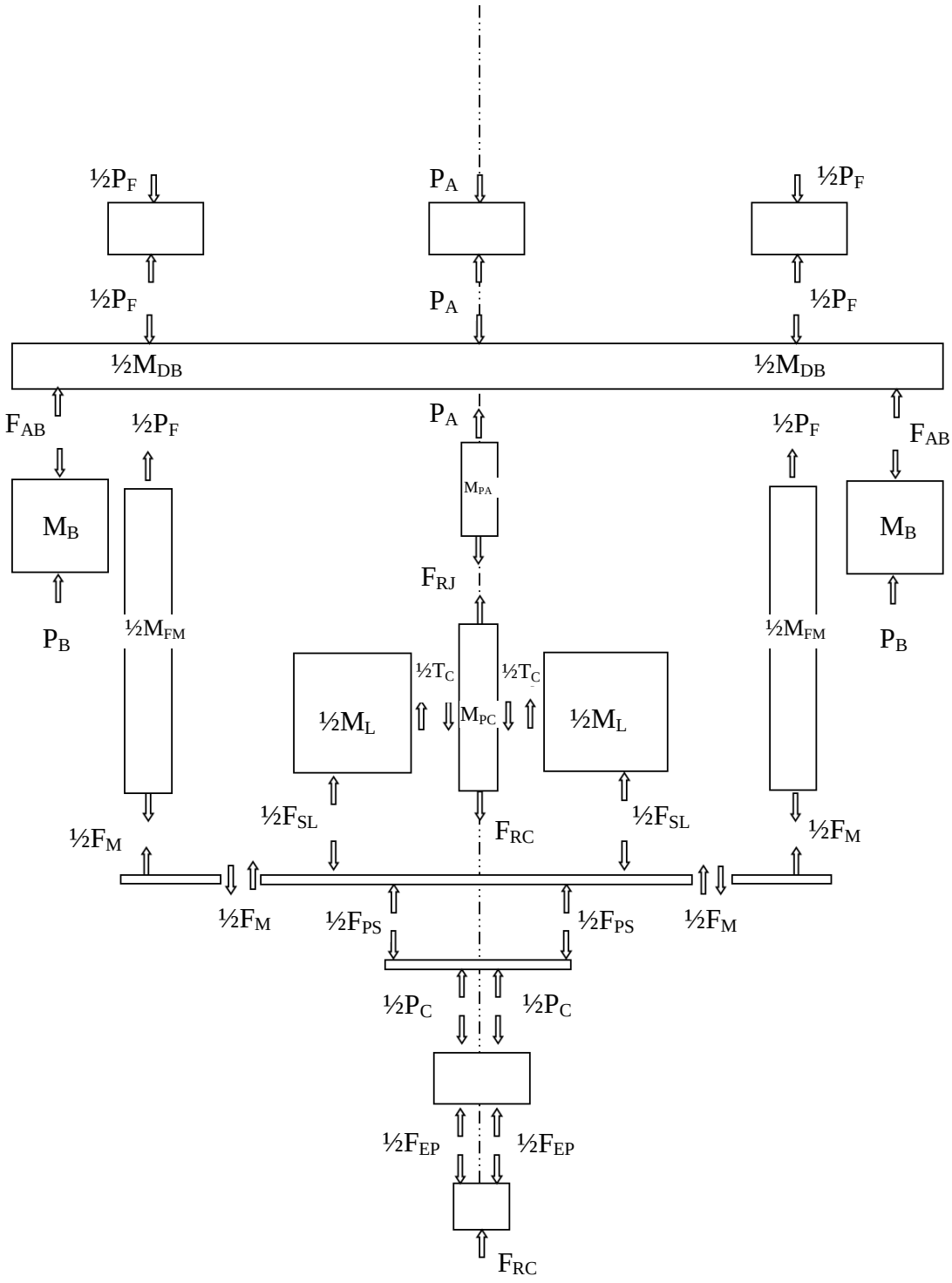

Figure 32: Schematic of load transfer mechanism for a combined scheme in the WASM Dynamic Test Facility.

4.3 The Data Acquisition System and Sensors used in the Test Facility

The load transfer mechanisms clearly identified in the previous section were used to design the instrumentation to measure selected forces, displacements, accelerations and strain of the:

- Reinforcement system (bolts, surface hardware, collar and anchor)
- Simulated ejected rock (the integrated steel rings and lower pipe length)
- Simulated stable rock mass (the drop beam and upper pipe length)
- Buffers (the impact surface), Player et al. (2004)

In addition, mesh was used in this combined test program. The characteristic displacement of the mesh is assumed to be same as the collar fixture on the reinforcement system. The instrumentation data is recorded at a very high frequency (very small time interval).

4.3.1 Data Acquisition System

Midas 2.0 (Xcitex Inc 2002) was used as the video control and analysis software to record the high speed video data. A National Instruments - PCI6071E data acquisition (DAQ) board was used to control the acquisition of test data. A schematic diagram of the DAQ board and the instrumentation are shown in Figure 33.

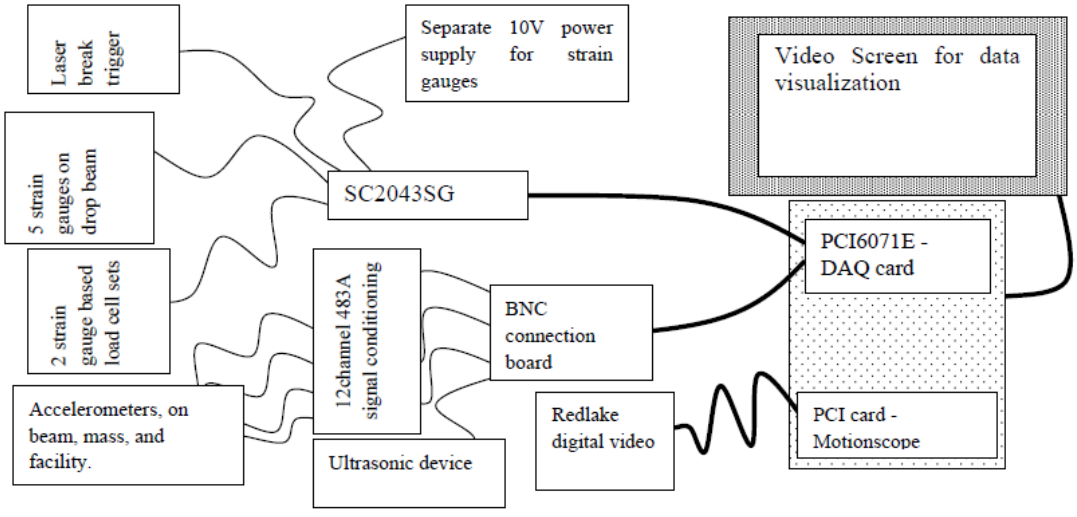

Figure 33: Schematic of instrumentation and data acquisition (Player et al., 2004).

The DAQ board has a capacity of 32 channels with a sample rate of 25,000 samples per second for each channel and operates simultaneously with the video camera.

The DAQ board starts recording data (sensor data and video data) continuously in a two-second window as soon as it is powered. The system is triggered when a laser beam is broken when the drop beam passes through as shown in Figure 34. Two lasers, the upper laser and the lower laser, were used for two reasons. Firstly to trigger the data recording process and secondly to calculate the impact velocity of the drop beam. After the system is triggered, the data are recorded in a two second time window.

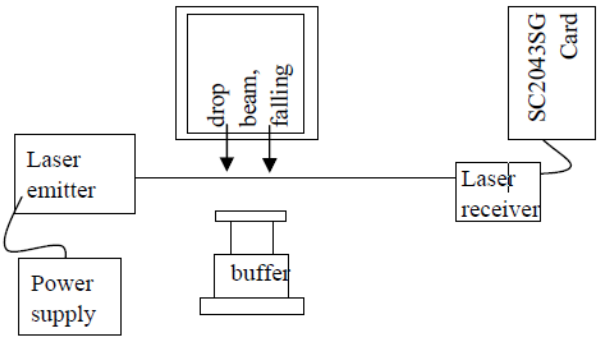

Figure 34: Laser break trigger of instrumentation (Player et al., 2004).

A strain gauge signal conditioning card (NI-SC2043SG) was used to detect the laser break. When the system is triggered, a percentage of data is recorded as pre-trigger data.

4.3.2 Sensors

As mentioned previously, sensors include accelerometers, potentiometers, load cells, lasers and strain gauges. All the sensors were calibrated prior to the test or the manufacturer's specifications were used. The quality of the measured data point is a function of the combined accuracy and precision of both sensor and the DAQ board (Player et al., 2004).

4.3.2.1 Accelerometers

Two shock accelerometers were installed on the beam above the buffers and a tri-axial accelerometer was installed in between the shock accelerometer and the centre of the beam (2/3 from the centre) as shown in Figure 21. Two accelerometers, shock accelerometer and a tri-axial accelerometer were installed on the top of the mass as shown in Figure 29 .

Mechanical filters and rubber pads were fixed on to the tri-axial accelerometers to protect them from high frequency and saturation. Tri-axial accelerometers have an acquisition range of 1Hz to 5kHz and shock accelerometers have a range of 1kHz to 10kHz.

4.3.2.2 Load Cells

Two types of load cells were installed in the WASM dynamic testing facility. Anchor load cells were bolted to the drop beam as shown in Figure 35 and the collar load cell installed with the surface hardware at the collar end as shown in Figure 36.

Anchor load is measured by averaging the outputs form the four load cells arranged in a Wheatstone bridge circuit. The nominal capacity of the cells is 300kN which are used to identify the force transfer from the loading mass to the drop beam through the reinforcement system.

A single 356kN capacity load cell was installed to measure the collar force developed in the reinforcement. The collar load cell is basically used to assess the performance of surface hardware and to measures the load transfer between the reinforcement element and the simulated borehole. It was identified that the anchor load cells and the DAQ board have a combined error of 3.53kN and 14.1kN of error during commissioning tests while the collar load cell and the board showed a combined error of 1.28kN and 5.3kN during commissioning tests (Player et al., 2004).

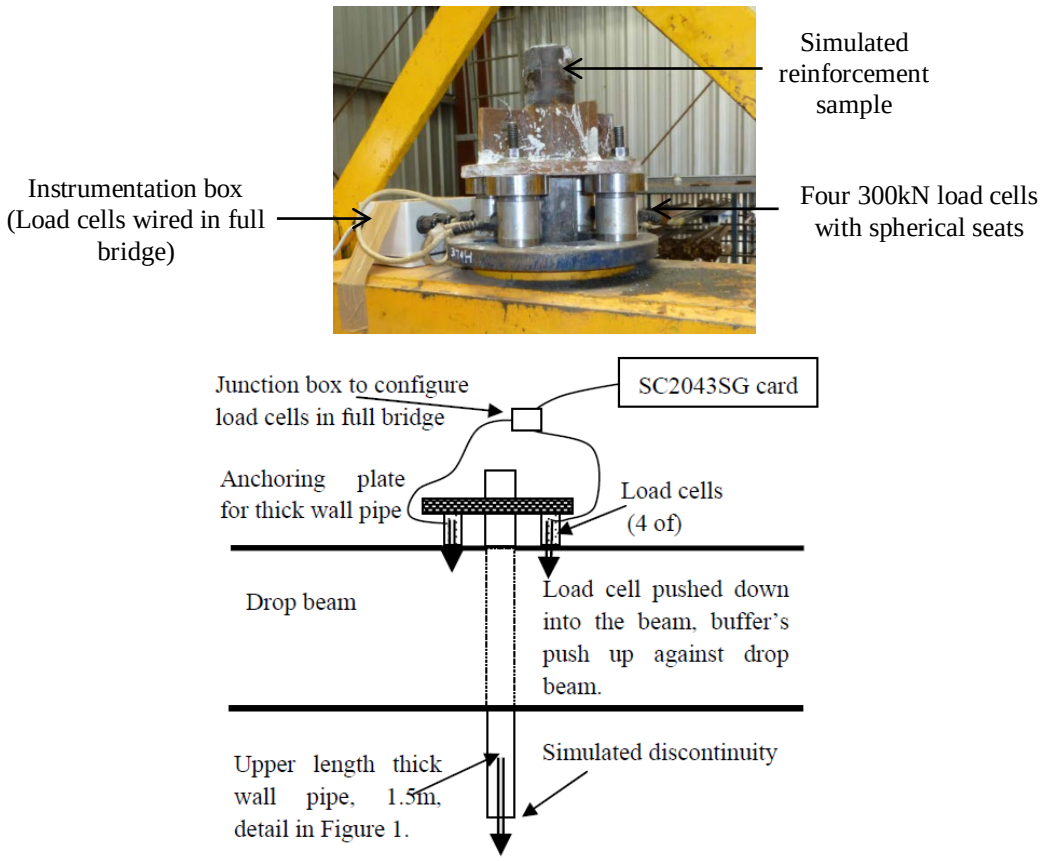

Figure 35: Anchor load cells setup (Player et al., 2004).

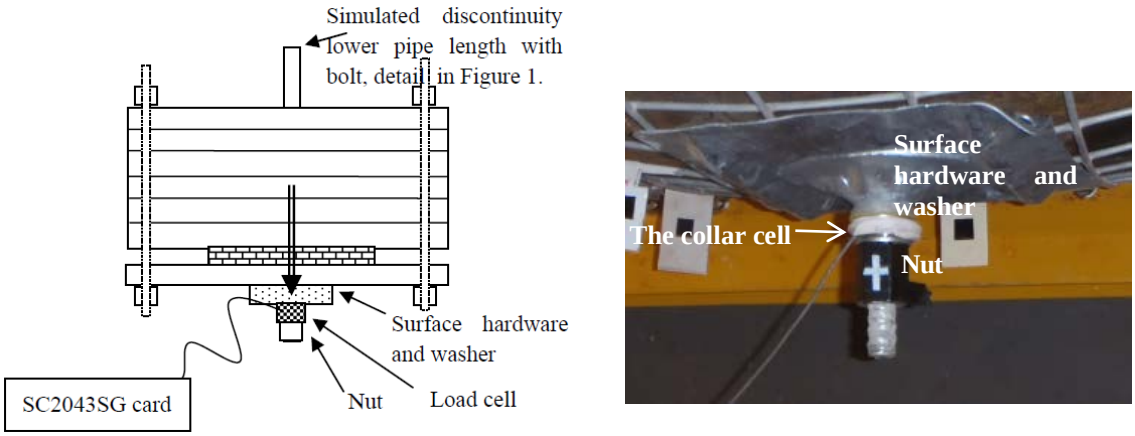

Figure 36: Collar load cell setup (Player et al., 2004).

4.4 PREVIOUS TESTING

4.4.1 Background

Reinforcement systems and support systems should withstand both static and dynamic loading conditions. A large number of tests have been conducted at the WASM static and dynamic test facilities prior to the combined testing. Static testing for reinforcement systems are conducted at the WASM rock mechanics laboratory. An Avery machine is used with instrumentation to conduct static tests as shown in Figure 37.

Figure 37: Static test setup for reinforcement

The static test facility shown in Figure 38 for weld mesh and woven wire (chain link) mesh was described by Morton et al. (2007). Moreover, the WASM static test results for weld mesh and woven wire mesh are described by Villaescusa (2014, pp. 392-394).

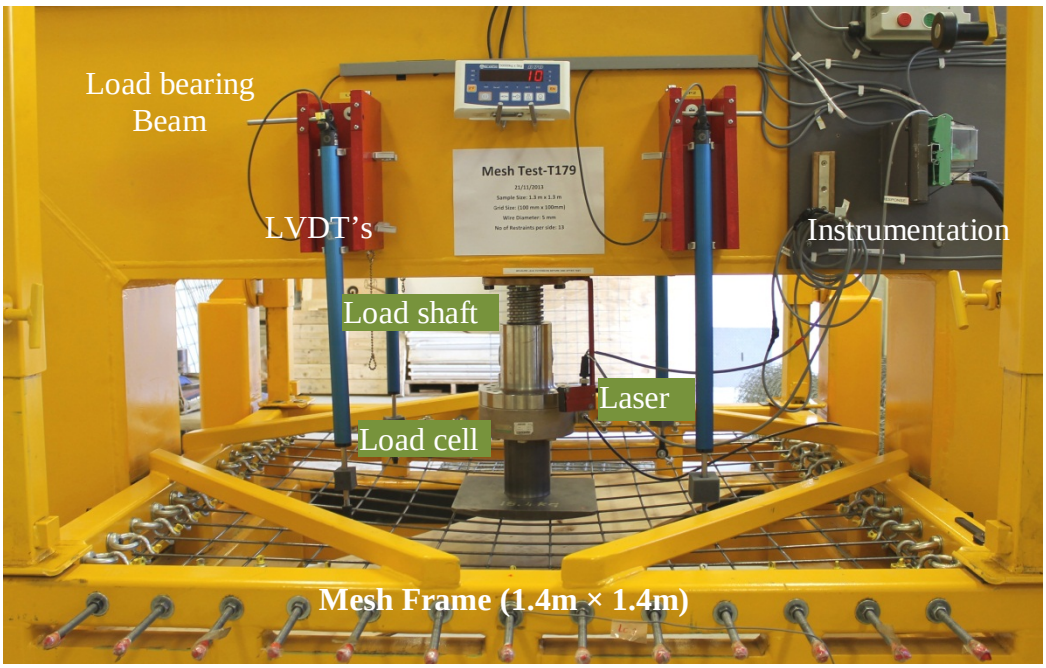

Figure 38: The configuration of WASM static test facility for mesh testing (Morton et al., 2007).

Furthermore, Morton et al. (2007) has described the static testing of sprayed layers (shotcrete and membranes) as shown in Figure 39.

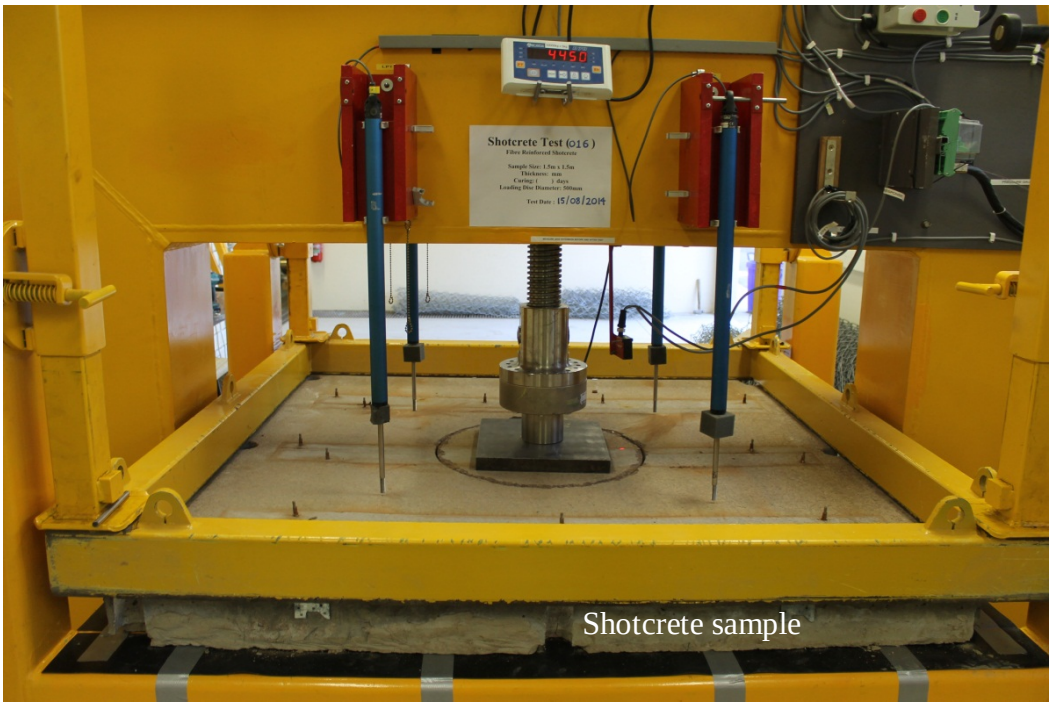

Figure 39: The configuration of WASM static test facility for shotcrete testing (Morton et al., 2007).

Individually, the behaviour of reinforcement systems and support systems were well understood at the WASM laboratories and this thesis focuses on understanding of combined schemes.

The summary descriptions of some of the WASM dynamic and static test results are presented in the following sections. This study of combined systems involved threaded bar and mesh systems. Consequently, the following section presents a summary of threaded bar mesh results from the WASM test facility.

4.4.1.2 WASM Dynamic Test Results of 20mm Threaded Bar

Player et al. (2004, 2008) tested and examined the performance of 20mm threaded bar under dynamic loading conditions at WASM Dynamic Test Facility. Tests were conducted under three categories. Fully bonded threaded bar encapsulated in cement grout, partially decoupled threaded bar encapsulated in cement grout and resin encapsulated toe anchored threaded bar.

The dynamic force – displacement graphs of fully bonded threaded bar and the summary results are shown in Figure 40 and Table 2 respectively.

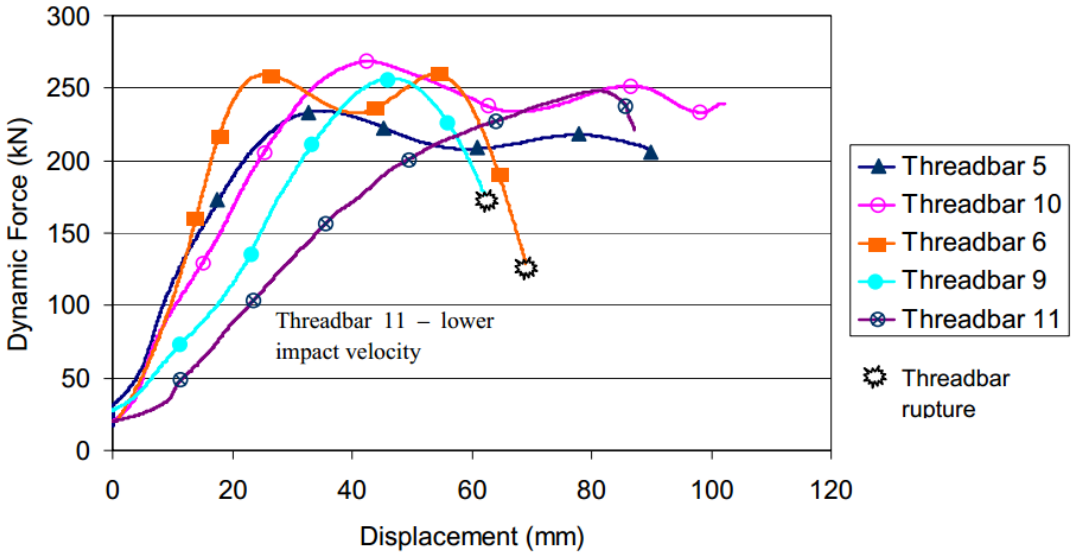

Figure 40: Dynamic force displacement response at simulated discontinuity – fully encapsulated threaded bar (Player et al., 2008).

Table 2: Fully encapsulated threaded bar summary results (Player et al., 2008)

Bolt Number	Load Time (ms)	Displacement (mm)	Peak Deceleration (g)	Peak Force (kN)	Peak Ejection Velocity (m/s)	Energy Absorbed (kJ)	Results
11	56	92	-12	248	2.2	14.8	Bar streched
9	26	62	-12	256	3.0	10.9	Bar fractured at simulated discontinuity
6	28	69	-12	260	3.1	13.9	Bar fractured at simulated discontinuity
10	56	100	-13	270	3.2	20.8	Bar streched, no surface hardware
5	100	91	-13	235	2.4	17.5	Bar streched and pulled in grout, 5 year old grout
Average:		82.8			2.8	15.6	

Player et al. (2004, 2008) defined the loading condition as critical and sub-critical where the critical loading caused the rupture of the bar and sub-critical loading allowed the bar to stretch (plastic deformation) at the simulated discontinuity. When the sub-critical loading occurs, the development of decoupled length helps the bolt to withstand the load by dissipating the input energy while stretching.

The dynamic force – displacement graphs of decoupled threaded bar and the summary results are shown in Figure 41 and Table 3 respectively.

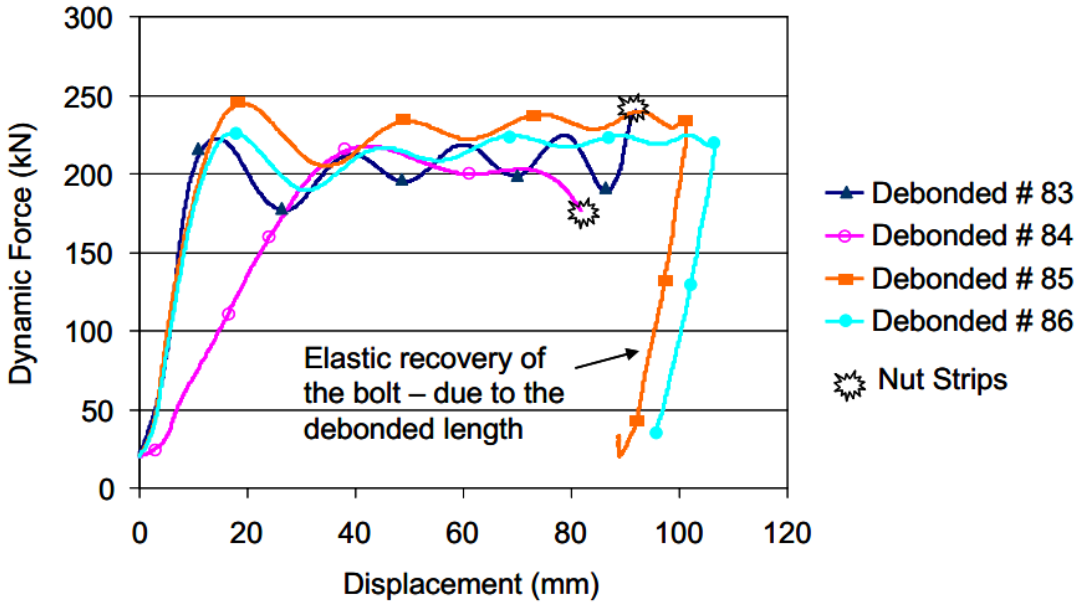

Figure 41: Dynamic force displacement response at simulated discontinuity - decoupled threaded bar (Player et al., 2008).

Table 3: Decoupled threaded bar summary results (John et al., 2008)

Bolt Number	Load Time (ms)	Displacement (mm)	Peak Deceleration (g)	Peak Force (kN)	Peak Ejection Velocity (m/s)	Energy Absorbed (kJ)	Results
83	55	93	-11	240	2.5	18	Nut stripped
84	35	82	-10	217	2.6	13.6	Nut stripped
85	58	101	-12	244	2.6	21.8	Reinforcement system survived two drops
86	62	106	-11	226	2.6	21.6	Reinforcement system partial thread shearing on second drop.

The decoupled threaded bar dissipates energy by plastic deforming the decoupled steel length. “The critical functionality for a decoupled threaded bar was the correct selection of the surface fixture” (Player et al. 2008). It was understood that when using the mine nut and a washer, the nut stripped over once the collar load reached 180kN and increased up to 200kN with a longer integrated nut and washer (Figure 42).

Figure 42: Mine nut (left), longer integrated nut (right).

Moreover, Player et al. (2008) concluded that the performance of complete reinforcement system depends on the encapsulation medium, toe and collar embedment lengths, surface hardware and loading conditions.

4.4.2 Testing of Mesh

4.4.2.1 Static Test Results for Welded Wire and Chain Link Mesh

Villaescusa (1999) conducted a weld shear test program (AS1304-1991 Welded wire reinforcement fabric for concrete) to understand the different failure modes in welded wire mesh. Three distinguish failure modes (Figure 8): shear failure at weld

point (weld failure), failure at the heat affected zone (HAZ) and tensile failure of the weld mesh wire were identified by Villaescusa and he suggested that “the weld strength must be designed to have strength at least equal that of the line wire strength”. Also he suggested that HAZ failure caused because of “weakening of the wire during the welding process due to excessive weld head pressure and temperature”.

Morton et al. (2008) have conducted a static test series for 5.6mm diameter galvanised welded wire mesh (welded wire mesh with 100mm square grid pattern) and 4mm high strength steel wire chain link mesh.

The summary of static force- displacement response is shown in Figure 43. The average rupture displacement for welded wire mesh and chain link mesh were 186mm and 307mm respectively.

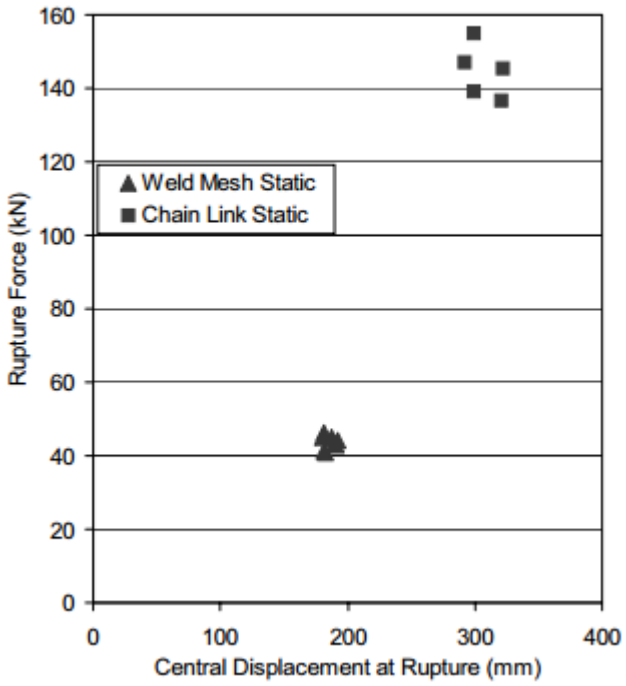

Figure 43: Summary of static force- displacement results for welded wire mesh and chain link mesh (Morton et al., 2008).

Initial displacements were considered as it varied due to the tension of the sample. But it was identified that the initial displacement did not significantly affect the overall performance of the mesh. The average rupture force for welded wire mesh was 44kN while the average rupture force for chain link mesh was 145kN.

4.4.2.2 Dynamic Test Results of Welded Mesh and Chain Link Mesh

Player et al. (2008) presented dynamic test results of welded mesh and high tensile chain link mesh, conducted at the WASM Dynamic Test Facility.

The Rupture Force- Displacement graph and the Rupture Energy- Displacement graph are shown in Figure 44 and Figure 45, respectively.

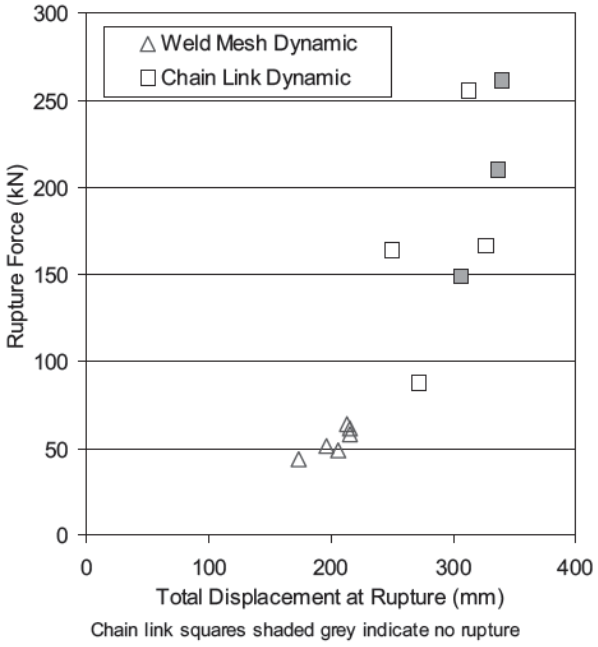

Figure 44: Summary of dynamic force-displacement results for welded mesh and chain link mesh (Player et al., 2008).

The force in the mesh was inferred from the deceleration of the loading mass. The displacement was calculated by subtracting the beam/frame displacement from the loading mass displacement (Thompson et al., 2013).

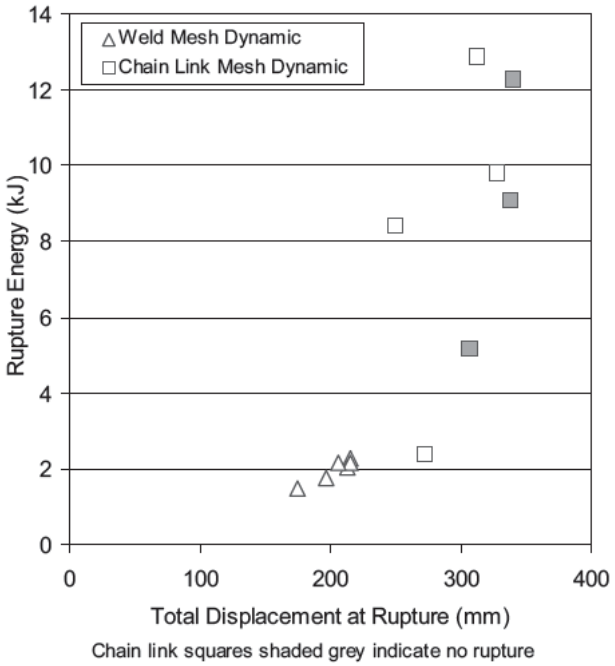

Figure 45: Rupture energy results for welded wire mesh and chain link mesh (Player et al., 2008).

The results have shown that 4mm high tensile chain link mesh can absorb energy of ~18kJ and withstand up to ~250kN of force while standard weld mesh only absorb up to ~2.7kJ of energy and ~55kN of force.

The average dynamic displacement for chain link mesh and weld mesh were respectively 306mm and 203mm. Player et al. (2008) concluded that high tensile 4mm diameter chain link mesh has much higher force, displacement and energy capabilities than standard weld mesh.

CHAPTER 5

PREPARATION OF TEST SAMPLES AND THE TEST PROCEDURE

5.1 TEST SAMPLES

The first bolt and mesh combined scheme test program involved a combination of two different types of reinforcement systems; namely:

- Fully coupled 20mm threaded bar.
- 1000mm decoupled 20mm threaded bar.

combined with two different types of mesh support systems; namely:

- TECCO G80 chain link mesh, 4mm wire diameter.
- Weld mesh, 5.6mm wire diameter.

A total of eight tests were performed.

The second bolt and mesh combined scheme test program involved 20mm bar diameter, 3m long, 1.4m decoupled DSI Posimix and three types of chain link mesh support systems; namely:

- CODELCO chain link mesh, 4mm wire diameter.
- CODELCO chain link mesh, 5mm wire diameter.
- TECCO G80 chain link mesh, 4mm wire diameter.

Note that the mesh designated “CODELCO” was supplied from Chile. The TECCO G80 chain link mesh is a proprietary product of Geobrugg, a company with headquarters in Switzerland. Some malfunctions during the second test program resulted in only four tests being reportable.

5.2 GROUTING OF SIMULATED BOREHOLES

The initial stage was the grouting of the simulated boreholes. Centralisers fixed to the threaded bar (Figure 46) were used to locate the rock bolt inside a steel pipe prior to the grouting process. Toe grout connections were fixed on to the pipe ends with duct tape as shown in Figure 47.

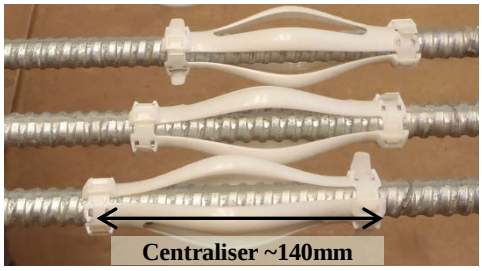

Figure 46: Fixing of centralisers.

Figure 47: The toe grout connection.

All the pipes were placed on two wooden blocks and fixed vertically near the collar end as shown in Figure 48. The 0.4 water/cement ratio grout was pumped from the collars to the tops of the pipes. After the pipes were completely filled with grout, the ends of the plastic pipes were blocked to prevent leaking of grout. Grouted simulated borehole samples were cured for 28 days inside the WASM Dynamic Test laboratory prior to testing.

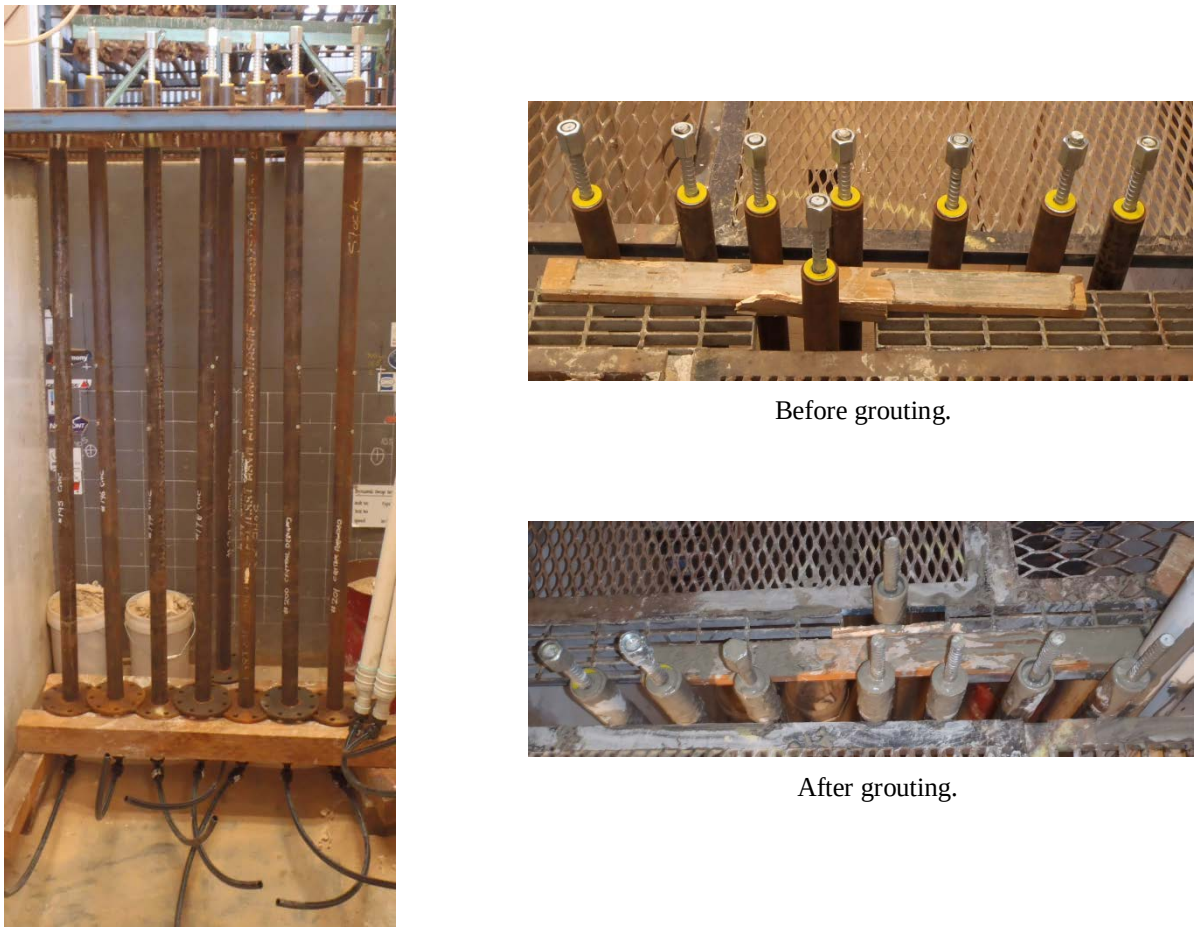

Before grouting.

After grouting.

Figure 48: The grouting process.

5.3 Attachment of Mesh on to the Mesh Frame

The mesh frame was lifted and placed on four stands as shown in Figure 49. The mesh was fixed onto the shackles followed by the eye bolts on the frame. Targets with black squares in a white background were positioned securely to the mesh to measure the initial mesh deflection and also to track the mesh deformation with the high speed video camera.

The number of restraints for each side depended on the type of mesh (chain link mesh or weld mesh) and the size of a mesh loop (typically a diamond shape for chain link mesh and square or rectangle for weld mesh).

Figure 49 : Fixing of the mesh on to the frame.

5.4 Placement of the Simulated Borehole onto the Drop Beam and to the Loading Mass

Initially, the drop beam was rested on the buffers as shown in Figure 50. The load mass was centralised and rested on two blue steel beams which were placed across the drop pit. The simulated borehole (the steel pipe configuration) was lifted with the use of the crane and positioned through the drop beam and the mass. Then the pipe was bolted onto the beam above the anchor load cells. A load transfer ring was welded onto the pipe.

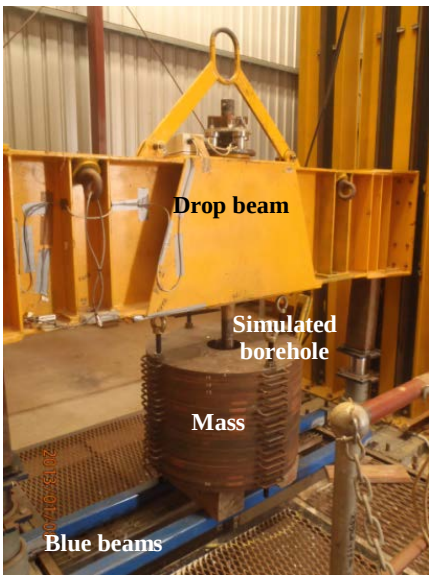

Figure 50: Setting up the reinforcement system.

5.5 Attachment of Mesh Frame on to the Drop Beam

Four ropes were attached to the system as shown in Figure 51. Then the beam was lifted and placed on top of the mesh and lowered onto the mesh frame. The collar pipe was positioned through the centralized curved plate while the mesh frame threads were positioned through the drop beam holes. These two steps were performed simultaneously.

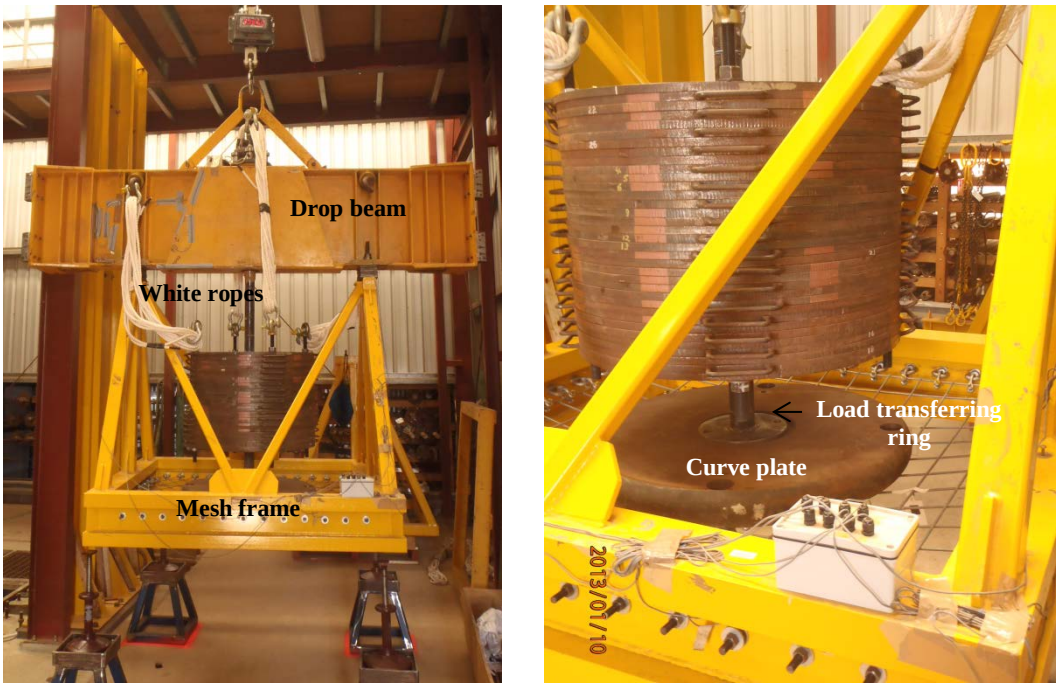

Figure 51: Fixing of the beam on to the mesh frame.

The curved plate was fixed on to the load mass and to the mesh. The frame threads were fixed on to the drop beam with the load cells. Then the total system (drop beam + mesh frame + reinforcement system + mass) was lifted with the crane and positioned at the drop pit. The system was lowered in the drop pit (Figure 52) until the complete system rested on the buffers.

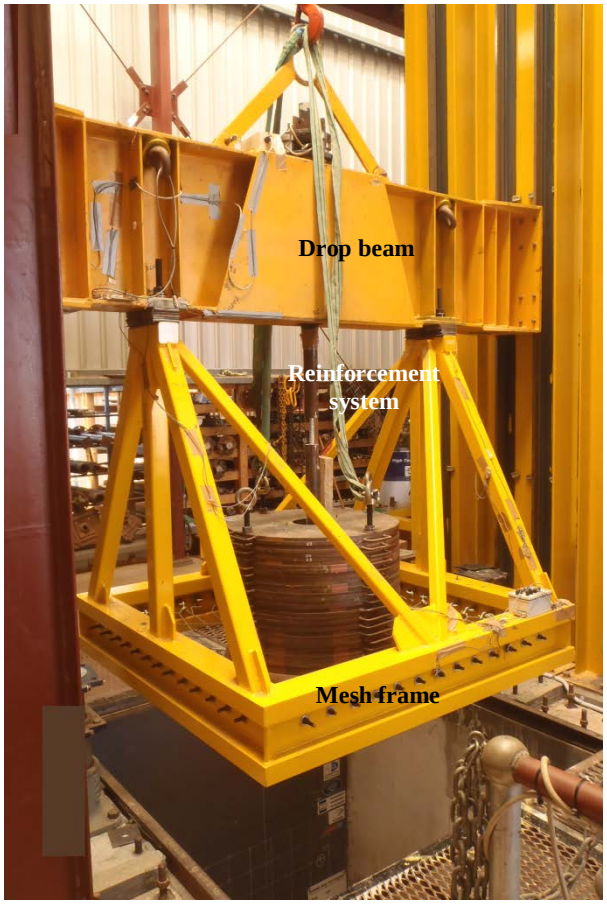

Figure 52: Lowering down the system onto the buffers.

5.6 Installation of Surface Hardware and the Collar Load Cell

The collar load cell was installed between the star plate and the nut as shown in Figure 53. The nut was rotated with a torque wrench and the bar tensioned to approximately 20kN. A dome washer was used between a flat washer and the star plate.

After installing the surface hardware, the nut was covered with black tape and white crosses were drawn on it as shown in Figure 53. Those targets were used to track the collar movement of the reinforcement in video data analysis process.

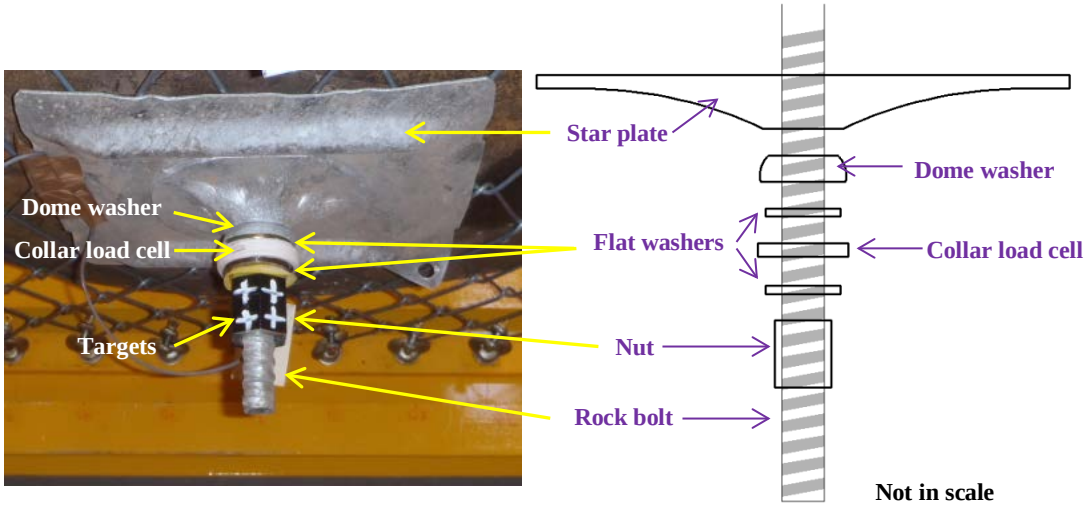

Figure 53: Collar load cell configuration.

5.7 INSTALLATION OF THE INSTRUMENTATION

The next step of the procedure was installation of the instrumentation to the test components. All the accelerometers were fixed onto the drop beam and to the loading mass as explained previously in Chapter 3.

A high speed video camera (fixed onto a tripod) was placed on the floor. The high speed video camera was adjusted to the correct aperture and zoomed to the centre plane of the pit with use of a calibrated board.

NI-SC2043SG board cables for the drop beam and the mesh frame were connected and checked for correct operation using the data acquisition software. The laser triggering process was checked manually by blocking the laser beam. In the final stage, the helicopter hook (release hook) was attached to the crane and the system raised to the required height above the impact surface on the buffer pistons.

5.8 PRE-TEST CHECKS AND MEASUREMENTS

A number of checks and important measurements needed to be made prior to and after the test. The checks included:

- Rubber pads were placed on both of the buffers to reduce the noise by preventing the metal to metal contact.
- Wires of accelerometers and load cells were taped to prevent damaging during the drop.
- Checking of the laser triggering process prior to the test.

The measurements included:

- Distance from the camera to the pit wall. This measurement was used in video data analysis software to calibrate the camera.
- Inclination of the mass before and after the test towards North-South and East-West.
- Exposed thread length: The extra thread length from the pipe to the nut.
- Separation of the simulated discontinuity before and after the test to calculate the total deformation of the reinforcement.
- Bar diameter of the reinforcement (includes the diameter at flat surface and diameter at the tooth). Post measurements of bar diameter were taken at the simulated discontinuity.
- Mesh deflection was measured as shown in Figure 54.

  Eye shackles were selected as the zero level and the distance from the metal frame to the eye shackle was taken as the zero measurement. The distances between the targets and the white metal frame were measured before and after the test.

  Post-test measurements were not defined for the tests where the mesh ruptured. Measurements of the test ID 195 are illustrated in Figure 55.

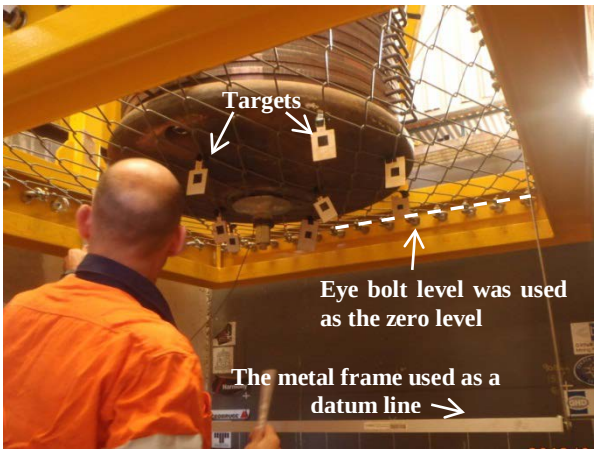

Figure 54: Pre mesh deflection measurements.

WASM Dynamic Testing – Reinforcement System

Bolt Number 195 Drop Number 1

Mesh measurements

Position	Pre -test X	Pre -test Y	Pre -test Z	Post - Test X	Post - Test Y	Post - Test Z	Comments
1-1	900	895	596	900	900	525	
1-2	610	895	570	600	900	493	
1-3	305	895	594	300	900	525	
2-1	1060	620	608	1055	620	548	
2-2	850	620	570	850	620	484	
2-3	350	620	566	340	620	482	
2-4	150	620	606	150	620	557	
3-1	900	350	595	900	350	522	
3-2	610	350	571	600	350	486	
3-3	300	350	585	305	350	524	

1st Row

2nd Row

3rd Row

Pre measurements of the mesh deflection

Post measurements of the mesh deflection

Zero Round 647mm → The distance between the zero level and the metal frame

Measurement of Rounded Bolt Deflection with Mesh on Mesh 91mm

Figure 55: Mesh measurements data sheet.

Mesh deformation measurements prior to the test and after the test are shown in Figure 56.

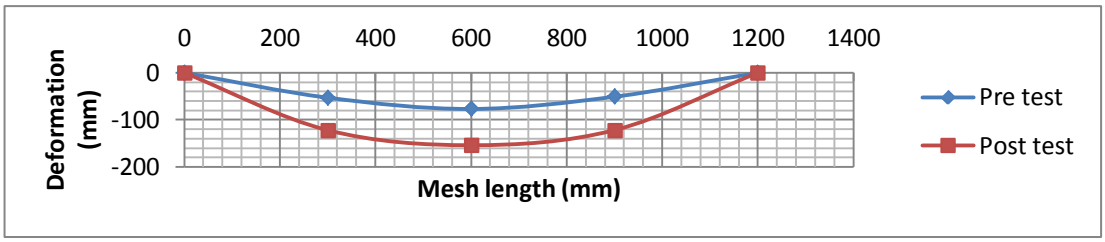

(a) Mesh deformation of first raw (Y = 900).

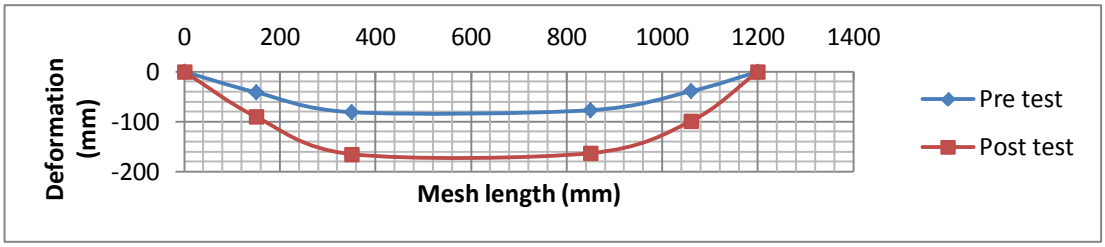

(b) Mesh deformation of second raw (Y = 620).

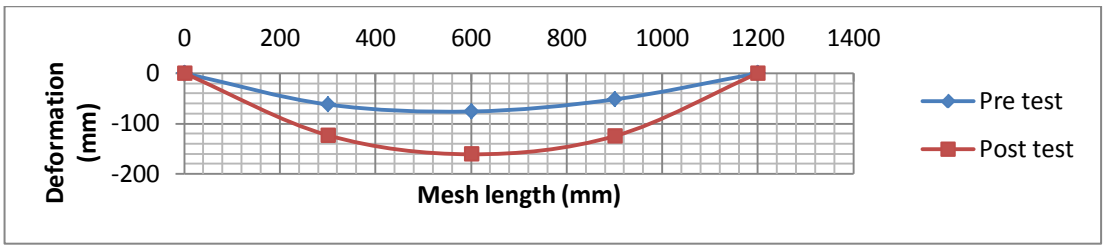

(c) Mesh deformation of third raw (Y = 350).

Figure 56: Mesh deformation details of test #195.

CHAPTER 6

TYPICAL DATA ANALYSIS PROCEDURE

Data analysis was critical to the investigations and needed to be done systematically and carefully to get the final results. The analysis associated with filtering and processing of the data from the accelerometers, load cells and potentiometers will be presented in detail using Test ID 195 as an example. All other tests used the same basic analysis methodology. Analysis software such as ProAnalyst, Midas and in-house software were used in the data analyses. A number of different filters are provided within the in-house software. The most used of the filters are the Fast Fourier Transform (FFT) for frequency analysis and the Butterworth filter for "smoothing" of data.

The analysis methodology consists of three stages;

- Reviewing and selecting data for analysis.
- Filtering of the selected data.
- Analysis of the filtered data over the required time interval.

Basically the analysis process can be divided into two sections: the video data analysis (calculated displacement tracked from the high speed camera) and the sensor data analysis (data from accelerometers, load cells and linear potentiometers).

6.1 VIDEO DATA ANALYSIS

The video data analysis comprises of several stages (Figure 57) and uses the ProAnalyst and the data smoothing software.

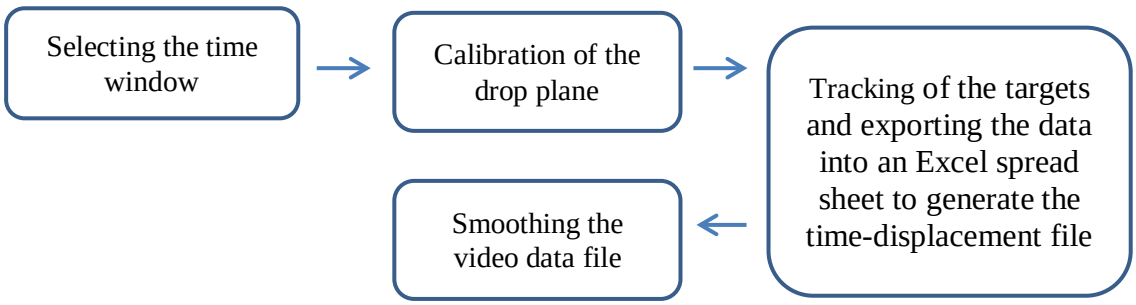

Figure 57: Video analysis process.

The main purpose of the video analysis was to track the path (movement) of the loading mass and the collar end of the reinforcement during the test. Selected points of the test specimen were tracked using the video recording software.

6.1.1 Selection of Time Window

The initial stage of the video data analysis was to window the raw data acquired from the high speed video camera. The raw data file was opened in ProAnalyst software and the time window was chosen as shown in Figure 58.

The noise at the starting point was the releasing of helicopter hook as shown in a yellow circle in Figure 58. The time window for further processing was selected to avoid the front end noise and the back end noise as shown in Figure 58.

The data after the impact is the important part of the analysis and should lie within the selected data window. As the camera and the sensors were synchronized, the time window is common for the both video and sensor data.

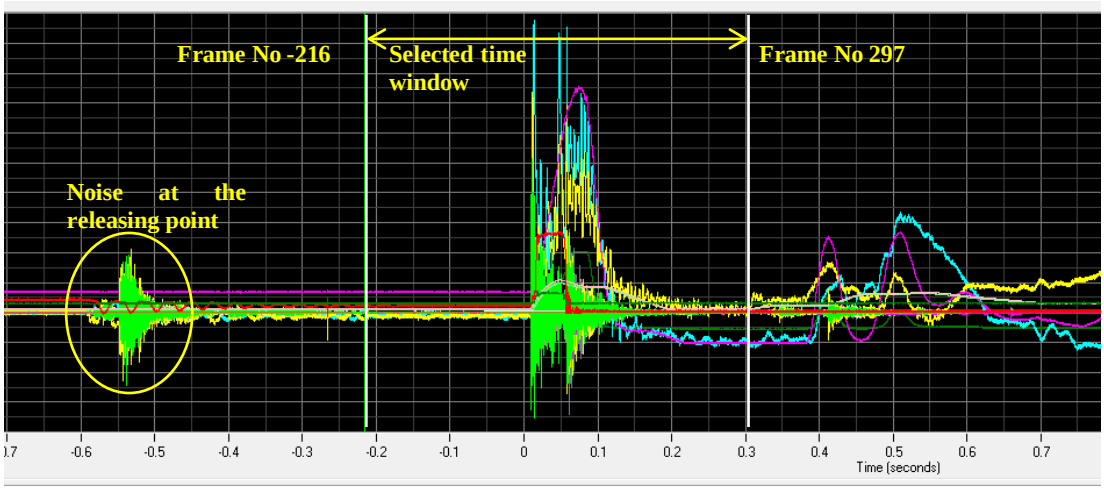

Figure 58: Selecting the time window (windowing).

Figure 59 illustrates the zoomed data of the selected time window of Figure 58. Only the windowed data was subjected to further processing using the in-house software.

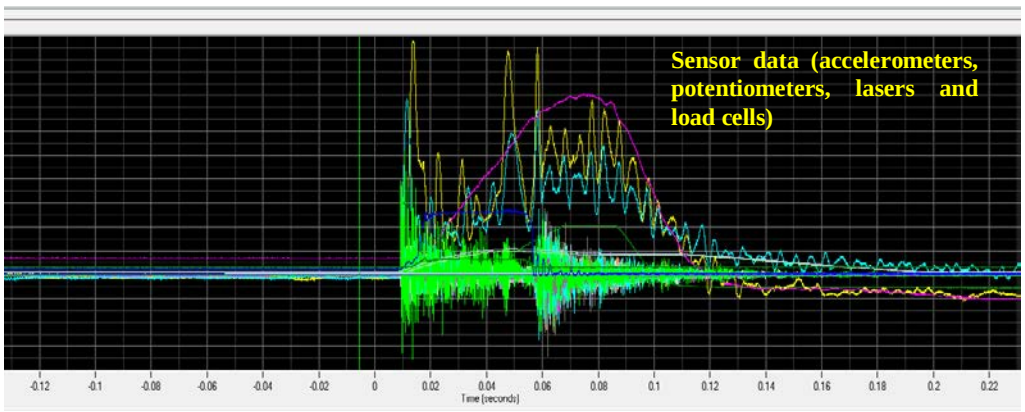

Figure 59: Zooming at windowed data.

6.1.2 Calibration of the Drop Plane Scale

The drop plane was calibrated with respect to the four points on the drop pit wall as shown in Figure 60. The calibration is required to convert video file pixels into millimetre scale.

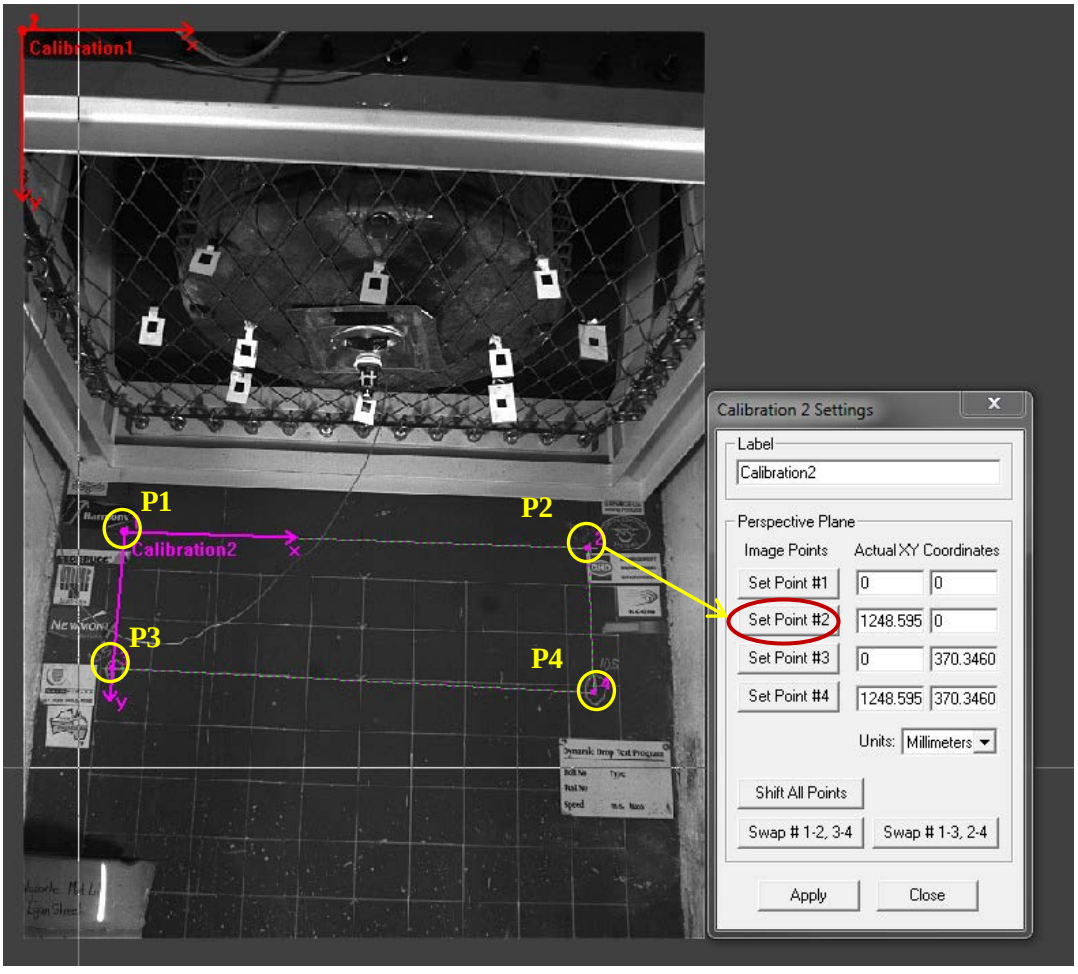

Figure 60: Calibration for the drop plane.

According to the horizontal distance between the camera lens and the pit wall, the actual coordinates for the four points were calculated using an Excel spread sheet.

6.1.3 Video Tracking of the Targets and Generation of Time-Displacement File

The nut (which is used to tighten the surface hardware) was covered with black tape and crosses were marked in white to use as a target to track the loading mass and the collar of the reinforcement. Targets with black squares in white backgrounds were tracked only in sample #195 as it was the only sample where the support system survived. The data were exported into an Excel spread sheet after the software tracked the targets up to the end time of the data window.

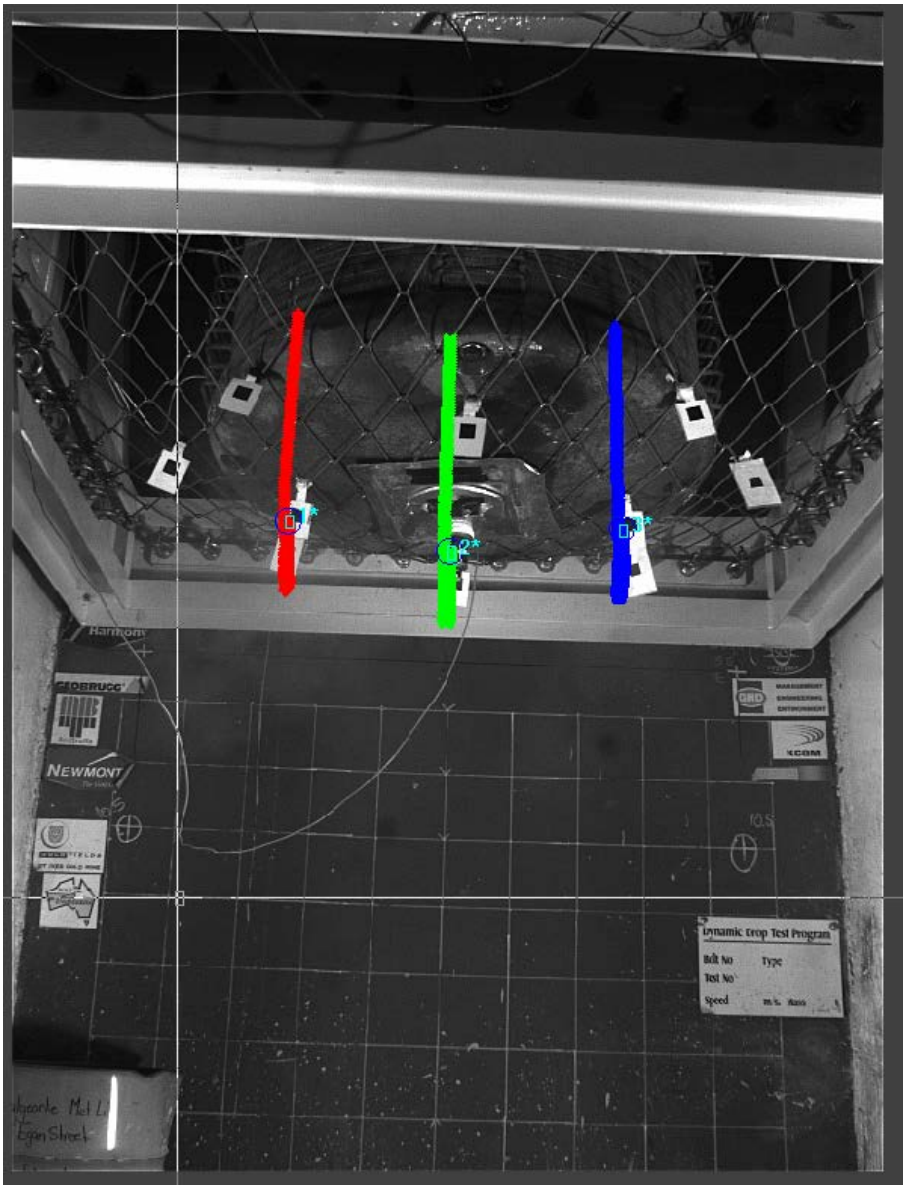

Figure 61: Progressive ProAnalyst tracks of the targets.

6.1.4 Data Pre-Processing Utility

A data pre-processing utility shown in Figure 62 was developed in-house. The utility is used for several purposes; namely:

- Definition of the test configuration file.
- Details of the instrumentation channels and calibration coefficients.
- Scaling of the native data saved from the data acquisition system.
- Creation of time-displacement data from the video tracking software file.

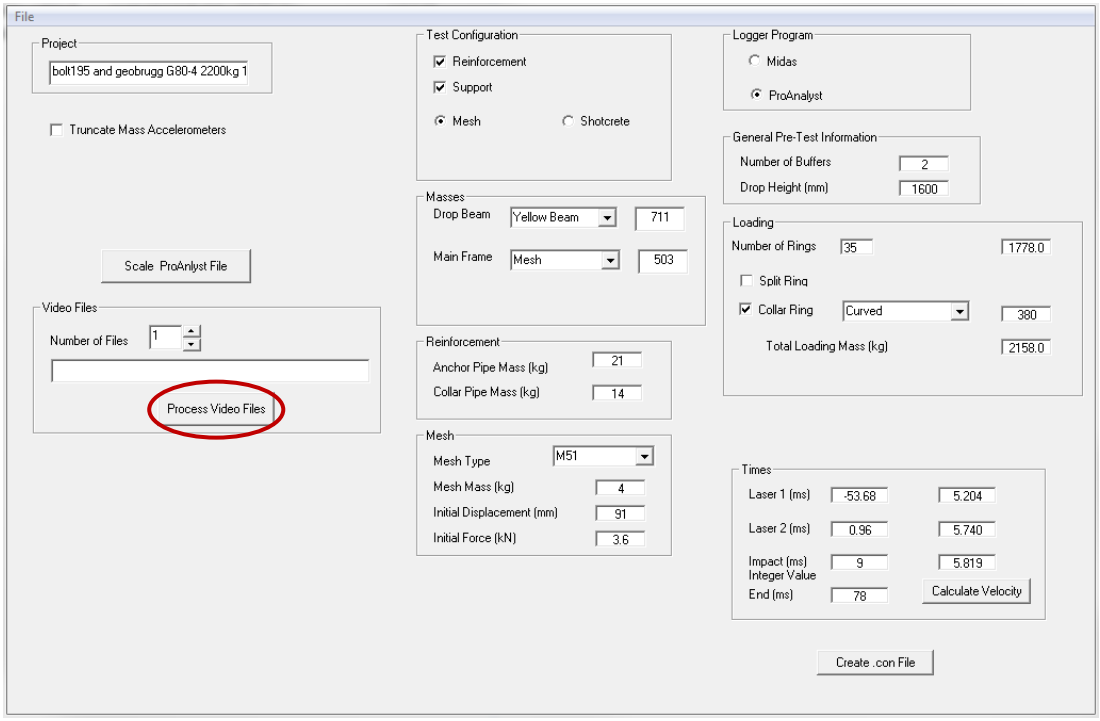

Figure 62: The interface of in-house pre-processing utility.

The video data tracking data in the Excel spread sheet is imported to the in-house software to generate the time-displacement data file.

6.1.5 Video Track Smoothing

The raw video data file (Figure 63) was subjected to filtering to acquire a smooth curve as shown in Figure 64. The in-house software was used to smooth the raw video data file. Basically the software averages five consecutive data points to create a smooth curve.

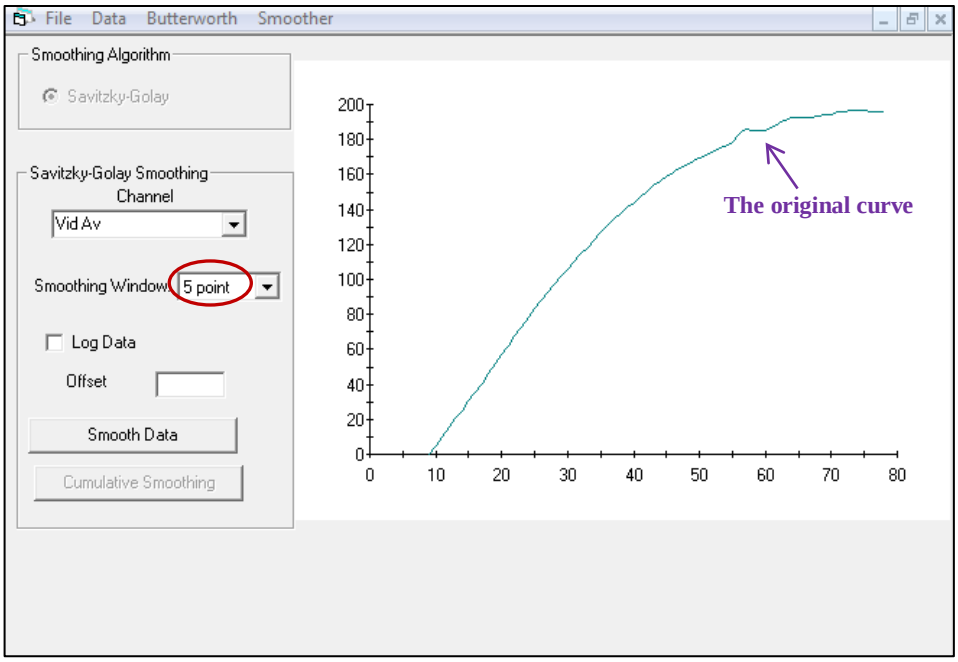

Figure 63: Raw video data response.

The smoothing process was repeated several times by clicking the "Cumulative Smoothing" button until an acceptable curve was obtain. The same process was followed for all the other video tracks. The smoothed .vid file was saved for further reference.

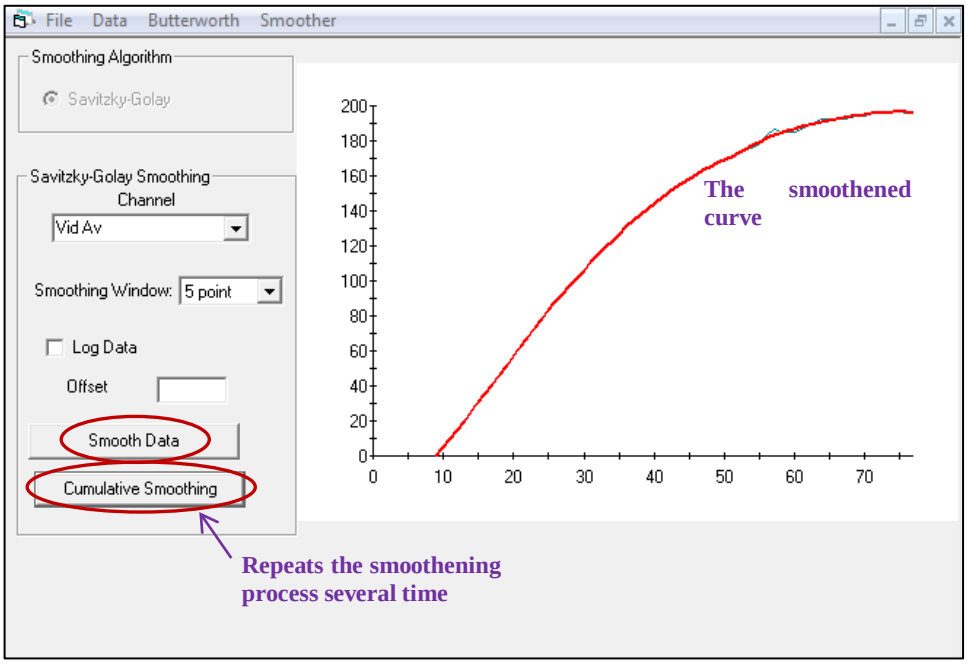

Figure 64: Smoothed video data file.

6.2 SENSOR DATA ANALYSIS

In this section, analyses of raw data including accelerometer data, potentiometer data and load cell data are discussed in detail. In-house developed software was used for sensor data analysis and the steps are illustrated in Figure 65.

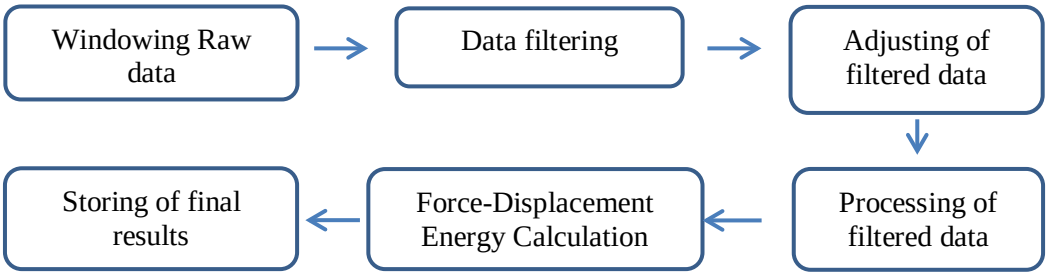

Figure 65: Sensor data analysis process.

Initially the windowed data was subjected to filtering. The filtered data was then adjusted to a same starting time prior to further processing. The smoothed video file was imported to the software and processed together with adjusted sensor data. The processing determined the accelerations, velocities and displacements for all components involved in a test.

The acceptable sensor data for the final stage of processing was selected at the calculation step to acquire the final force-displacement response curves from which energy dissipation could be determined for the reinforcement and mesh. The results from the analysis were stored for additional processing using Windows Excel.

6.2.1 Time Window for Raw Data

The initial step of sensor data processing was defining a time window for the raw data. Windowing of raw data is used mainly for eliminating unwanted data at the beginning of the test and end of the test prior to data processing as described in the section 6.1.1.

From the experience gained through data processing, it was identified that the end of a stable test (a test in which the reinforcement survives) is a point after the loading velocity is zero and for a rupture test a (test in which the reinforcement ruptures), the end of the test is defined as the reinforcement rupture point.

A screen capture of raw data for sample #195 is shown in Figure 66. The loading started with an impact on buffers and the reinforcement rupture point is marked in red.

The next step was filtering the windowed sensor data using the FFT filter and the Butterworth filters.

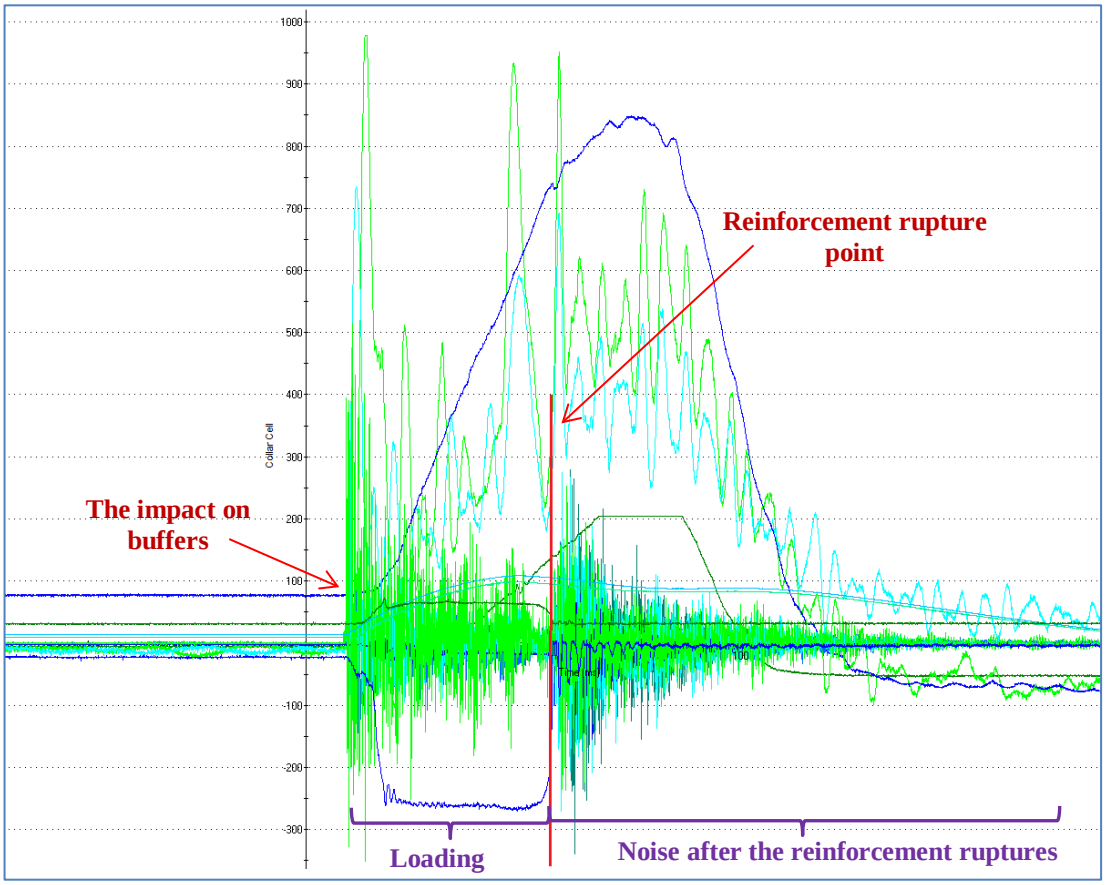

Figure 66: Raw data recorded for sample #195.

6.2.2 Filtering the Windowed Data

Normally the raw data is disturbed by mechanical and electrical noise due to the vibration and metal to metal contact during the impact. The filtering of the raw data is essential to interpret the results in a meaningful way. Different types of filtering techniques such as the Fast Fourier Transform filter (FFT) and Butterworth filter were implemented for analysing the raw data.

6.2.2.1 Fast Fourier Transform (FFT) Filtering

The FFT filtering is one of the commonly used filters and was primarily used to filter accelerometer signals. Initially, a time window of 2^n samples (where n is an integer) was selected For FFT filtering.

A frequency-signal strength analysis was performed on the raw data. A cut-off frequency was then selected to eliminate the higher frequencies prior to performing the Inverse analysis to create the filtered reponse. The data window and the frequency analysis for the mass accelerometer (ac02z) of sample #195 are shown in Figure 67 and Figure 68, respectively.

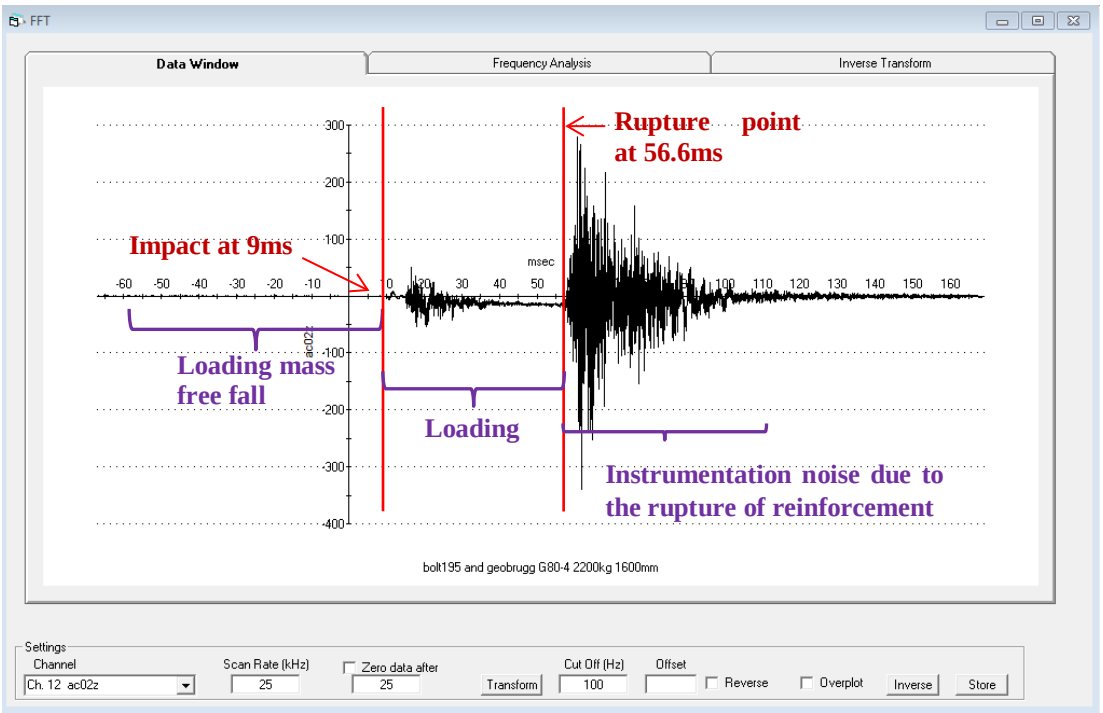

Figure 67: Windowed raw data of the loading mass accelerometer of sample #195.

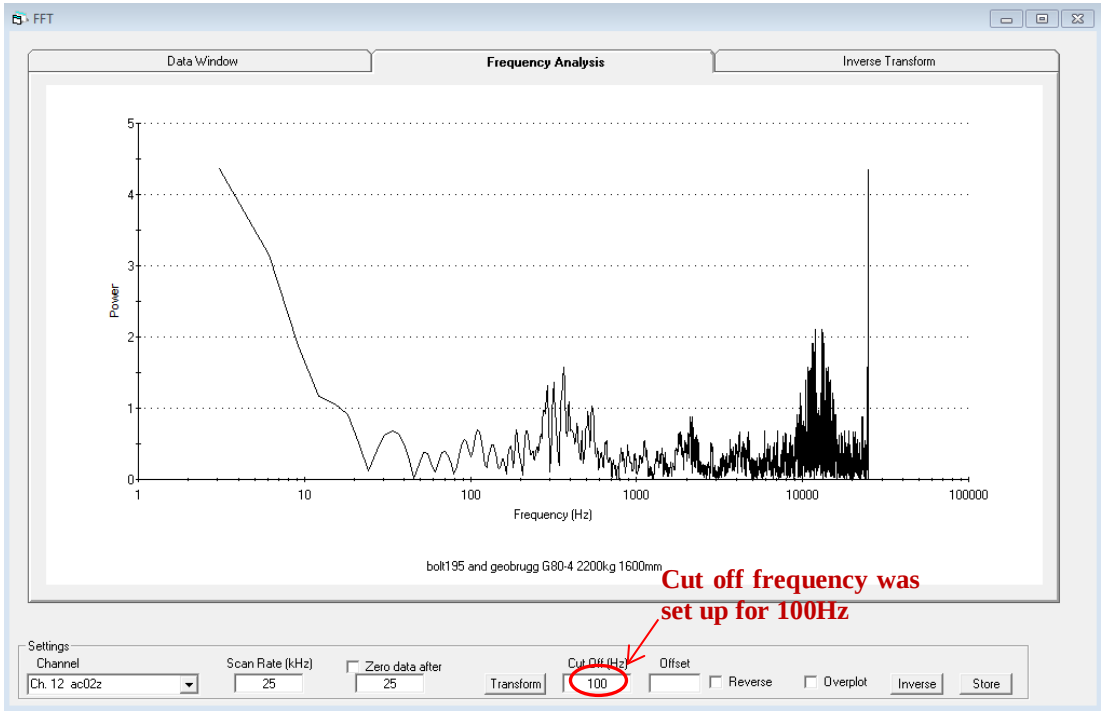

Figure 68: Frequency analysis for the loading mass accelerometer of sample #195.

A cut off frequency of 100Hz was selected and used to create the inverse transform shown in Figure 69.

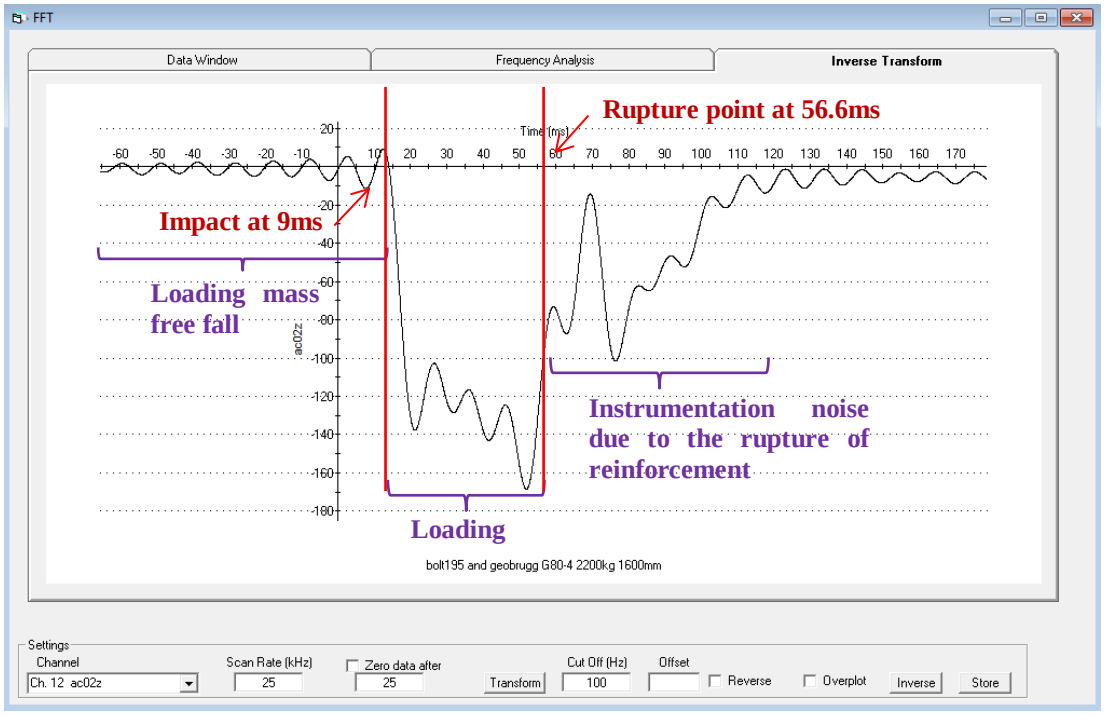

Figure 69: 100Hz filter for loading mass accelerometer of sample #195.

For sample #195, the impact time (9ms) was selected as the start point for the test. The reinforcement rupture point (end of the test) was noted as 47.6ms. The filtered beam-accelerometer data and the mass accelerometer data for sample #195 are shown in Figure 70.

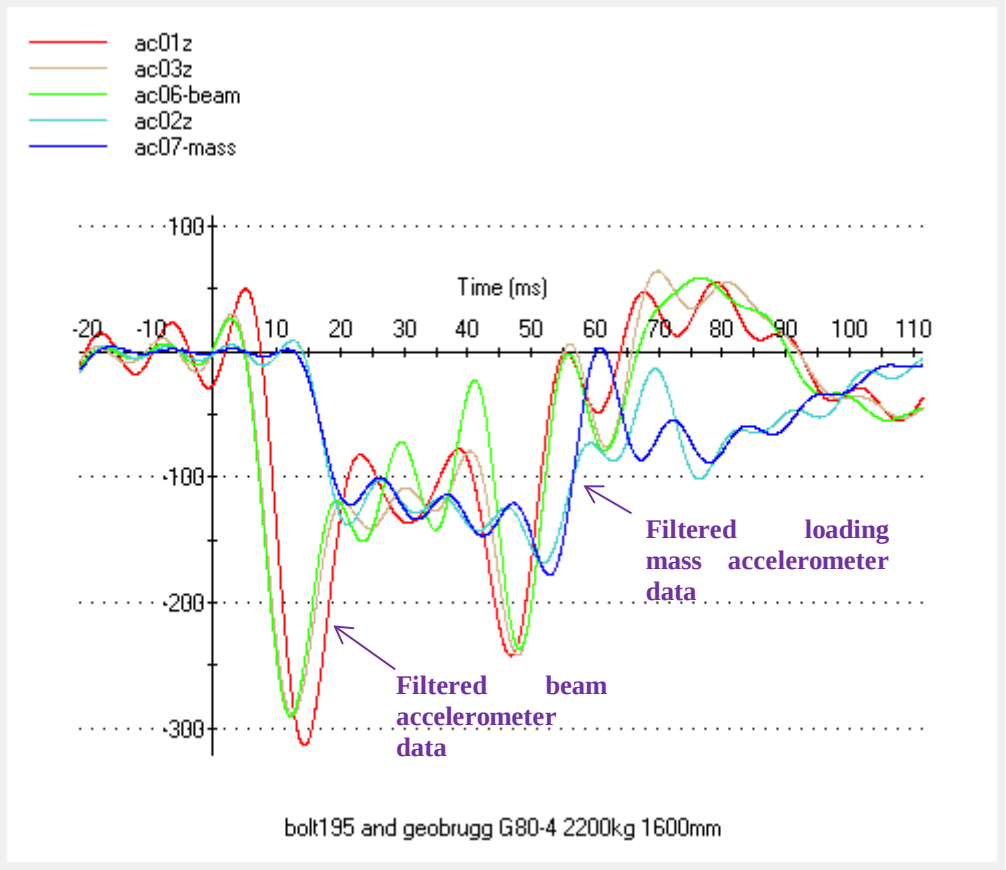

Figure 70: Filtered accelerometer data of sample #195.

6.2.2.2 Butterworth Filtering

The Butterworth filter was used to filter the potentiometer data and the load cells' data. Figure 71 refers to the left buffer potentiometer response and Figure 72 refers to the filtered potentiometer data after use of the Butterworth filter. A 10% cut-off value was used for potentiometer data filtering. The cut-off percentage to begin the attenuation was determined from the equation:

$$\text{Cut-off value} = \%\ \text{value} * \tfrac{1}{2} * \text{number of samples in time window} \qquad \text{Eq 10}$$

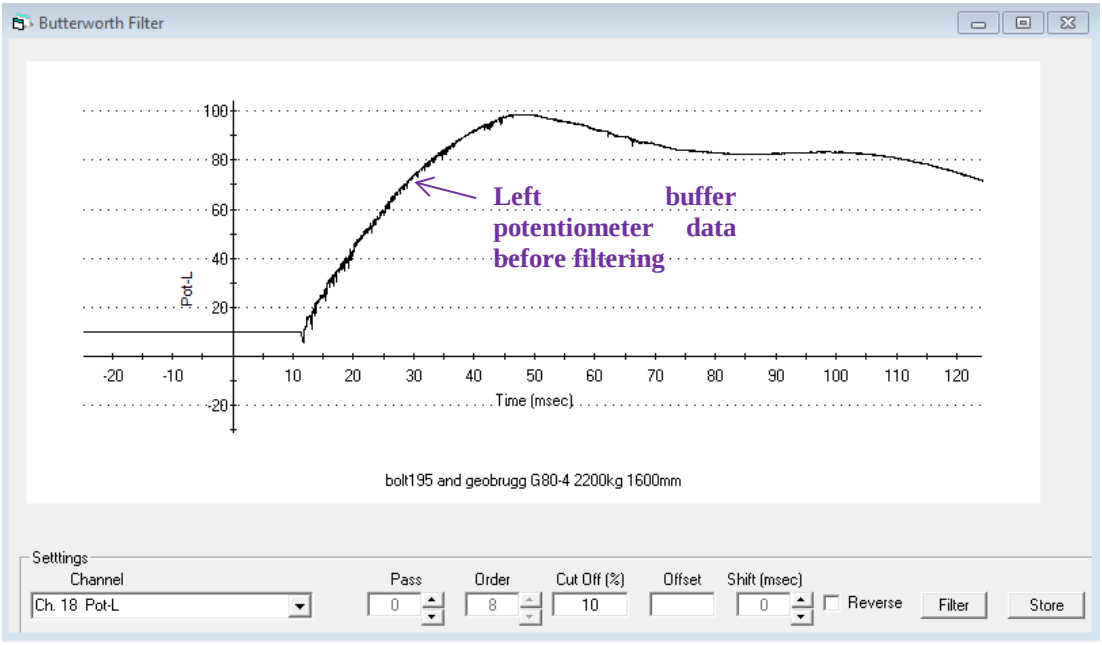

Figure 71: The left buffer potentiometer data for the sample #195.

An offset of -9.9 in Y-axis was applied during the filtering process to set the initial displacement to zero.

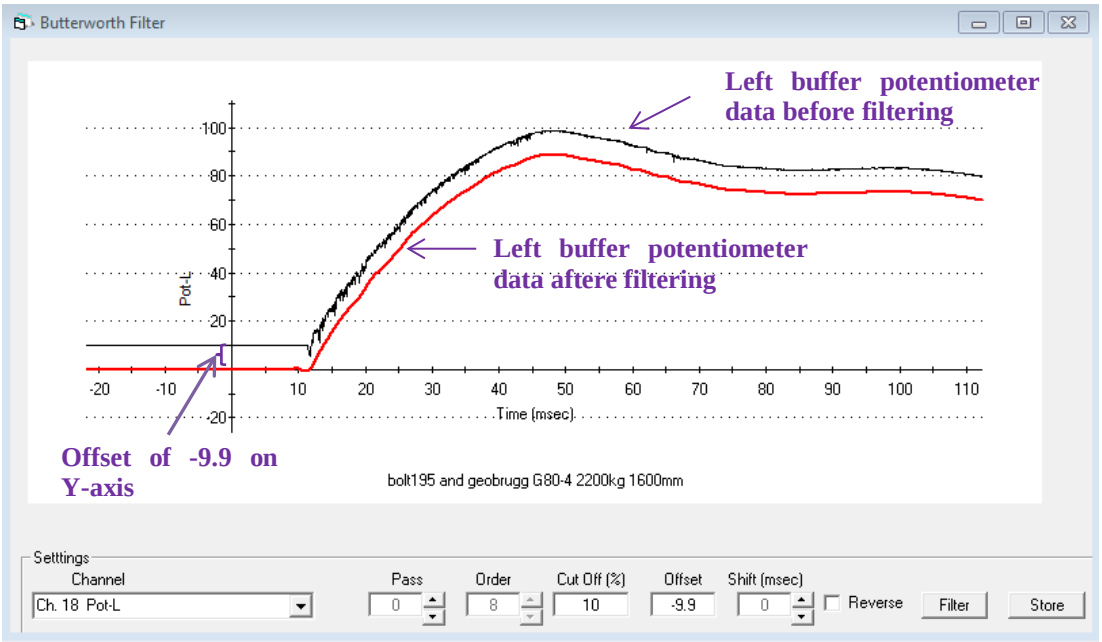

Figure 72: Filtered left buffer potentiometer data using Butterworth filter.

The filtered potentiometer data and load cell data are shown in Figure 73.

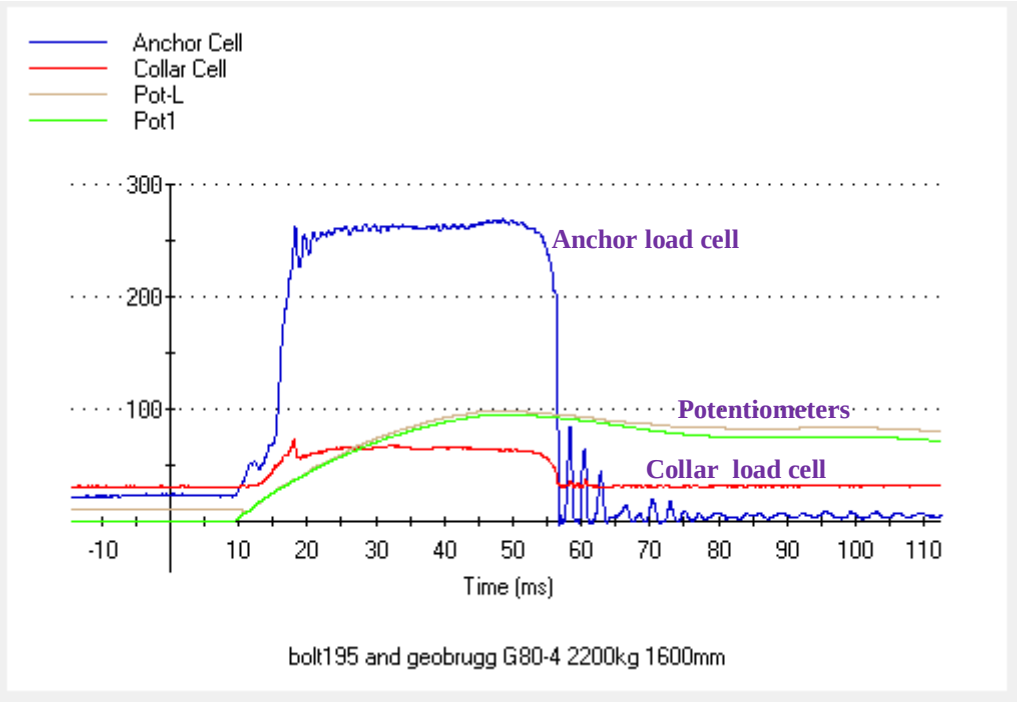

Figure 73: Potentiometers and load cells filtered data with use of the Butterworth filter.

6.2.3 Adjusting the Filtered Data

The next stage of processing was adjusting the filtered sensor data in to a common starting time. Phase shifts occurred for the processed waveforms due to the application of the FFT filter. All the filtered sensor data for sample #195 are shown in Figure 74.

A screen capture of the in-house software which is used to adjust the data is shown in Figure 75. The adjustments were done simply by changing the start time column highlighted in red. The sensor data starting time was fixed to the video start time (impact) which was 9ms for this test.

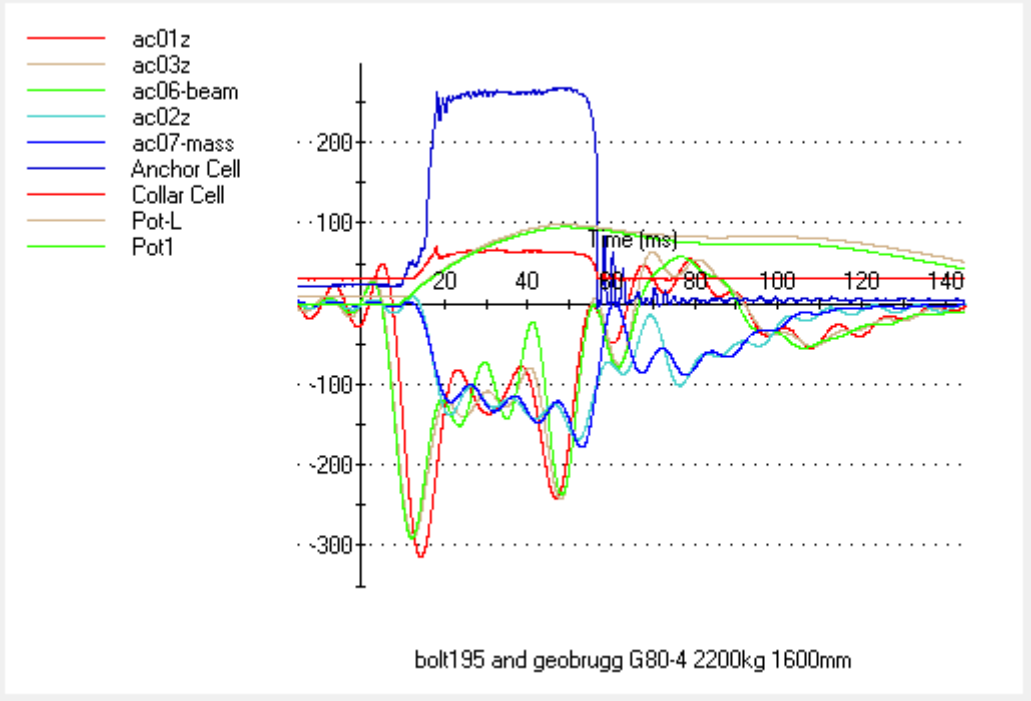

Figure 74: Filtered sensor data before time synchronization.

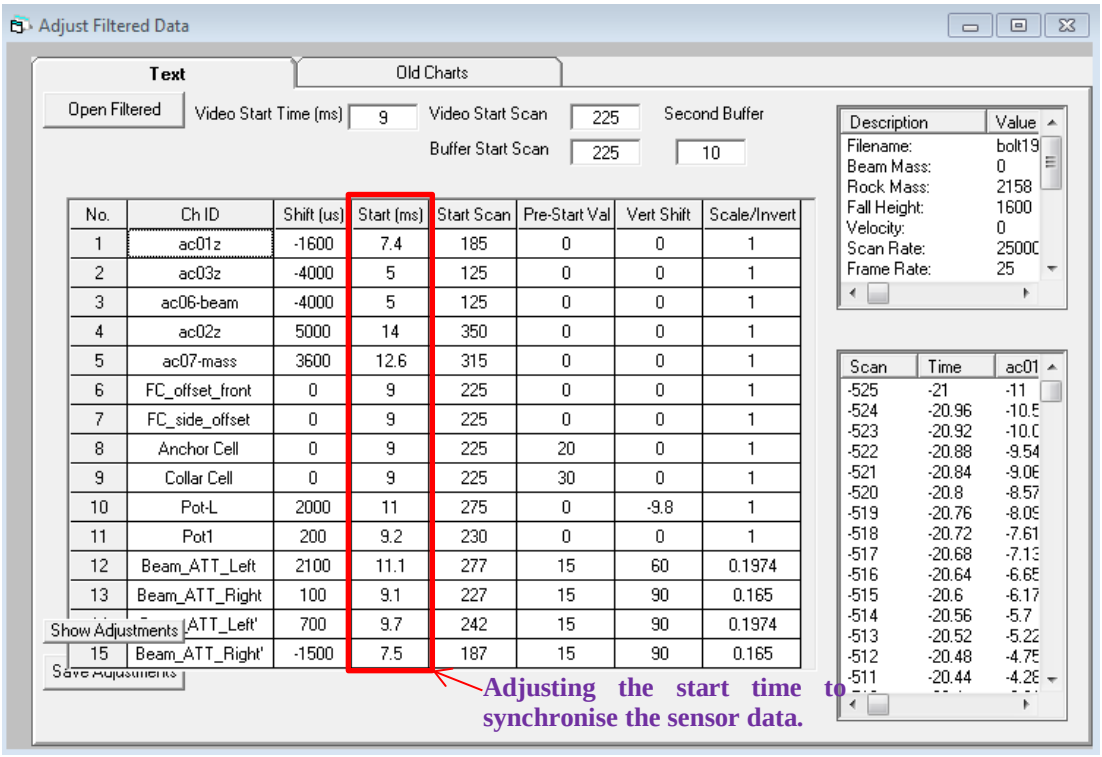

Figure 75: Adjusting of filtered data using the in-house software.

After adjusting the start time, the software was used to generate a file for final processing. The adjusted sensor data shown in Figure 76.

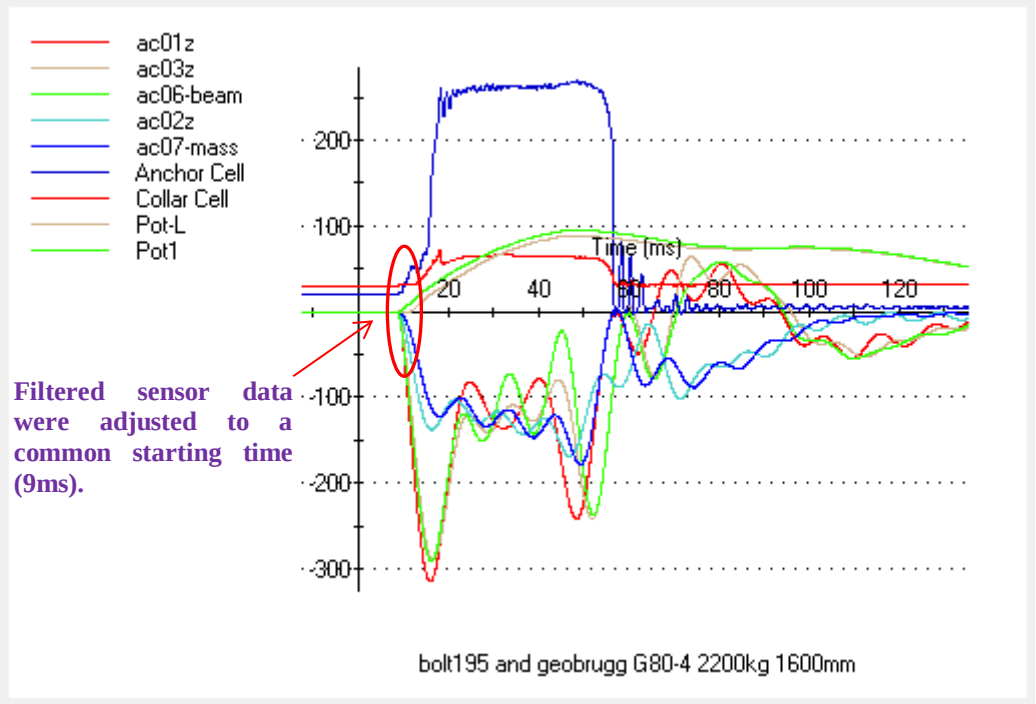

Figure 76: Adjusted sensor data file.

6.2.4 Processing the Adjusted Data

In the processing stage, the adjusted data and the video data were imported to the in-house software. Then both set of data were processed to generate the final graphs.

6.2.4.1 Data Processing

The objective of data processing is firstly to determine the variations with time of accelerations, velocities and displacements for all the components in a test. The equations given previously in Section 4.2.9 were then used to calculate forces based on the mass of the component and the corresponding accelerations/declerations. The masses and their velocities were used to calculate the kinetic energies of the components. In addition, the loss of potential energy during the test after impact was calculated.

The force time responses for sample #195 are represented in below graphs. The reinforcement system ruptured at 47.6ms after impact. Following rupture of the bolt, mesh force increased and the mass was brought to rest.

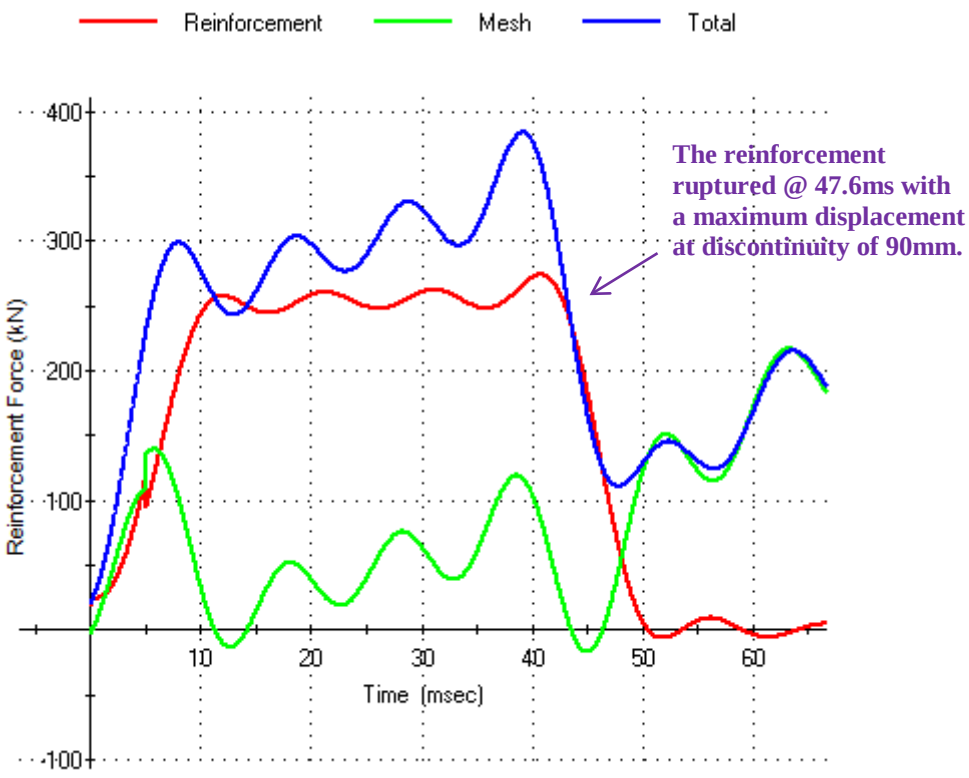

Figure 77: Support Scheme Force – Time response of sample #195.

The threaded bar was ruptured with a maximum displacement at discontinuity of 90mm while the chain link mesh survived with a maximum displacement of 115mm.

Secondly, the force-displacement responses for the reinforcement and mesh were defined and the energy dissipation calculated.

6.2.4.2 Energy Balance

The energy balance is defined as the sum of dissipated energy (the sum of energy dissipated by the reinforcement system, support system, buffers and residual kinetic energy of the loading mass, the beam and the mesh frame) divided by the input energy (kinetic energy of the entire system at impact plus the change in potential energy).

The energy balance for a test is calculated at the rupture point or when the relative velocity between the loading mass and the drop beam become zero. The end point for the test #195 was defined at 47.6ms, which was the reinforcement rupture point. Therefor the energy balance was determined at 47.6ms. The energy summary graph of sample #195 is shown in Figure 78. The red vertical line is the end of the test.

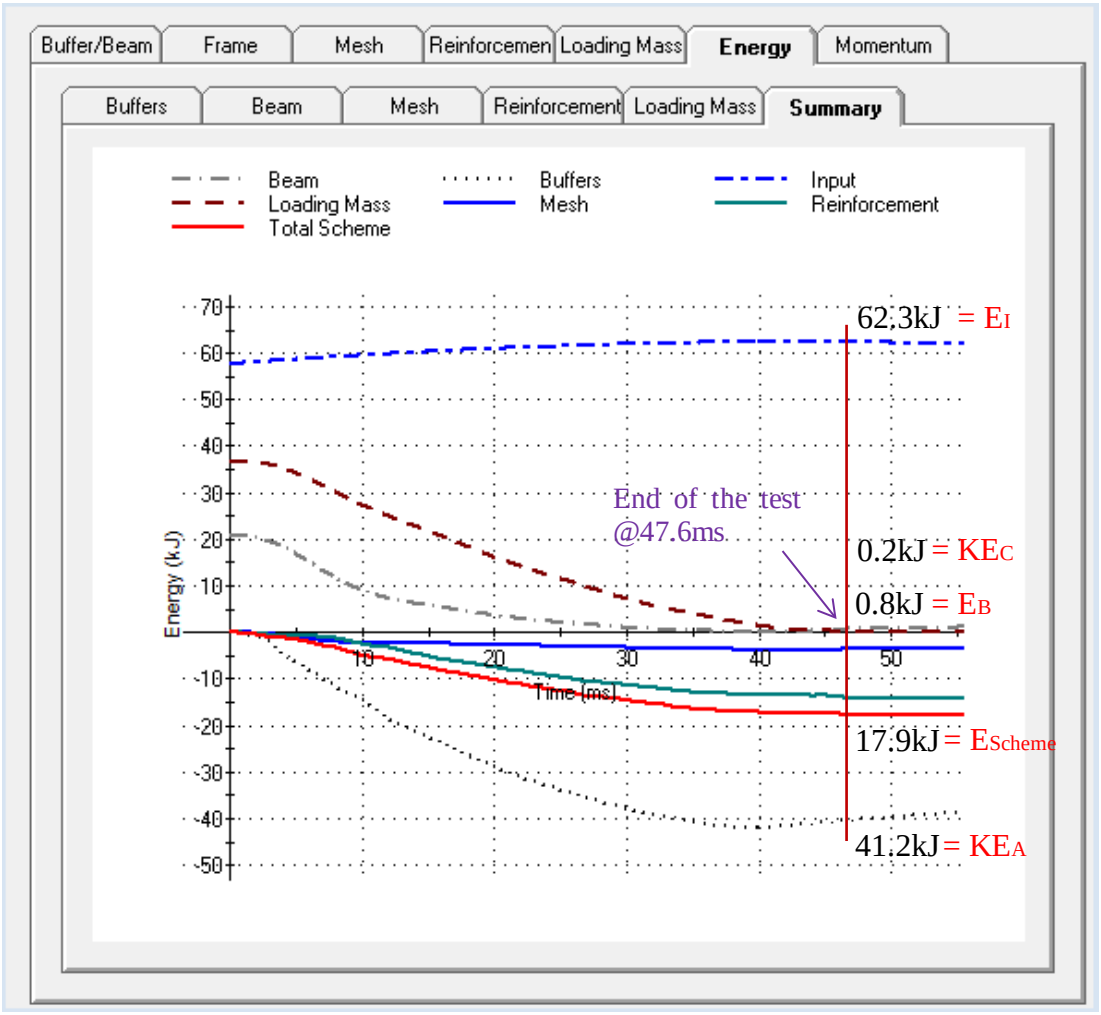

Figure 78: The energy summary graph of sample #195.

According to the above figure, the input energy (E_I) is approximately equal to the sum of the energies dissipated by the buffers (E_B), the reinforcement system (E_R), the support system (E_S) and, the residual kinetic energies of the loading mass (KE_C) and the beam (KE_A).

$$E_I \approx E_B + E_{Scheme} + KE_C + KE_A \quad \text{Eq 11}$$

$$E_{Scheme} = E_R + E_S \quad \text{Eq 12}$$

The energy balance of the above test is 96.5%.

6.3 Dissection Analysis.

Simulated boreholes were dissected after the test to inspect the grout and bar interface and fractures along the simulated bore hole. Sections of the "Collar" and the "Toe" of sample #195 are shown in Figure 79 and Figure 80, respectively.

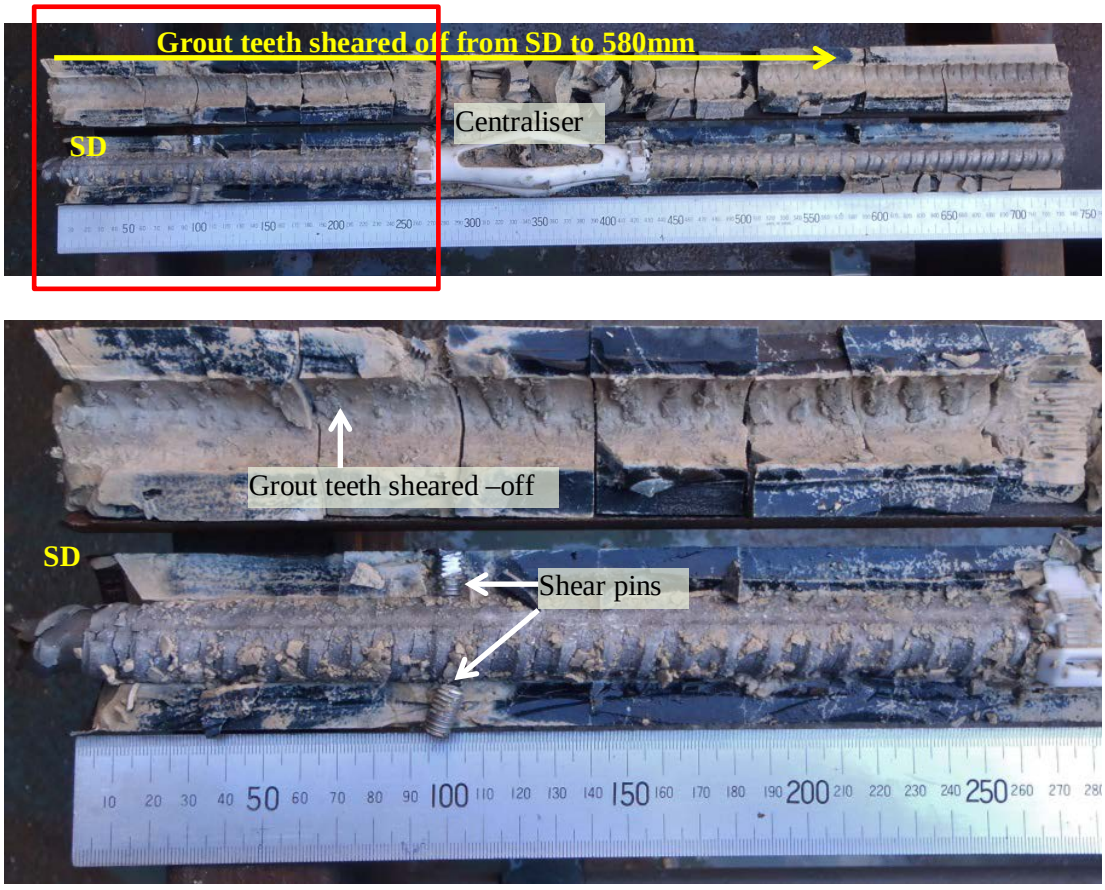

Figure 79: Collar section of sample #195.

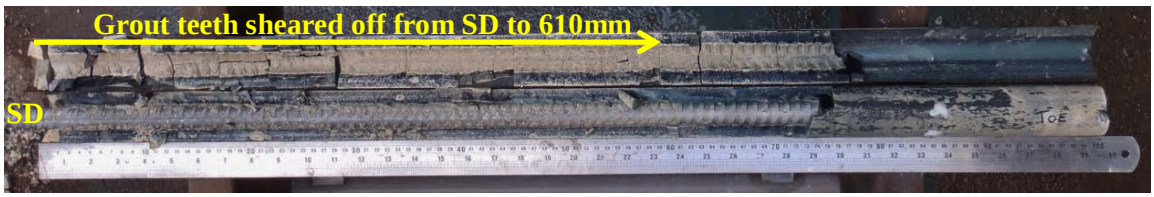

Figure 80: Toe section of sample #195.

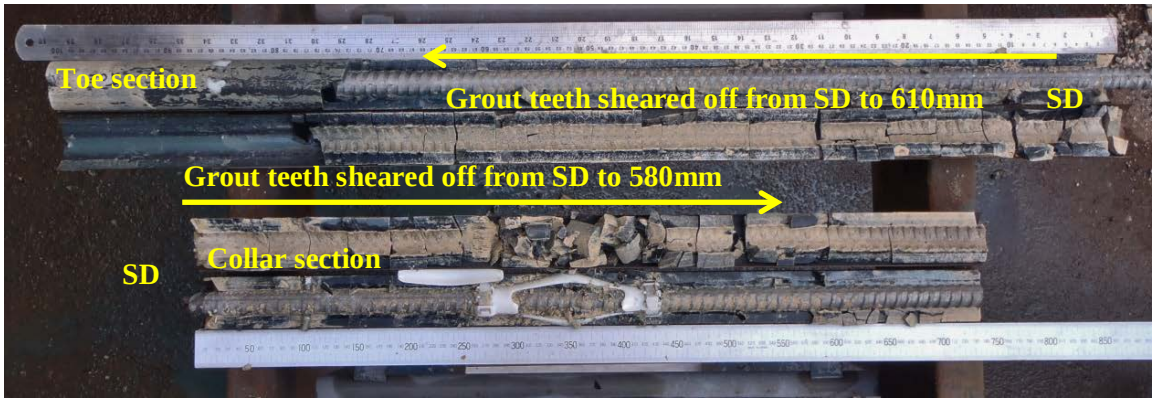

Figure 81: Both the toe and the collar sections.

Heavy galvanise flaking was identified at 360mm from the simulated discontinuity in collar section and at 180mm from the simulated discontinuity in toe section. Light galvanise flaking were visible from 180mm to 335mm from the simulated discontinuity. Grout porosity or air-bubbles were not visible in this sample.

Surface hardware did not fail in any of the bolt and mesh samples during the test. Pre- test and post-test pictures of the surface hardware of sample #197 is shown in Figure 82.

Figure 82: (L) Pre-test and (R) Post-test surface hardware of sample #197.

CHAPTER 7

PRESENTATION AND INTERPRETATION OF RESULTS

The results of two combined scheme test programs will be presented in this chapter. The individual contributions of reinforcement and support systems towards the overall performance of combined schemes are presented.

7.1 COMBINED TEST SPECIFICATIONS

Table 4 and Table 5, respectively, detail the sample specifications of the two combined scheme test programs.

Table 4: Sample specifications – Program 1

Test ID	Reinforcement System	Bar length (mm)	Bar diameter (mm)	Decoupled length (mm)	Support System	Wire diameter (mm)
195	Fully encapsulated threaded bar	2400	20	0	T/ECCO 80	4
196	Fully encapsulated threaded bar	2400	20	0	TECCO 80	4
197	Fully encapsulated threaded bar	2400	20	0	Weld mesh	5.6
198	Fully encapsulated threaded bar	2400	20	0	Weld mesh	5.6
199	Decoupled Posimix	2400	20	1000	Weld mesh	5.6
200	Decoupled Posimix	2400	20	1000	TECCO 80	4
201	Decoupled Posimix	2400	20	1000	TECCO 80	4
202	Decoupled Posimix	2400	20	1000	Weld mesh	5.6

Table 5: Sample specifications – Program 2

Test ID	Reinforcement System	Bar length (mm)	Bar diameter (mm)	Decoupled length (mm)	Support System	Wire diameter (mm)
231	DSI Posimix	3000	20	1400	CODELCO	4
232	DSI Posimix	3000	20	1400	CODELCO	4
233	DSI Posimix	3000	20	1400	CODELCO	5
234	DSI Posimix	3000	20	1400	CODELCO	5
235	DSI Posimix	3000	20	1400	GEOBRUGG	G80-4
236	DSI Posimix	3000	20	1400	GEOBRUGG	G80-4

Table 6 shows the test specifications of impact velocity, total loading mass and the nominal input energy for the two combined test programs.

Table 6: Test sample configurations

Test ID		Impact velocity (m/s)	Total loading mass (kg)	Initial input energy (kJ)
Program 1	195	5.8	2158	36.6
	196	6	1778	32
	197	5.4	1869	27
	198	5.8	2248	38.7
	199	6.8	2248	53.2
	200	6.1	2158	40.9
	201	6.8	1778	41.6
	202	5.8	2158	37
Program 2	231	7.2	2158	56
	234	7.1	2158	54.9
	235	7.3	2158	57.5
	236	7	2158	52.8

For Test Program 1, the input velocities varied from 5.4m/s to 6.8m/s while the respective energies varied from 27kJ to 53.2kJ. The second test program involved high impacts where the velocities varied from 7.0m/s to 7.3m/s with respective

energies ranging from 52.8 kJ to 57.5kJ. The results for Test ID.232 and 233 are not reported due to instrumentation failure.

The following sections summarise the pre-test setup and post-test observations of performance of the various combined schemes.

7.2 Overall Photos and Failure Mechanisms of Test Samples (Program 1)

7.2.1 Sample 195: Fully encapsulated threaded bar with 4mm chain link mesh

7.2.1.1 Pre-test photos of sample 195

Pre-test photos of sample 195 are shown in Figure 83.

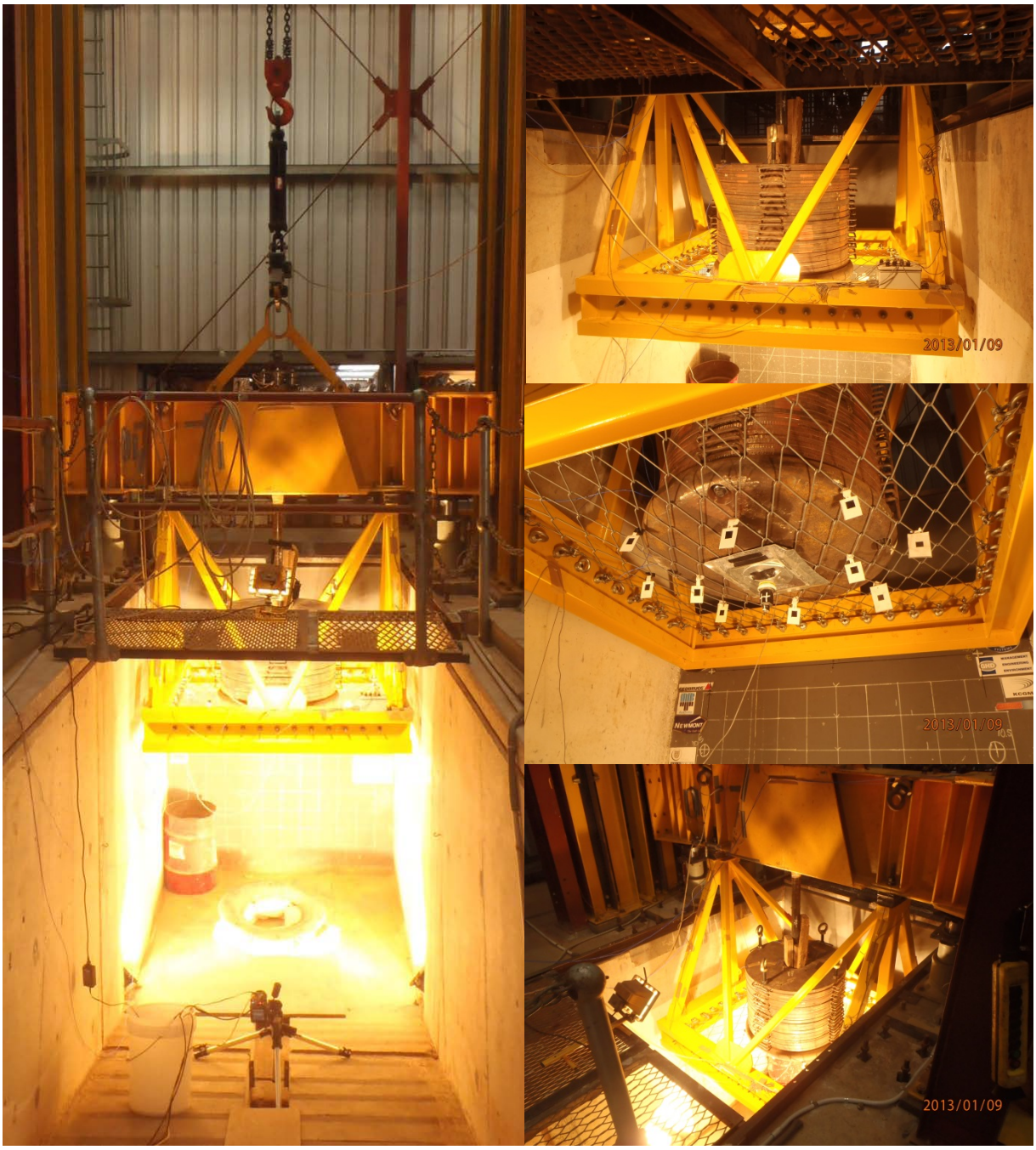

Figure 83: Pre-test setup of sample 195

7.2.1.2 Post-test photos of sample 195

Post-test photos of sample 195 are shown in Figure 84. Figure 85 refers to the yielding of the bar resulting in galvanise flacking at simulated discontinuity.

Figure 84: Post-test photos of sample 195

Figure 85: Displacement at the simulated discontinuity

7.2.1.3 Yield / failure Mechanism

Figure 86 shows the anchor and collar load cells responses of sample #195. The beam impacts on buffers at 0.009s and 0.011s respectively. Anchor load reaches up to 265kN rapidly after the impact and then the bar ruptures at 0.047s. The loading mass rests on the mesh and the mesh survives with a maximum displacement of 115mm. The combined system was stable.

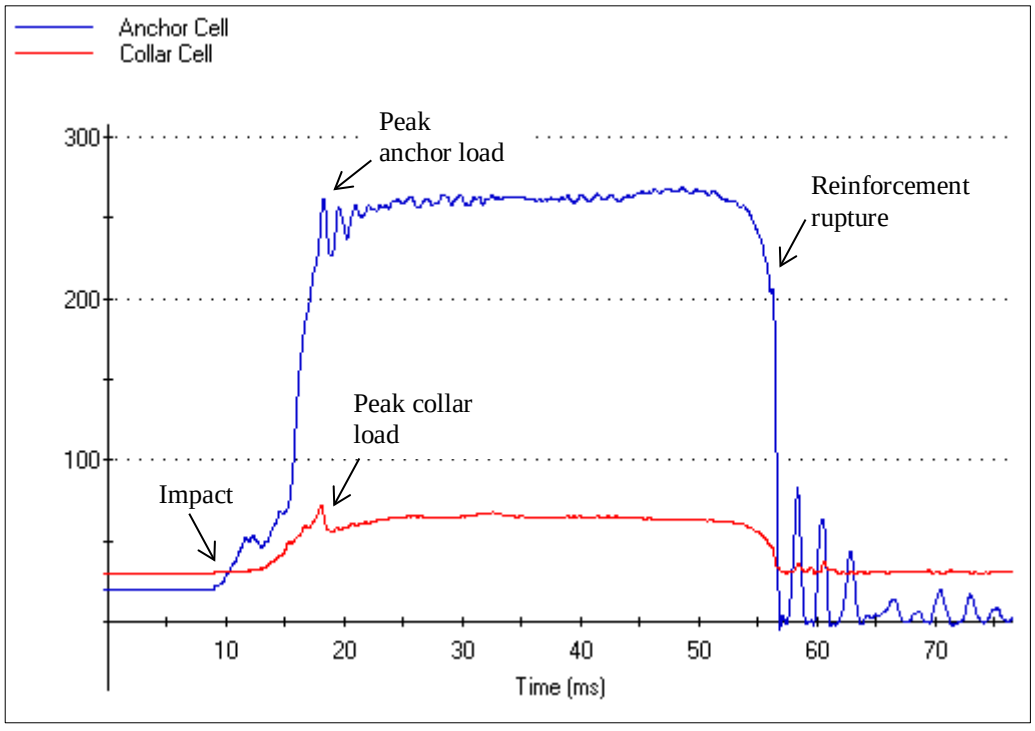

Figure 86: Anchor cells and load cell response of sample #195.

7.2.2 Sample 196: Fully encapsulated threaded bar with 4mm chain link mesh

7.2.2.1 Pre-test photos of sample 196

Pre-test photos of sample 196 are shown in Figure 87.

Figure 87: Pre-test setup of sample 196

7.2.2.2 Post-test photos of sample 196

Post-test photos of sample 196 are shown in Figure 88.

Figure 88: Post-test setup of sample 196

7.2.2.3 Yield / failure Mechanism

Figure 89 shows the anchor and collar load cells response of sample #196. The beam impacts on buffers at 0.011s. Anchor load reaches up to 265kN and then the bar ruptures at 0.052s followed by the mesh rupturing at 0.043s respectively. Total of 5 wires rupture on mesh. The combined system failed.

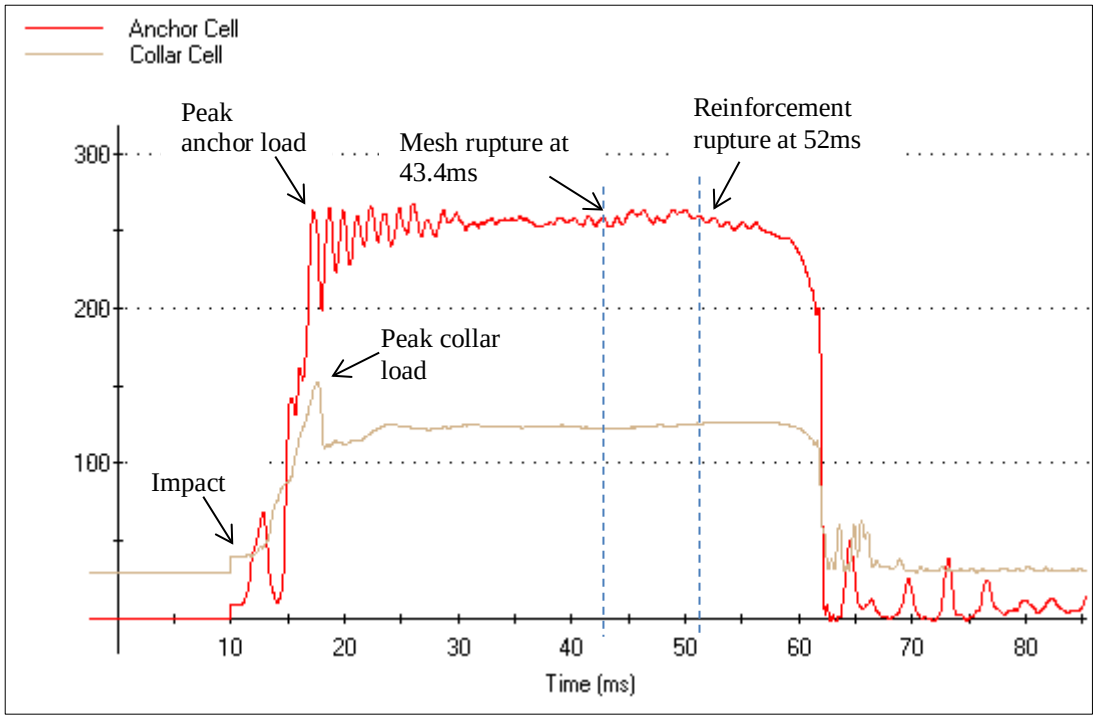

Figure 89: Anchor cells and load cell response of sample #196.

7.2.3 Sample 197: Fully encapsulated threaded bar with 5.6mm weld mesh

7.2.3.1 Pre-test photos of sample 197

Pre-test photos of sample 197 are shown in Figure 90.

Figure 90: Pre-test setup of sample 197

7.2.3.2 Post-test phots of sample 197

Post-test photos of sample 197 are shown in Figure 91.

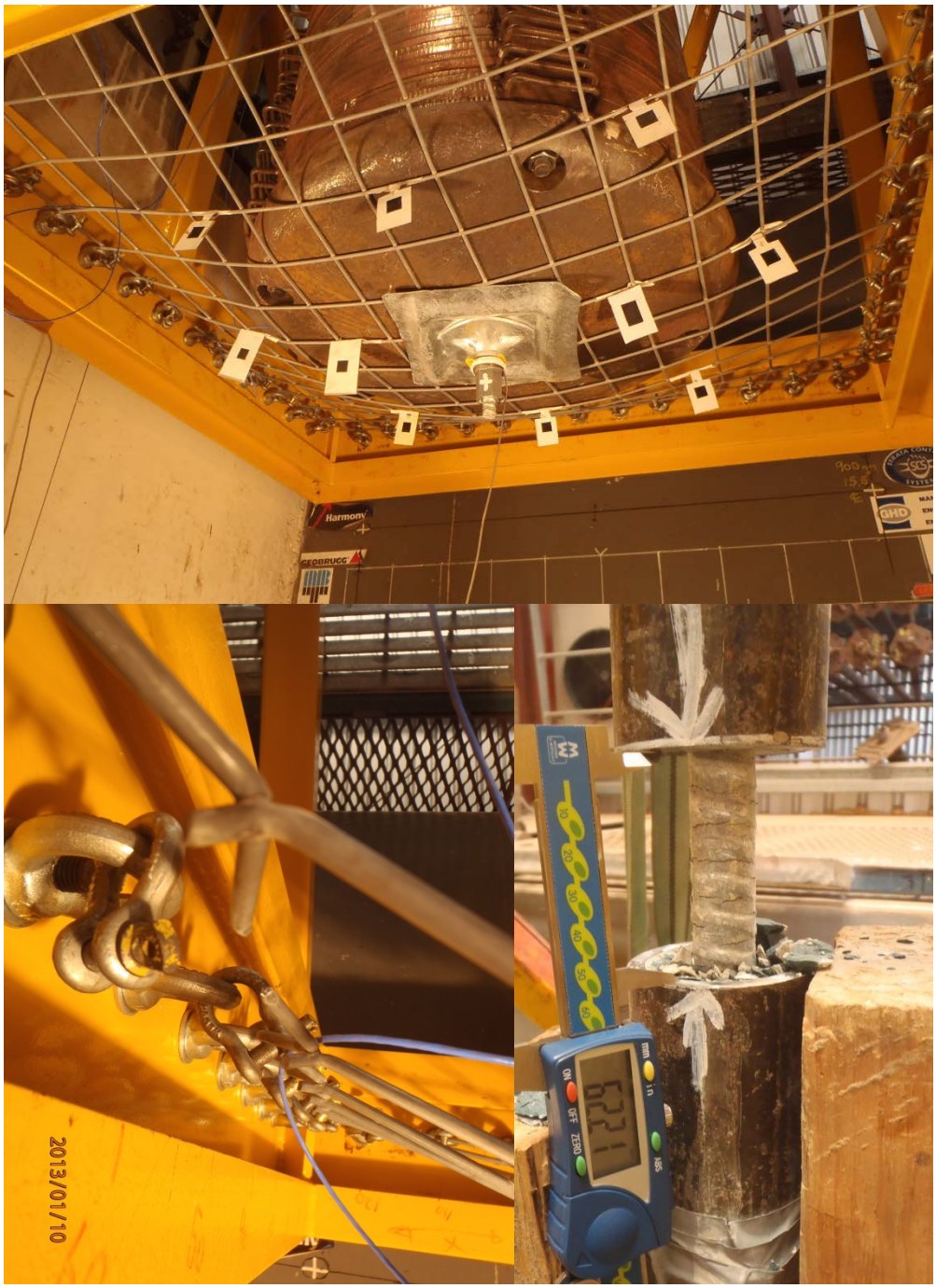

Figure 91: Post-test setup of sample 197

7.2.3.3 Yield / failure Mechanism

Figure 92 shows the anchor and collar load cells response of sample #197. The beam impacts on buffers at 0.011s. Anchor load reaches up to 252kN and the load remain nearly constant until the end of the test. The bar yielded up to a maximum of 59mm. The combined system was stable with 4 ruptured wires.

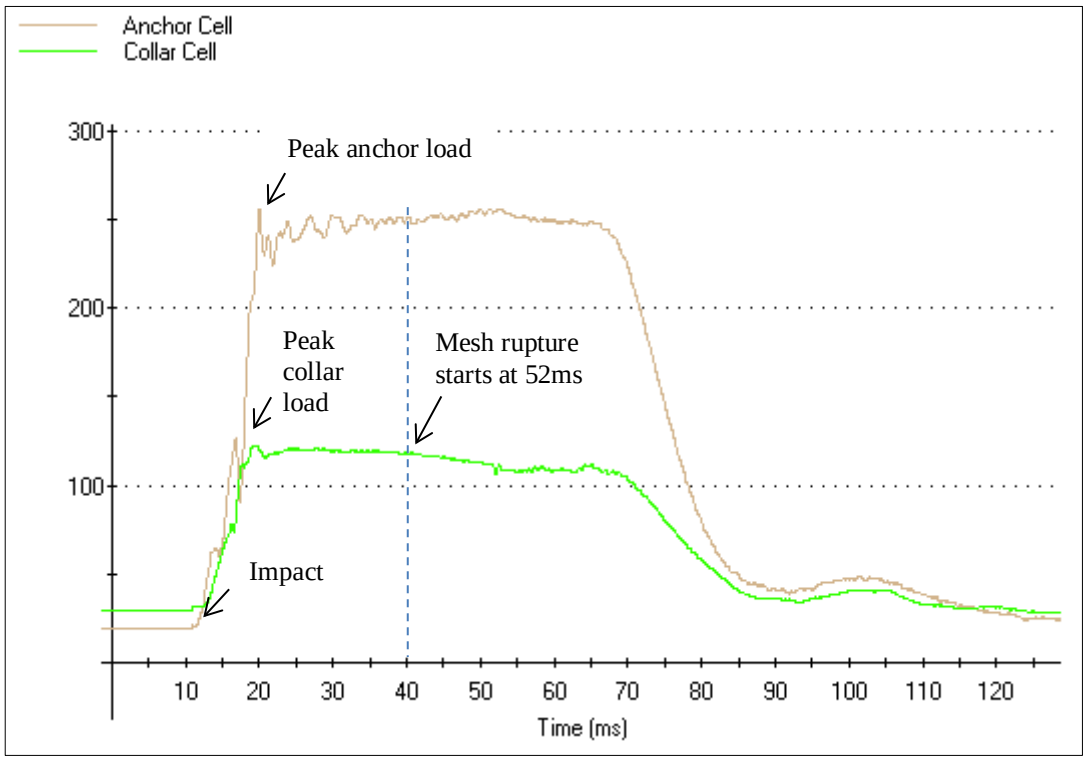

Figure 92: Anchor cells and load cell response of sample #197.

7.2.4 Sample 198: Fully encapsulated threaded bar with 5.6mm weld mesh

7.2.4.1 Pre-test photos of sample 198

Pre-test photos of sample 198 are shown in Figure 93.

Figure 93: Pre-test setup of sample 198

7.2.4.2 Post-test phots of sample 198

Post-test photos of sample 198 are shown in Figure 94.

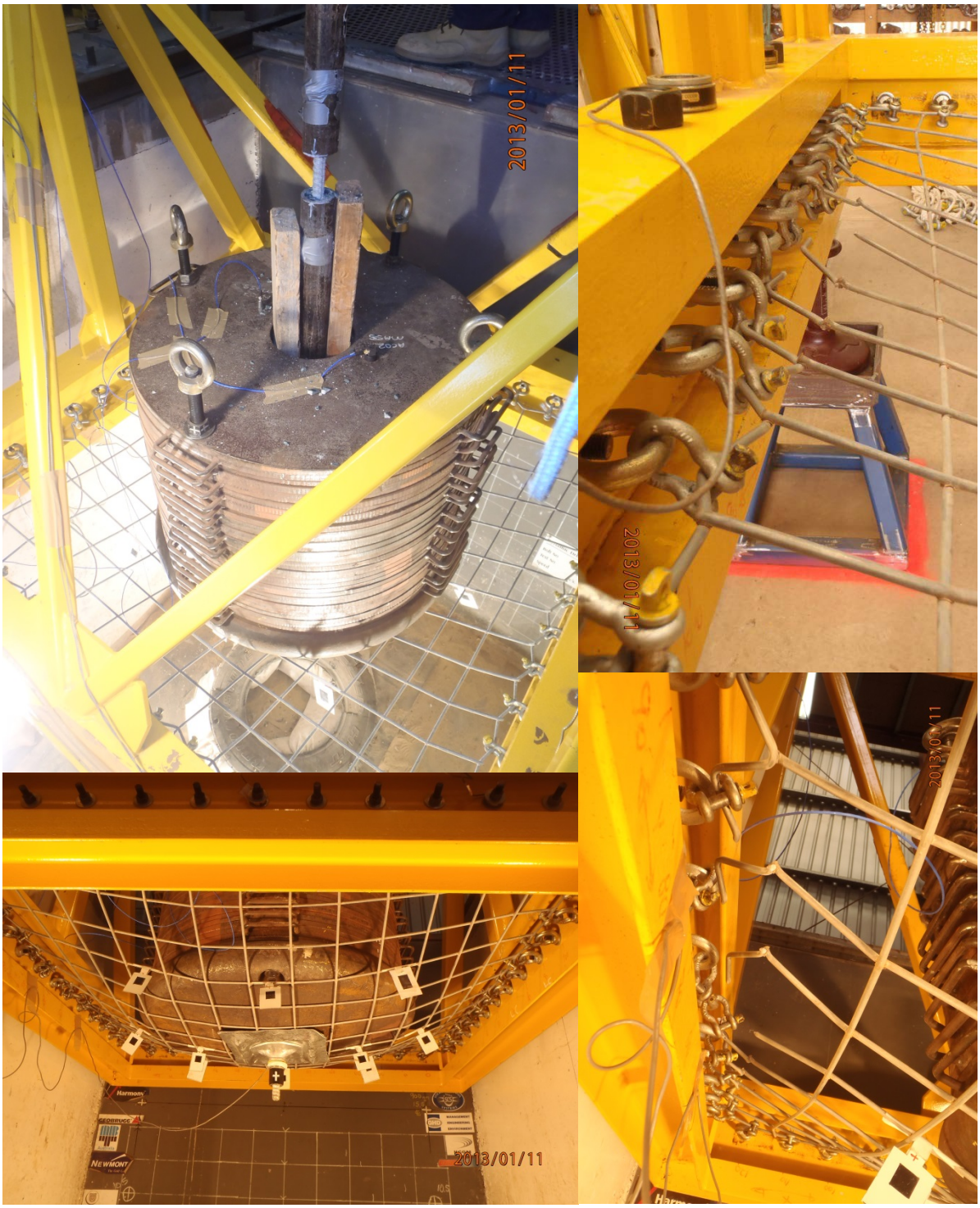

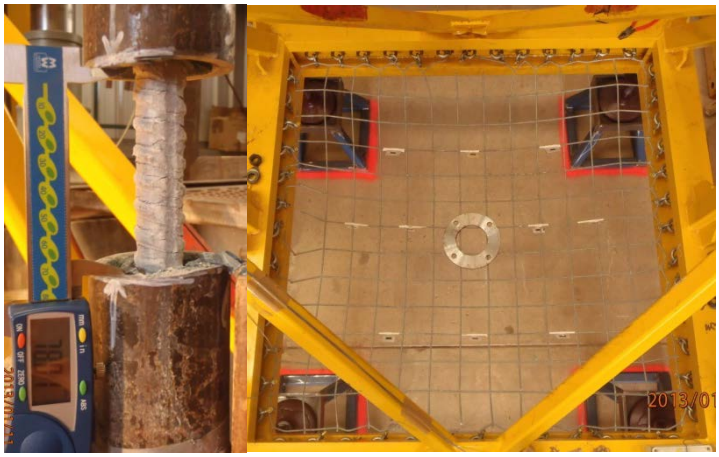

Figure 94: Post-test setup of sample 198

7.2.4.3 Yield / failure Mechanism

Figure 95 shows the anchor and collar load cells response of sample #198. The beam impacts on buffers at 0.010s. The anchor load reaches rapidly up to 260kN after the impact and remains nearly constant until the end of the test. The reinforcement was stable with a maximum yield of 85.4mm at the simulated discontinuity and the mesh ruptured at 39.4ms with a total no of 10 ruptured wires. The combined system was stable.

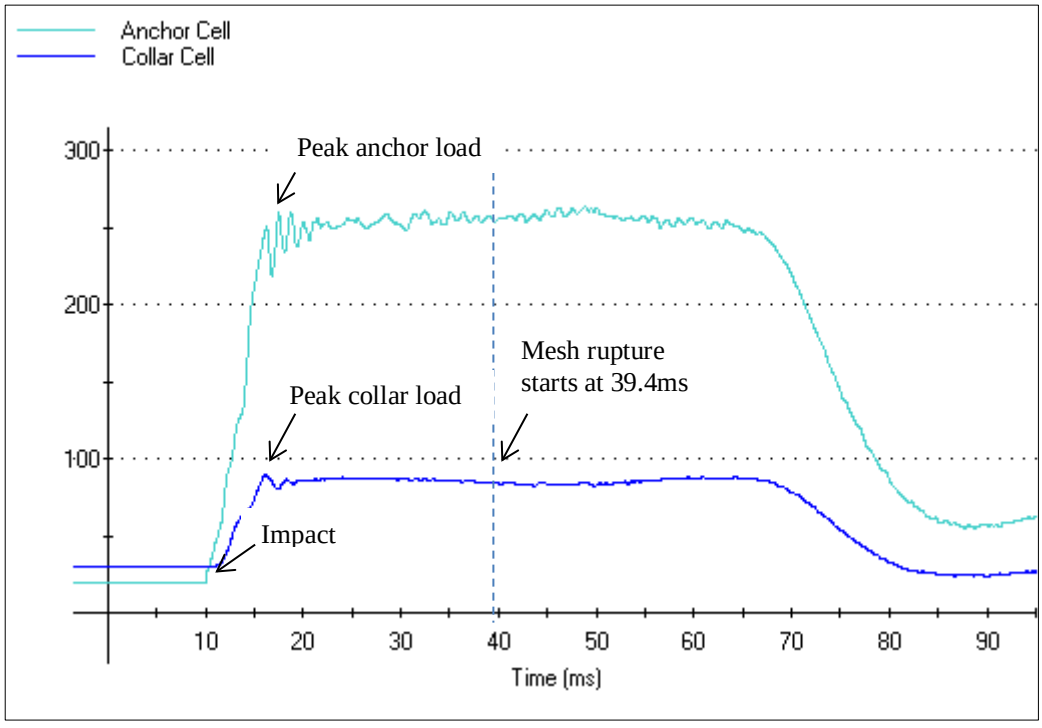

Figure 95: Anchor cells and load cell response of sample #198.

7.2.5 Sample 199: Decoupled Posimix bar with 5.6mm weld mesh

7.2.5.1 Post-test phots of sample 199

Post-test photos of sample 199 are shown in Figure 96.

Figure 96: Post-test setup of sample 199

7.2.5.2 Yield / failure Mechanism

Figure 97 shows the anchor and collar load cells response of sample #199. The beam impacts on buffers at 0.008s. The anchor load reaches up to 220kN and gradually increased up to 250kN until the reinforcement failed. The reinforcement failed at 55.6ms followed by the mesh rupture at 35.7ms. The mesh totally ruptured during the test. The combined scheme failed.

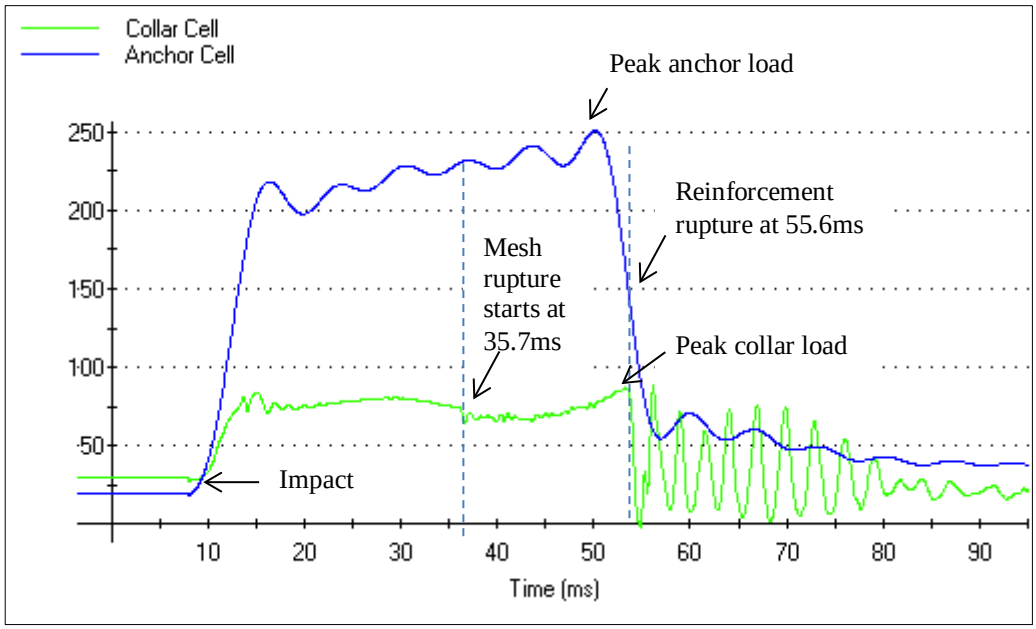

Figure 97: Anchor cells and load cell response of sample #199.

7.2.6 Sample 200: Decoupled Posimix bar with 4mm chain link mesh

7.2.6.1 Pre-test photos of sample 200

Pre-test photos of sample 200 are shown in Figure 98.

Figure 98: Pre-test setup of sample 200

7.2.6.2 Post-test phots of sample 200

Post-test photos of sample 200 are shown in Figure 99.

Figure 99: Post-test setup of sample 200

7.2.6.3 Yield / failure Mechanism

Figure 100 shows the anchor and collar load cells response of sample #200. The beam impacts on buffers at 0.009s. The anchor load rapidly reaches up to 262kN during the impact. The bar started to pull out at 50.8ms. Total of 15 wires failed on the mesh. The combined system was stable with a 174.5mm of displacement.

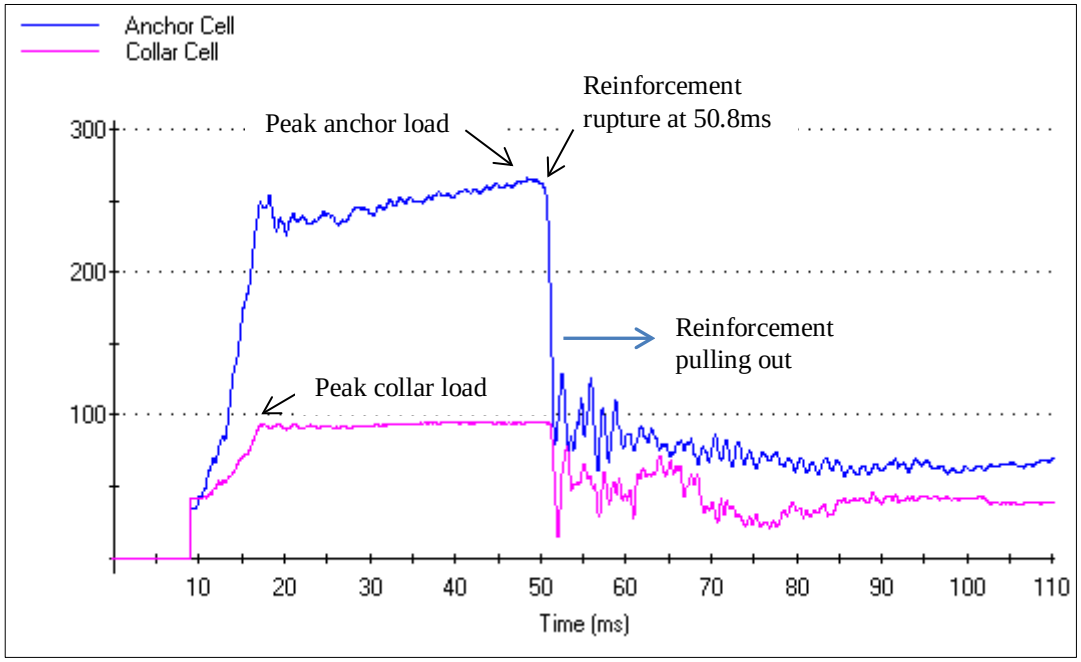

Figure 100: Anchor cells and load cell response of sample #200.

7.2.7 Sample 201: Decoupled Posimix bar with 4mm chain link mesh

7.2.7.1 Pre-test photos of sample 201

Pre-test photos of sample 201 are shown in Figure 101.

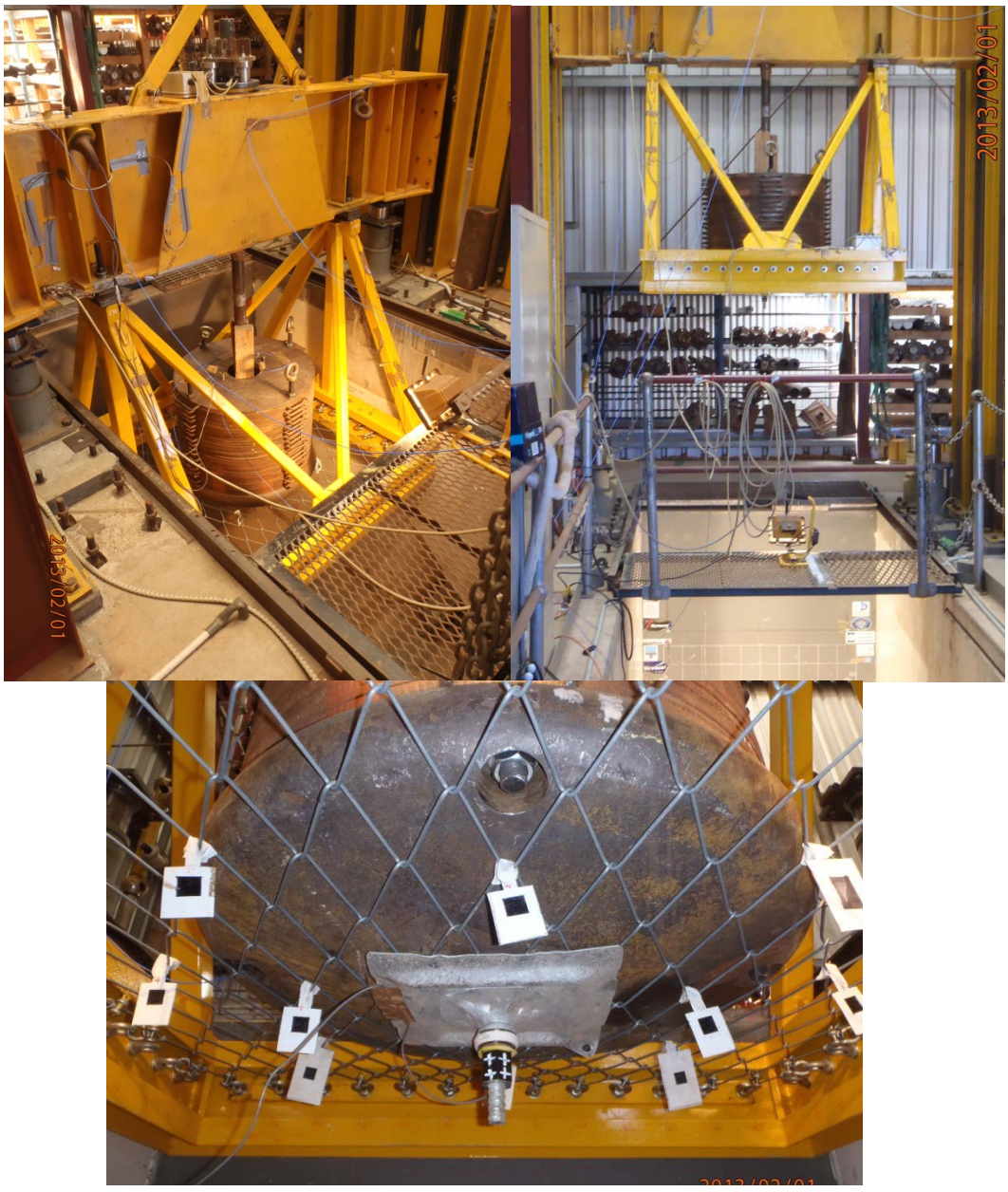

Figure 101: Pre-test setup of sample 201

7.2.7.2 Post-test phots of sample 201

Post-test photos of sample 201 are shown in Figure 102.

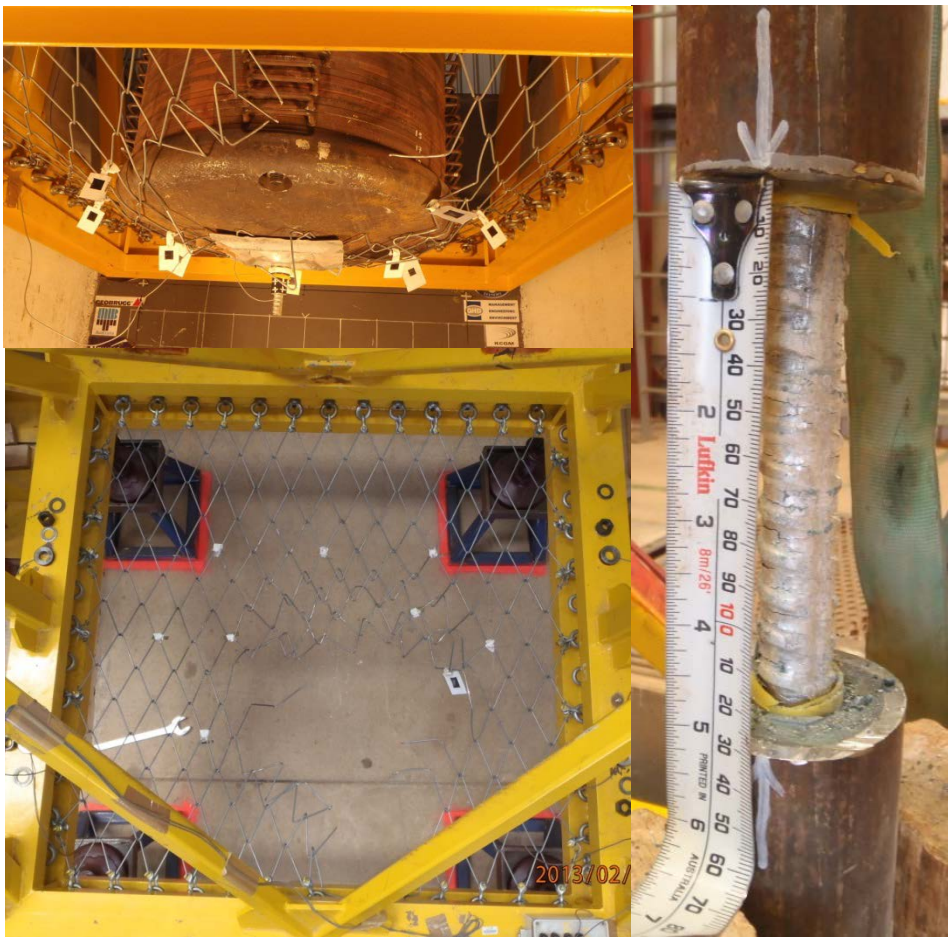

Figure 102: Post-test setup of sample 201

7.2.7.3 Yield / failure Mechanism

Figure 103 shows the anchor and collar load cells response of sample #201. The beam impacts on buffers at 0.009s. The anchor load rapidly reaches up to 251kN after the impact. Reinforcement survived after a maximum yield of 128mm at the simulated discontinuity. Total of 5 wires ruptured on the mesh. Overall the combined scheme was stable.

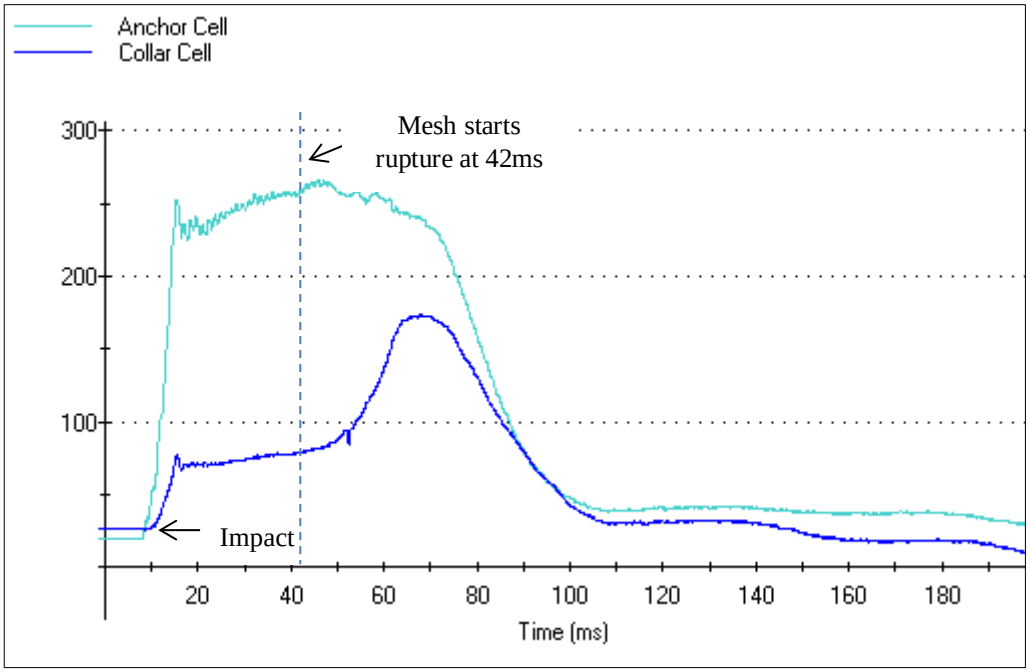

Figure 103: Anchor cells and load cell response of sample #201.

7.2.8 Sample 202: Decoupled Posimix bar with 5.6mm weld mesh

7.2.8.1 Pre-test photos of sample 202

Pre-test photos of sample 202 are shown in Figure 104.

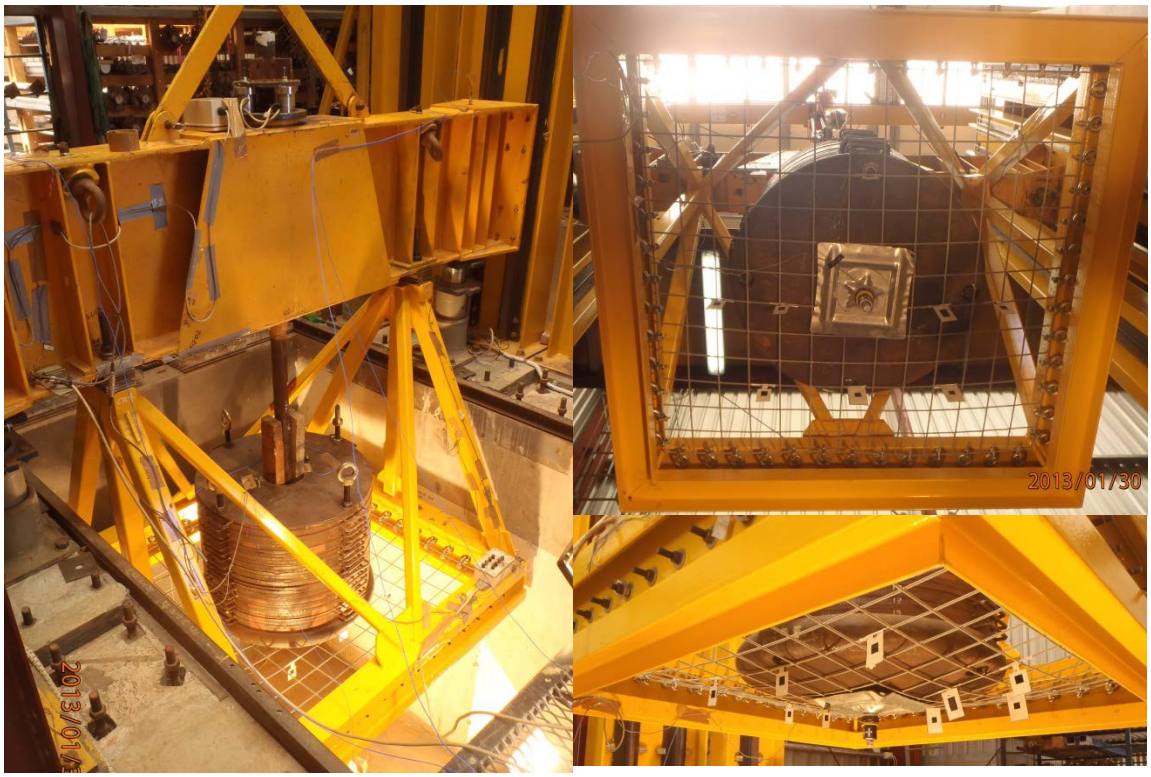

Figure 104: Pre-test setup of sample 202

7.2.8.2 Post-test phots of sample 202

Post-test photos of sample 202 are shown in Figure 105.

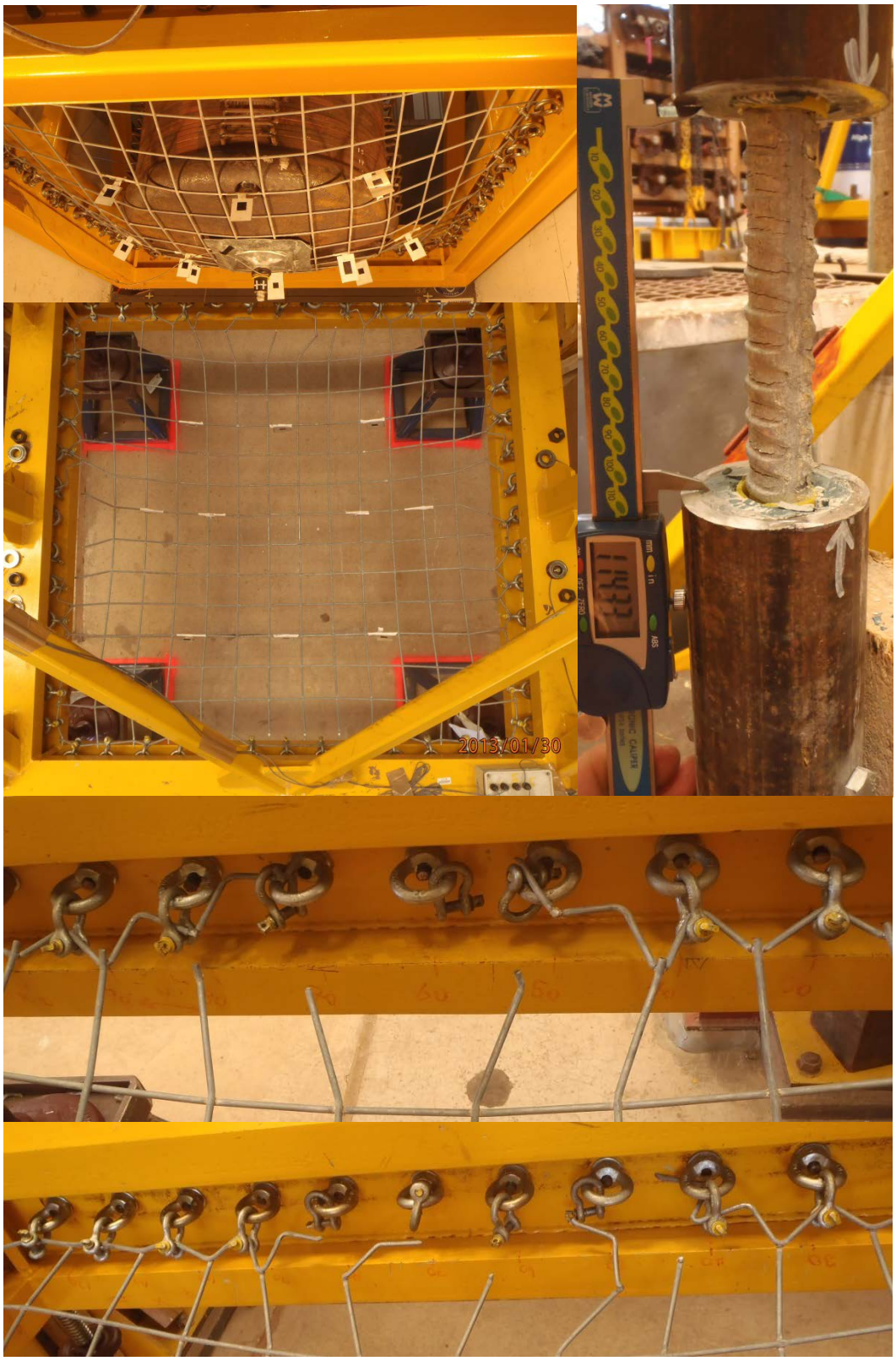

Figure 105: Post-test setup of sample 202

7.2.8.3 Yield / failure Mechanism

Figure 106 shows the anchor and collar load cells response of sample #202. The beam impacts on buffers at 0.010s. The anchor load rapidly reaches up to 251kN after the impact. The reinforcement was stable after a 121mm of yield at the simulated discontinuity. A total of 6 wires ruptured on the mesh. The combined scheme was stable.

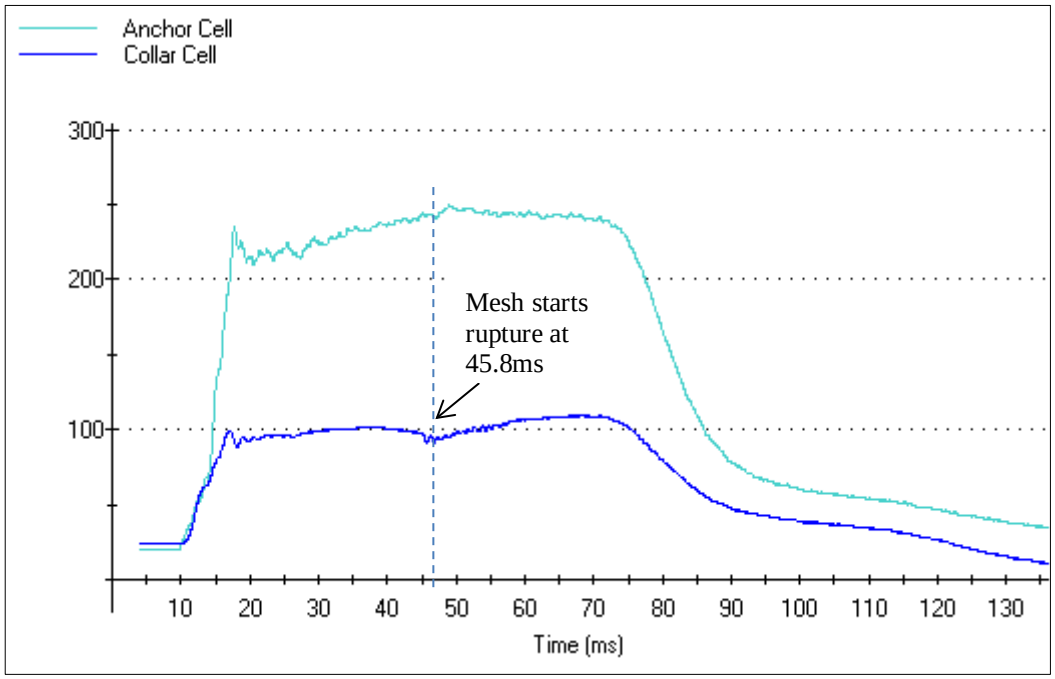

Figure 106: Anchor cells and load cell response of sample #202.

7.3 Overall Photos and Failure Mechanisms of Test Samples (Program 2)

7.3.1 Sample 231: Decoupled DSI Posimix bar with 4mm CODELCO chain link mesh

7.3.1.1 Pre-test photos of sample 231

Pre-test photos of sample 231 are shown in Figure 107.

Figure 107: Pre-test setup of sample 231

7.3.1.2 Post-test photos of sample 231

Post-test photos of sample 231 are shown in Figure 108.

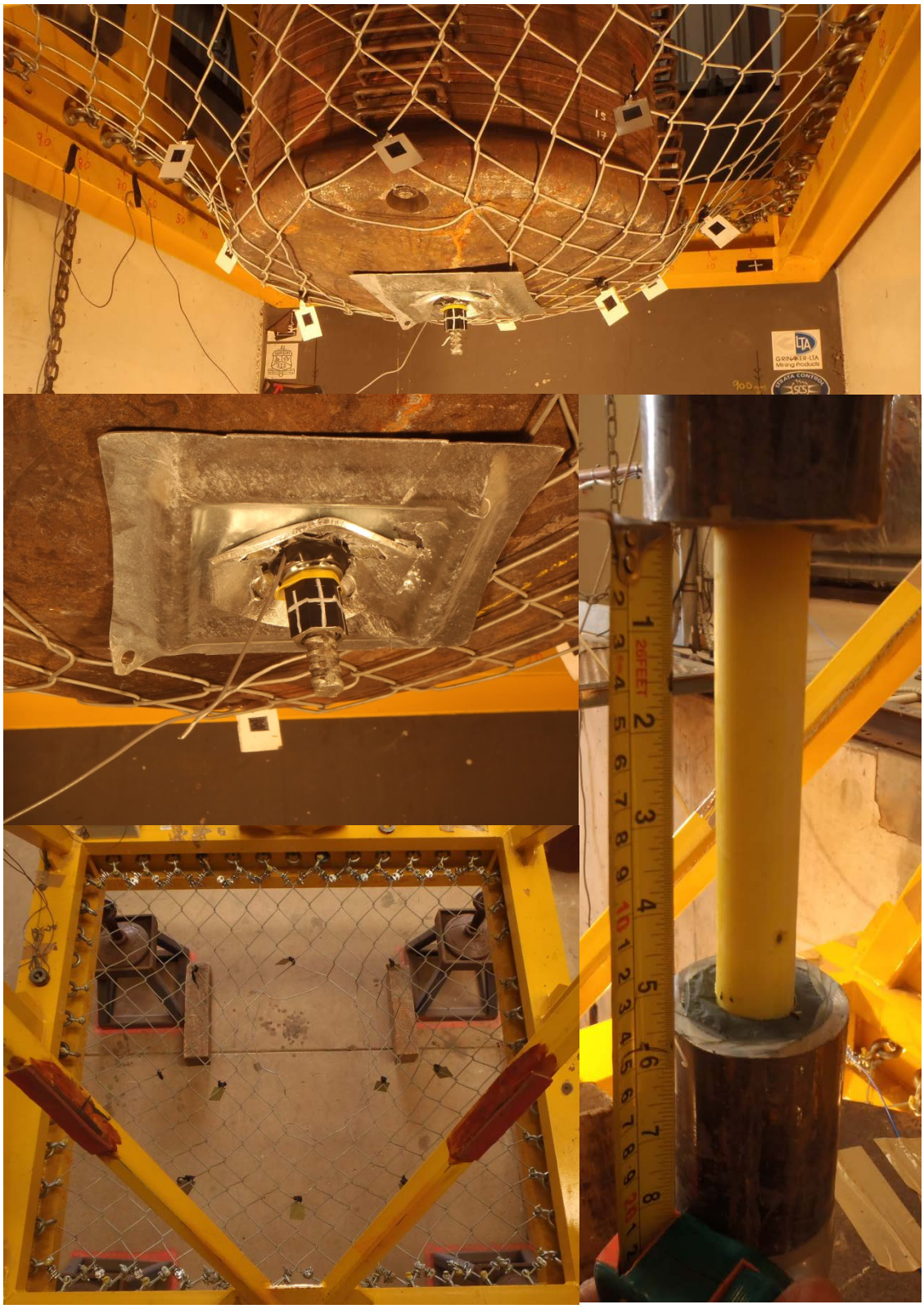

Figure 108: Post-test setup of sample 231

7.3.1.3 Yield / failure Mechanism

Figure 109 shows the anchor and collar load cells response of sample #231. The beam impacts on buffers at 0.03s. The anchor load rapidly reaches up to 301kN after the impact. The reinforcement was stable after a 142mm of yield at the simulated discontinuity. A single wire ruptured on the mesh. The combined scheme was stable.

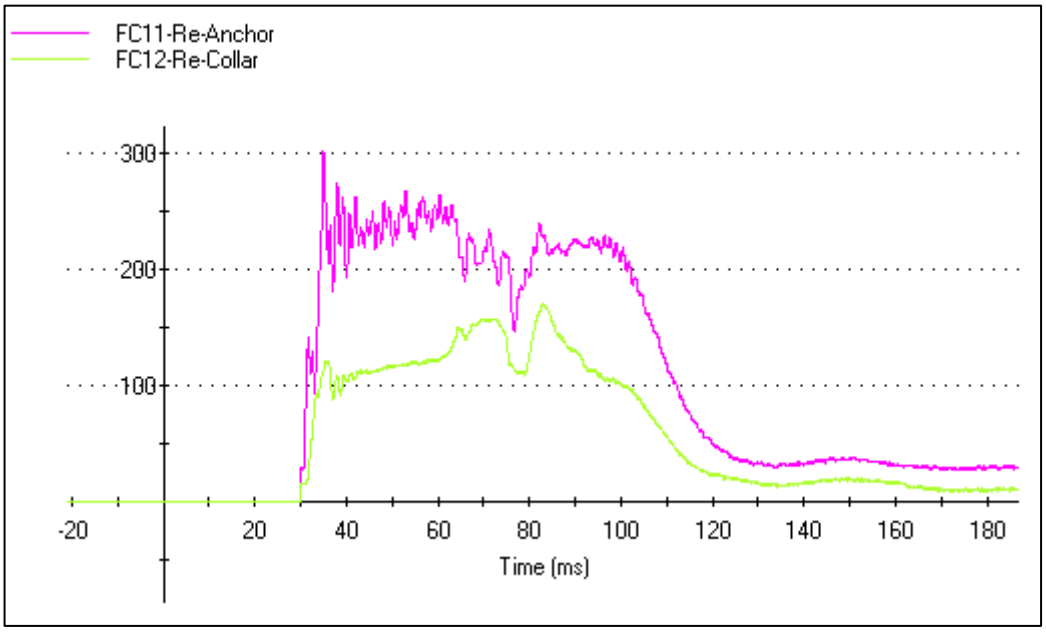

Figure 109: Anchor cells and load cell response of sample #231

7.3.2 Sample 234: Decoupled DSI Posimix bar with 5mm CODELCO chain link mesh

7.3.2.1 Pre-test photos of sample 234

Pre-test photos of sample 234 are shown in Figure 110.

Figure 110: Pre-test setup of sample 234

7.3.2.2 Post-test photos of sample 234

Post-test photos of sample 234 are shown in Figure 111.

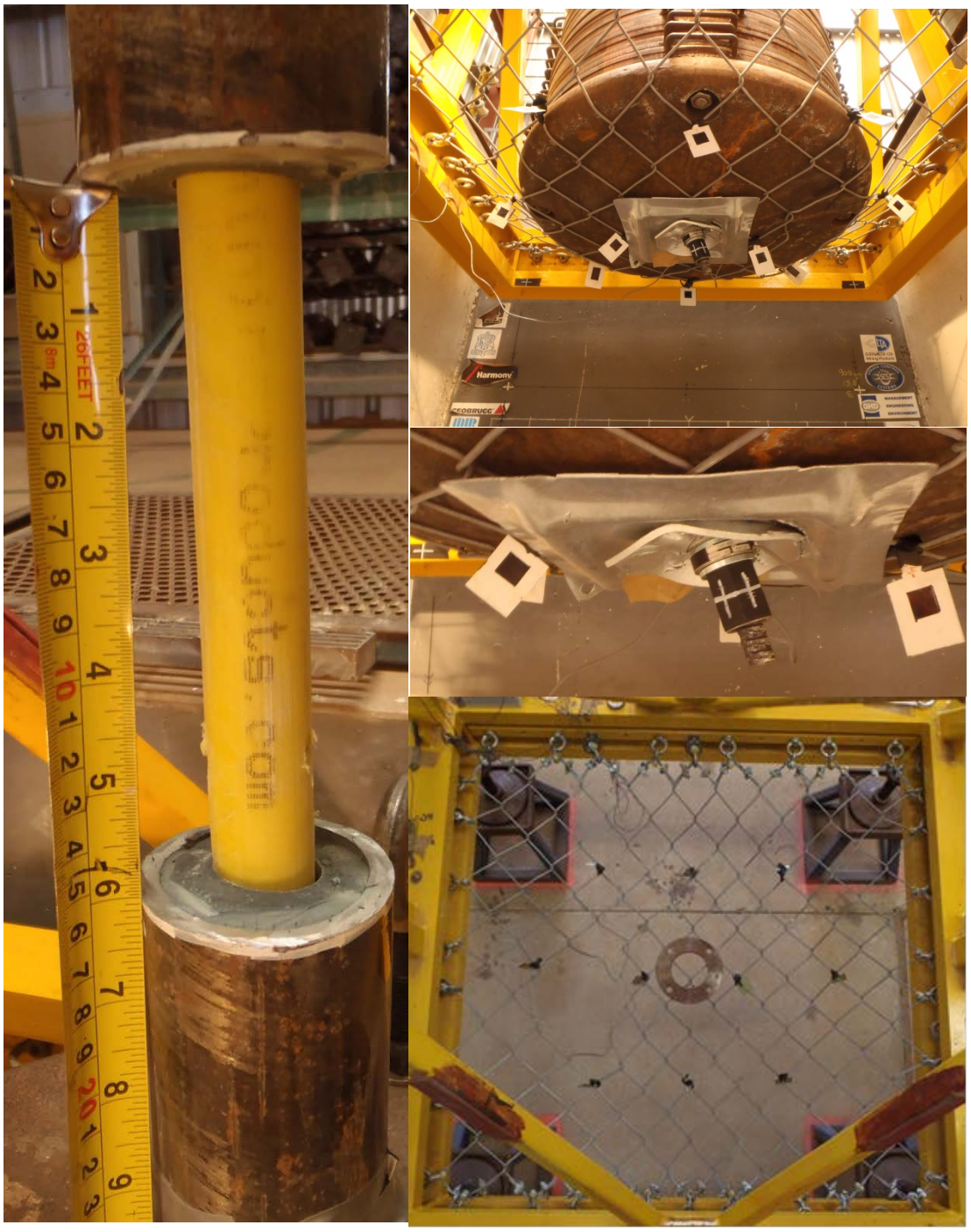

Figure 111: Post-test setup of sample 234

7.3.2.3 Yield / failure Mechanism

Figure 112 shows the anchor and collar load cells response of sample #234. The beam impacts on buffers at 0.030s. Anchor load collar load reach up to 350kN and 155kN respectively. The reinforcement was stable after a 155mm of yield at the simulated discontinuity. A single wire ruptured on the mesh. The combined scheme was stable.

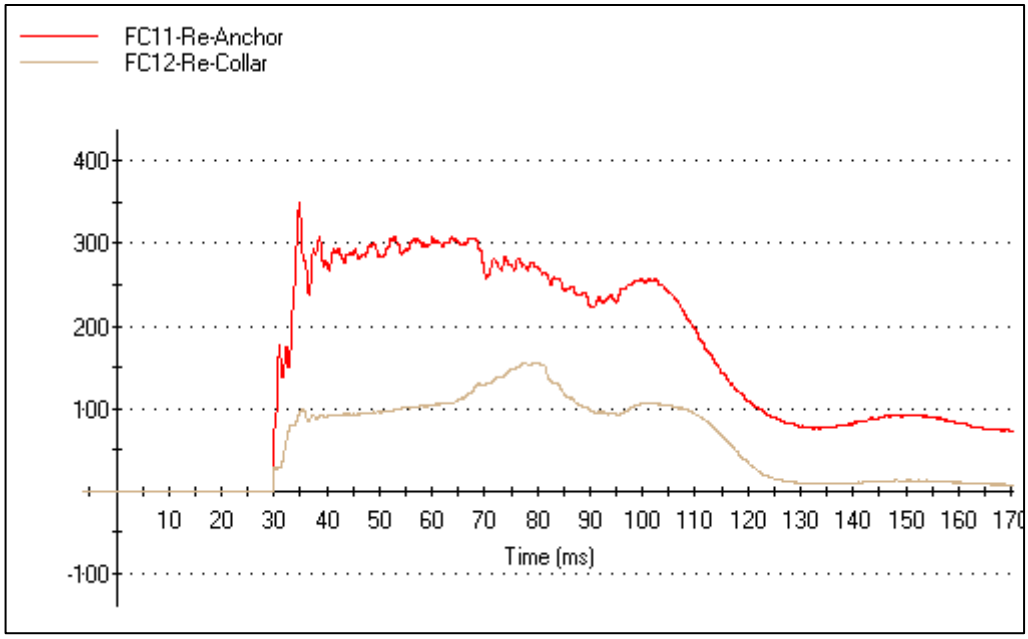

Figure 112: Anchor cells and load cell response of sample #234

7.3.3 Sample 235: Decoupled DSI Posimix bar with 4mm Geobrugg chain link mesh (G80-4)

7.3.3.1 Pre-test photos of sample 235

Pre-test photos of sample 235 are shown in Figure 113.

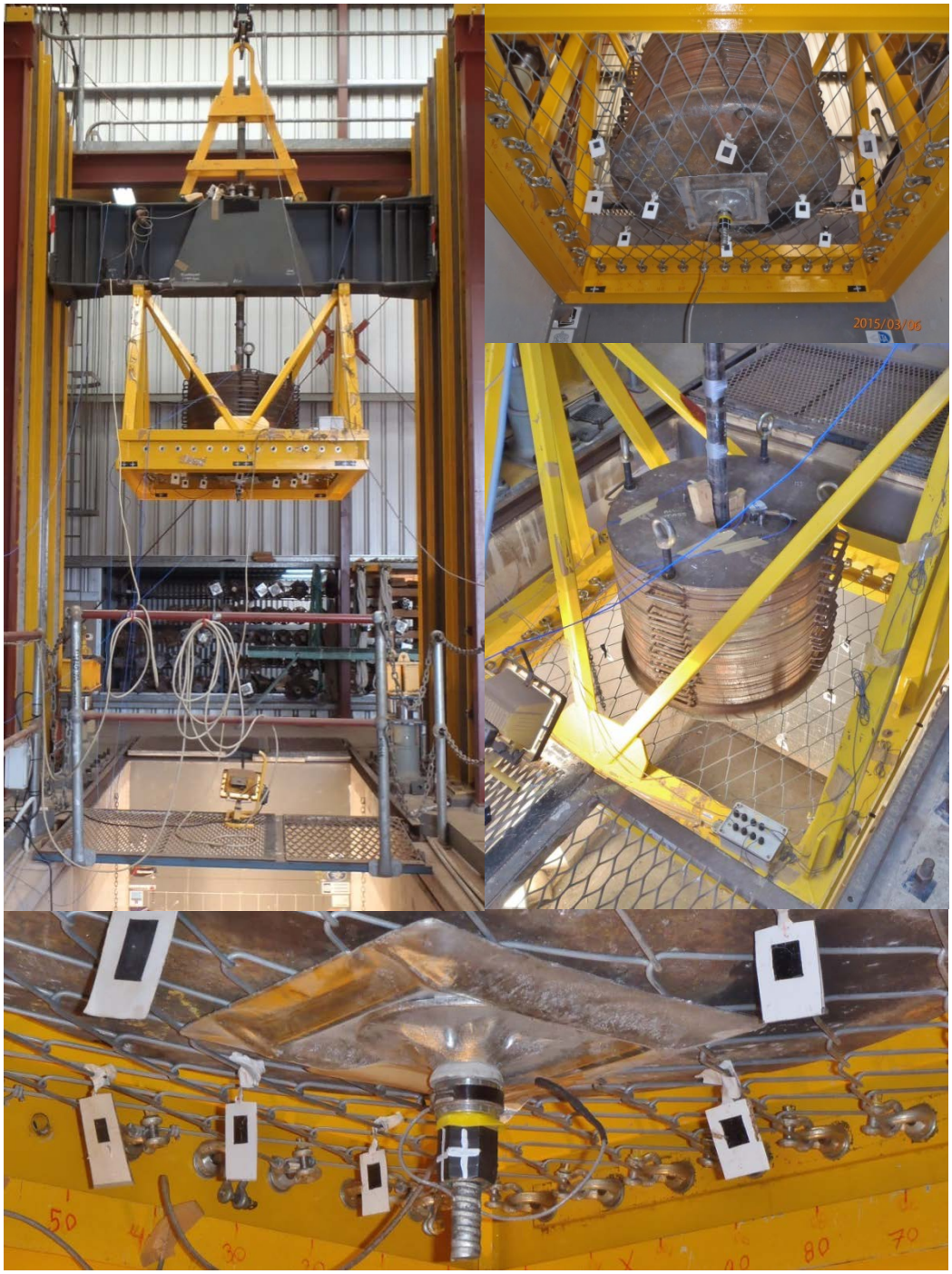

Figure 113: Pre-test setup of sample 235

7.3.3.2 Post-test photos of sample 235

Post-test photos of sample 235 are shown in Figure 114.

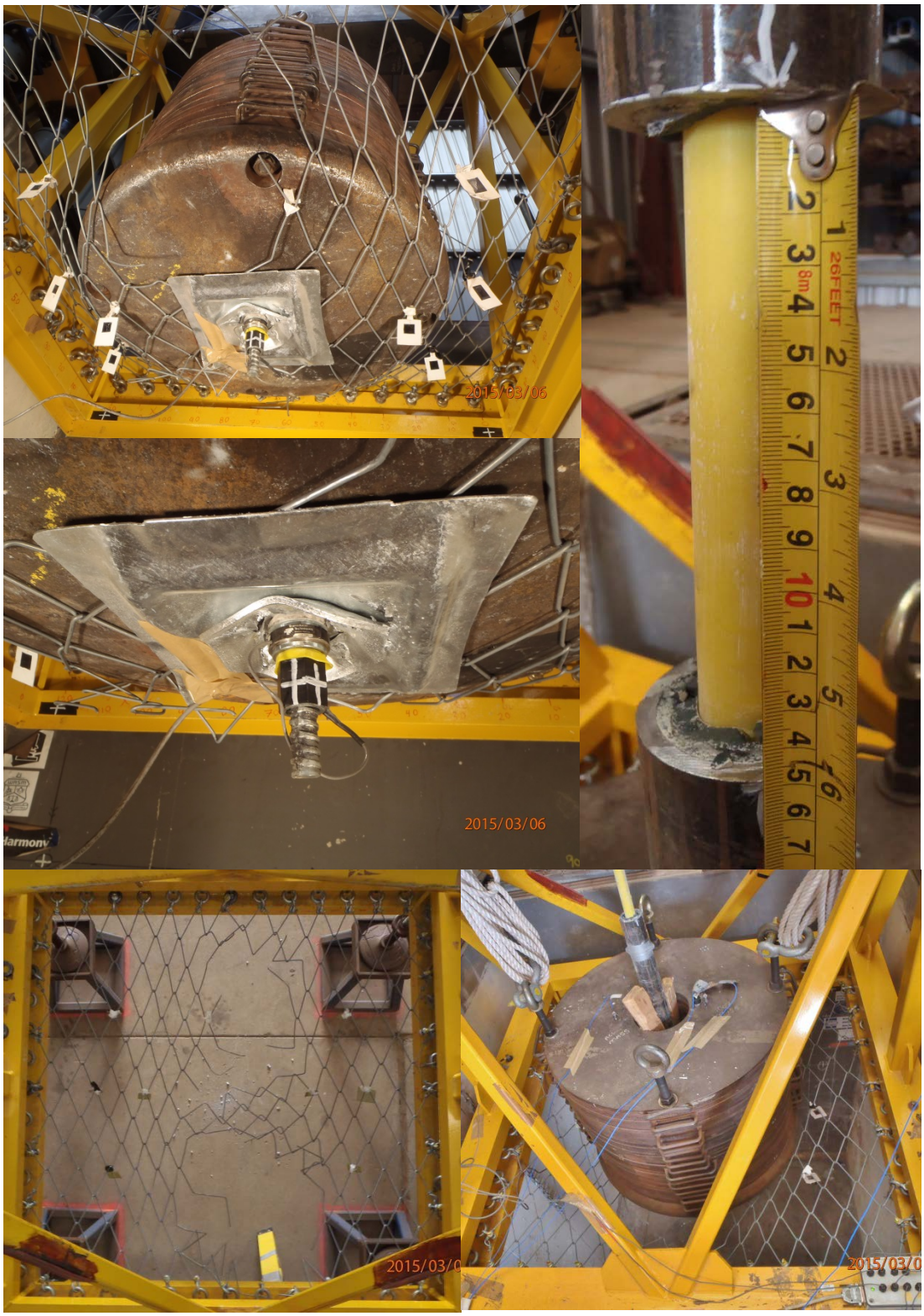

Figure 114: Post-test setup of sample 235

7.3.3.3 Yield / failure Mechanism

Figure 115 shows the anchor and collar load cells response of sample #235. The beam impacts on buffers at 0.030s. Anchor load collar load reach up to 310kN and 230kN respectively. The reinforcement was stable after a 149mm of yield at the simulated discontinuity. A total of nine wires ruptured on the mesh. The combined scheme was stable.

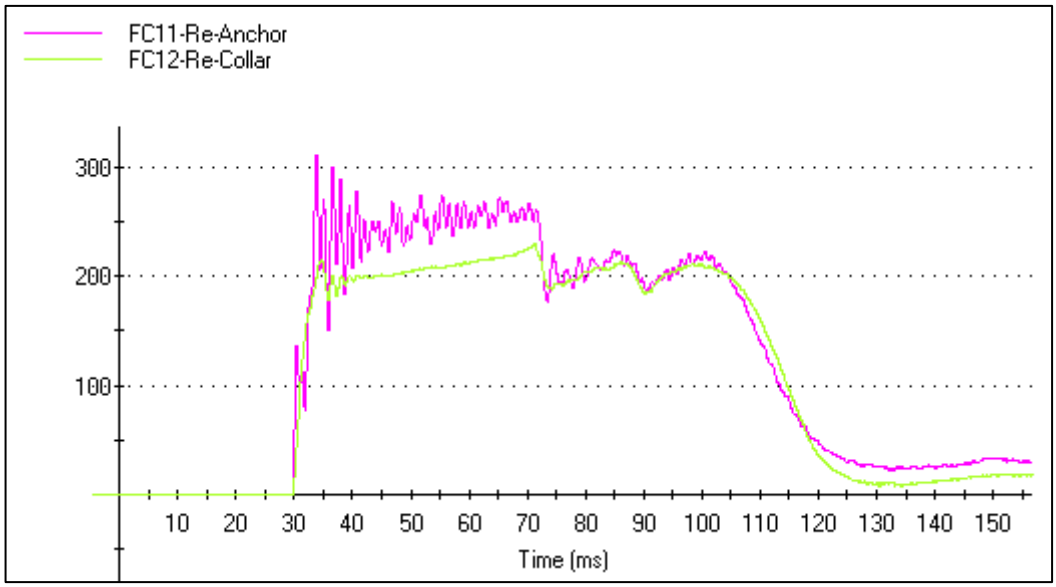

Figure 115: Anchor cells and load cell response of sample #235

7.3.4 Sample 236: Decoupled DSI Posimix bar with 4mm Geobrugg chain link mesh (G80-4)

7.3.4.1 Pre-test photos of sample 236

Pre-test photos of sample 236 are shown in Figure 116.

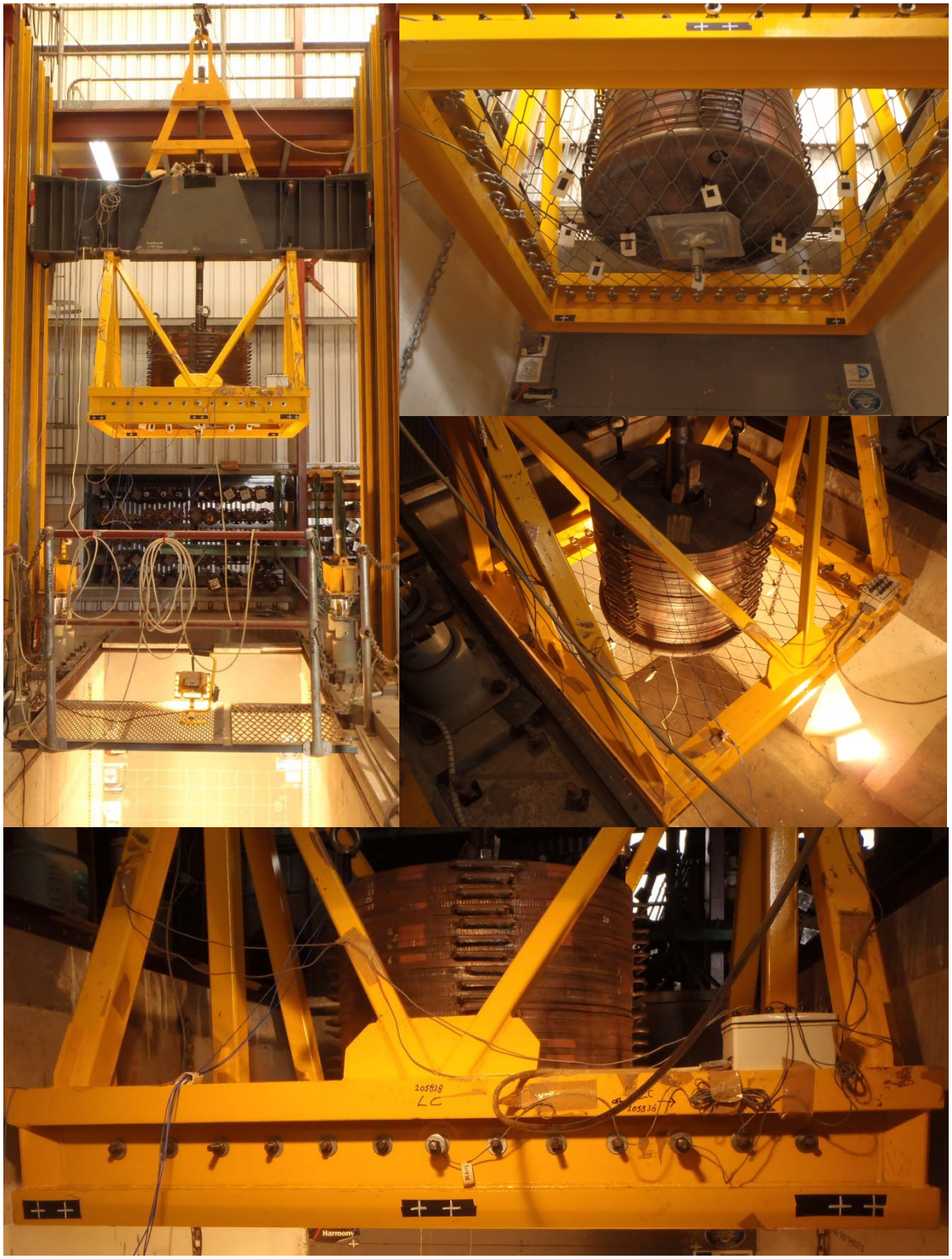

Figure 116: Pre-test setup of sample 236

7.3.4.2 Post-test photos of sample 236

Post-test photos of sample 236 are shown in Figure 117.

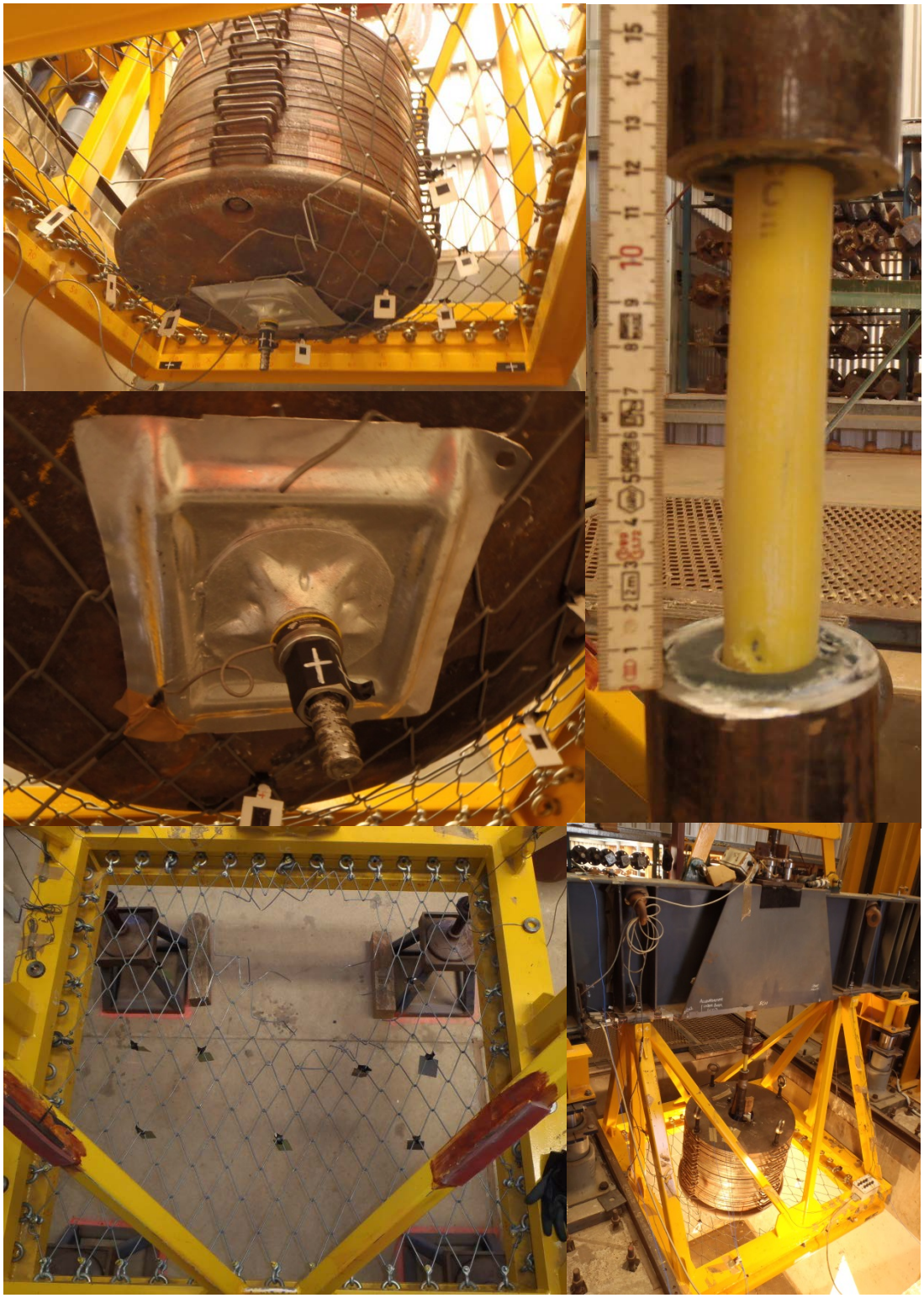

Figure 117: Post-test setup of sample 236

7.3.4.3 Yield / failure Mechanism

Figure 118 shows the anchor and collar load cells response of sample #236. The beam impacts on buffers at 0.031s. Anchor load collar load reach up to 300kN and 227kN respectively. The reinforcement was stable after a 121mm of yield at the simulated discontinuity. A total of four wires ruptured on the mesh. The combined scheme was stable.

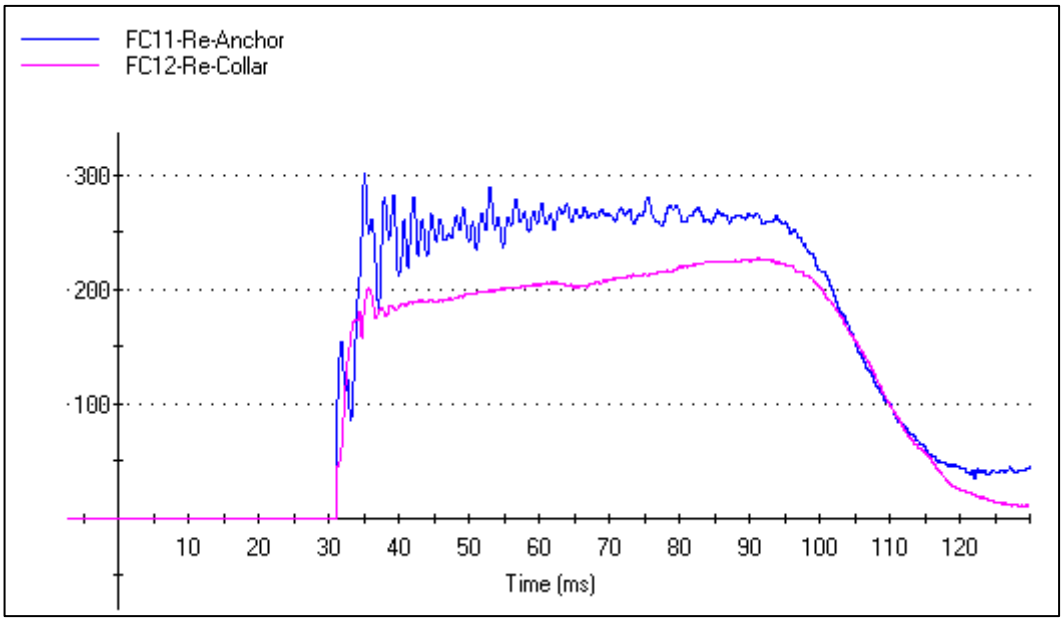

Figure 118: Anchor cells and load cell response of sample #236

7.4 SUMMARY OF RESULTS AND COMMENTS

The summaries of the test results for Program 1 and Program 2 are presented in Table 7 and Table 8, respectively.

The maximum separation of 155mm at the simulated discontinuity was measured in sample #234. The maximum energy input of 57.5kJ was applied to sample #235 while the minimum energy input of 52.8kJ was applied to sample #236. Combined scheme of sample #236 dissipated the highest energy of 43.4kJ.

Two fully encapsulated threaded bars with combination of a chain link mesh and a weld mesh and two decoupled threaded bars with combination of a chain link mesh and a weld mesh were ruptured in the first test program.

The support system (chain link mesh) of sample #195 was the only support system to survive while all the other support systems ruptured at least a single wire. In terms of overall performance, tests apart from test #196 and #199 were stable.

Deformations at the simulated discontinuity were measured for the reinforcement systems and the maximum displacement of the stable support system for sample #195. The measured maximum deformation of the reinforcement system was 136mm in sample #201 while the minimum was 67mm in sample #197.

The measured separation of the reinforcement systems were less than the calculated maximum deformation from the data acquisition software due to the recovery of elastic deformation at the simulated discontinuity.

The maximum energy input was applied to the sample #199 (53.2kJ) while the minimum was applied to the sample #197 (27kJ). Both the reinforcement and support systems failed in samples #196, #199 and #200. The threaded bar of sample #200 pulled out from the anchor section but was also marked as ruptured. In tests in which the element ruptured, the maximum deformations were estimated by holding the bolt parts together and then measuring the total length.

Table 7: Summary of program 1

Test ID	Reinforcement system	Support system	Total Energy Dissipated (kJ)	Comments
195	Ruptured	Survived	19.5	The reinforcement system ruptured with a maximum deformation of 77mm at the simulated discontinuity. The support system survived.
196	Ruptured	5 wires Ruptured	25.2	The combined scheme failed. The support system ruptured at 43.4ms followed by the reinforcement system at 47.6ms with a maximum deformation of 93mm at the simulated discontinuity.
197	Survived	4 wires Ruptured	16	The combined scheme was stable. The reinforcement system survived with a 59mm of separation at the simulated discontinuity. A total of 4 wires ruptured, one on each side of the support system.
198	Survived	10 wires Ruptured	25	The combined system was stable. The reinforcement system survived with a 75.5mm of separation at the simulated discontinuity. A total of 10 wires ruptured on 3 sides of the support system.
199	Pulled out	Completely Ruptured	37	Energy is calculated at the initiation of reinforcement sliding. The reinforcement system pulled out. The mass slipped onto the bottom of the pit. The support system completely failed.
200	Pulled out	15 wires Ruptured	24.8	Energy is calculated at the initiation of reinforcement sliding. The reinforcement pulled out with a separation of 174.5mm at the simulated discontinuity. A total of 15 wires failed ruptured on the support system.
201	Survived	5 wires Ruptured	29	The reinforcement system survived with a 128mm of separation at the simulated discontinuity while the support system failed.
202	Survived	6 wires Ruptured	34.3	The combined scheme was stable. The reinforcement system survived with a 112mm of separation at the simulated discontinuity. The support system was stable with 6 ruptured wires.

All the reinforcement systems of the Test Program 2 survived while the support systems ruptured at least from a single wire. In overall, all the tests were stable.

The maximum separation of 155mm at the simulated discontinuity was measured in sample #234. The maximum energy input of 57.5kJ was applied to sample #235 while the minimum energy input of 52.8kJ was applied to sample #236. Combined scheme of sample #234 dissipated the highest energy of 41.7kJ.

Table 8: Summary of program 2

Test ID	Reinforcement system	Support system	Total Energy Dissipated (kJ)	Comments
231	Survived	1 wires Ruptured	28.4	The combined system was stable. The reinforce system survived with a 142mm of separation at the simulated discontinuity and the support system was stable with a single ruptured wire.
232	Test error (Welding on the collar flange failed)			
233	Instrumentation error			
234	Survived	1 wire Ruptured	41.7	The combined system was stable. The reinforce system survived with a 155mm of separation at the simulated discontinuity and the support system was stable with a single ruptured wire.
235	Survived	9 wires Ruptured	30.8	The combined system was stable. The reinforce system survived with a 149mm of separation at the simulated discontinuity and the support system was stable with 9 ruptured wires.
236	Survived	4 wires Ruptured	37.4	The combined system was stable. The reinforce system survived with a 121mm of separation at the simulated discontinuity and the support system was stable with 4 ruptured wires.

Stable Ruptured Pulled out

The support system responses for each test are summarised in Table 9.

Table 9: Support system response

Test ID	Pre- test displacement (mm)	Post- test displacement (mm)	Total number of ruptures	Support System response
195	79	90	0	Stable
196	94	n/r	5	Cut by edge on turtle plate
197	118	173	4	4 failures (one on each side)
198	107	183	10	10 failure (on 3 edges)
199	96	n/r	38	Destroyed (no readings)
200	60	207	15	15 failure (on all sides)
201	74	222	5	Wires rupture start after bolt pulled off. Failure runs from back to front
202	99	196	6	Wire ruptures start from the front edge and work inwards
231	200	324	1	Wire cut by edge on surface hardware plate
234	140	282	1	Wire cut by edge on surface hardware plate
235	74	216	9	Wire ruptures are at the front and the back of the mass
236	76	192	4	Stable with 4 ruptured wires

Pre mesh displacements were compared with the static test results to calculate the respective loads. The chain link mesh of sample #200 was totally destroyed with a total number of 38 ruptures.

7.5 THE DYNAMIC FORCE – DISPLACEMENT RESPONSE

The overall dynamic force - displacement responses of threaded bars are shown in Figure 119. The ruptured threaded bars and the pulled out threaded bar of sample #199 are marked with end stars.

The decoupled threaded bars elongated more compared with the fully encapsulated threaded bars as shown in Figure 119. The decoupled length allows the bar to elongate with load increases. Conversely, fully encapsulated bars have limited

elongation due to the resistance between the grout and the bar. The peak dynamic forces for all the samples were in the range 300kN-410kN.

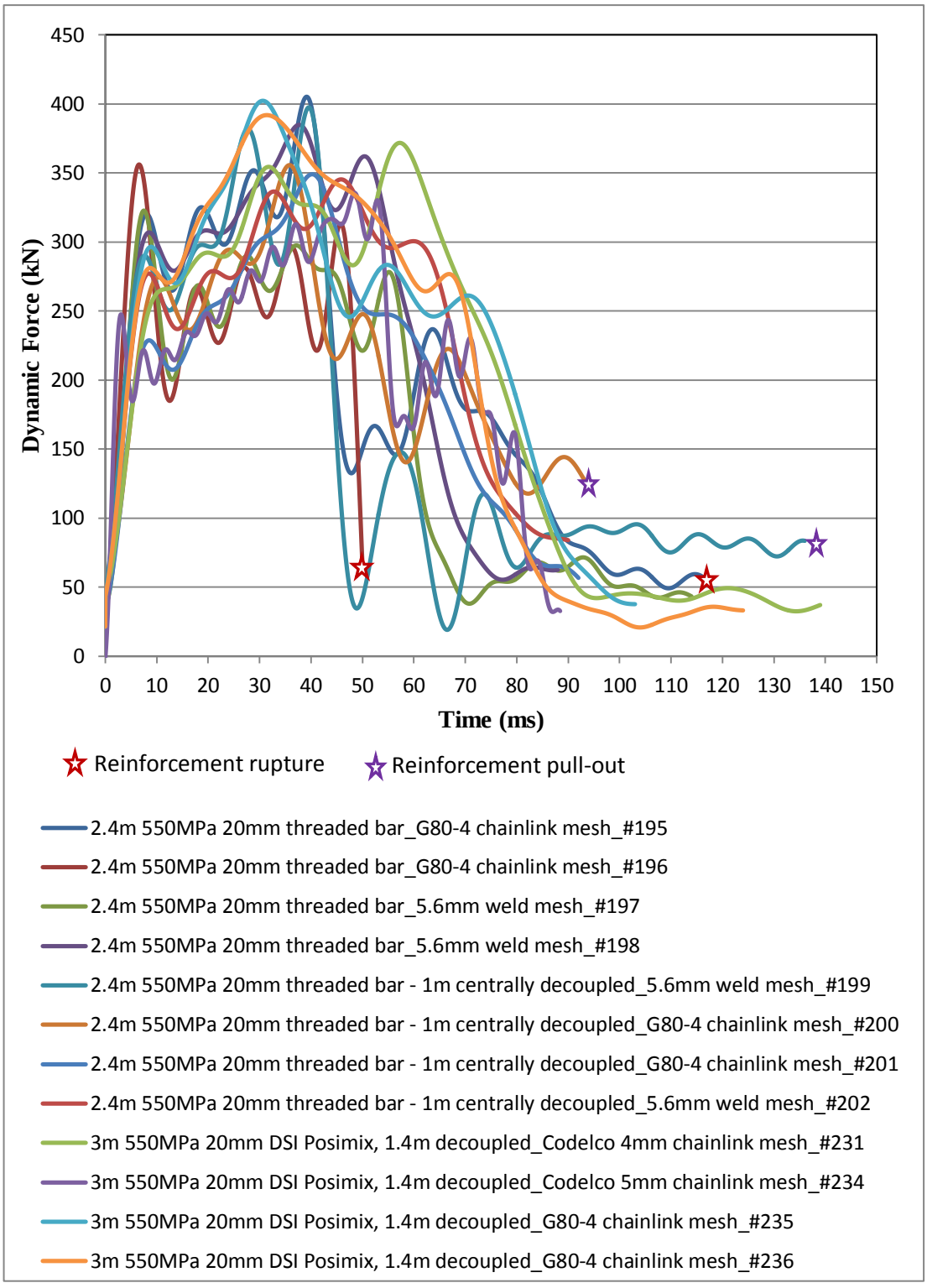

Figure 119: Dynamic force-time response of combined systems.

The combined scheme Dynamic Force – Time responses are categorised according to the type of reinforcement involved in as fully encapsulated threaded bar, 1m decoupled threaded bar and 1.4m decoupled DSI Posimix and are presented in Figure 120, Figure 121 and Figure 122 respectively.

After the dynamic force reached ~ 300kN in fully encapsulated threaded bars, the force remains nearly constant until the end of the test. A slightly increasing trend in force responses of decoupled threaded bars can be identified in Figure 119.

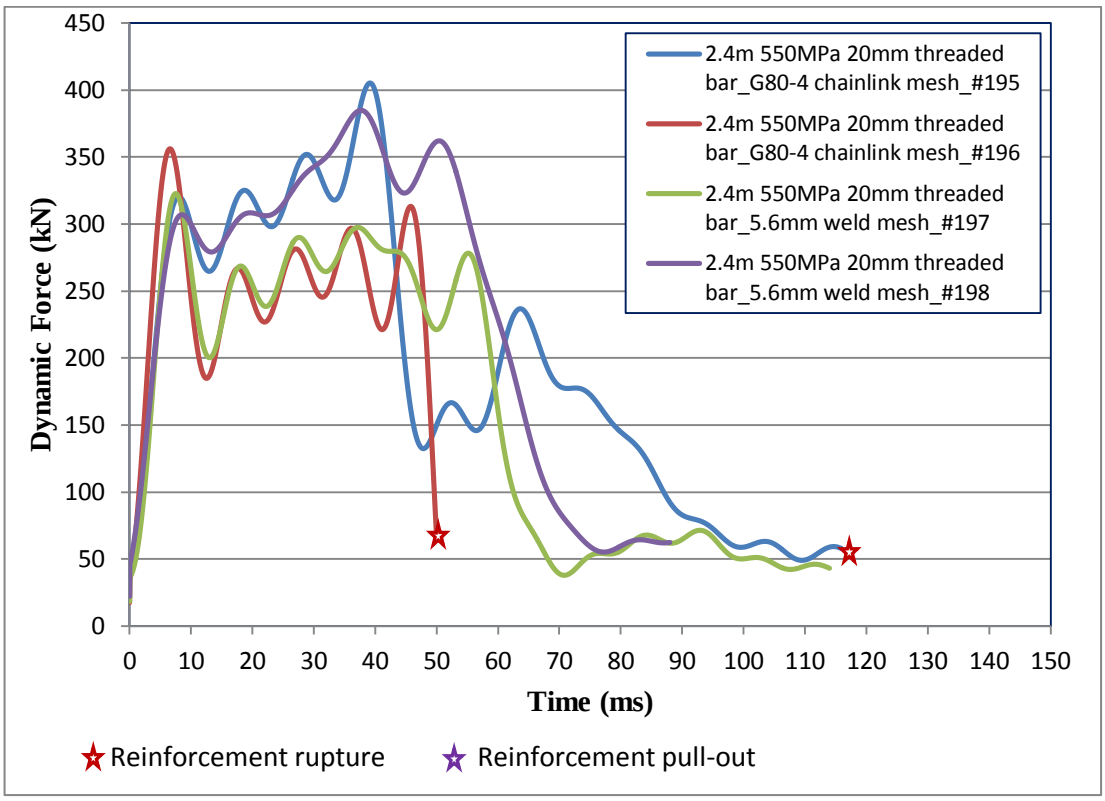

Figure 120: Dynamic Force – Time response of fully bonded threaded bars (Program 1).

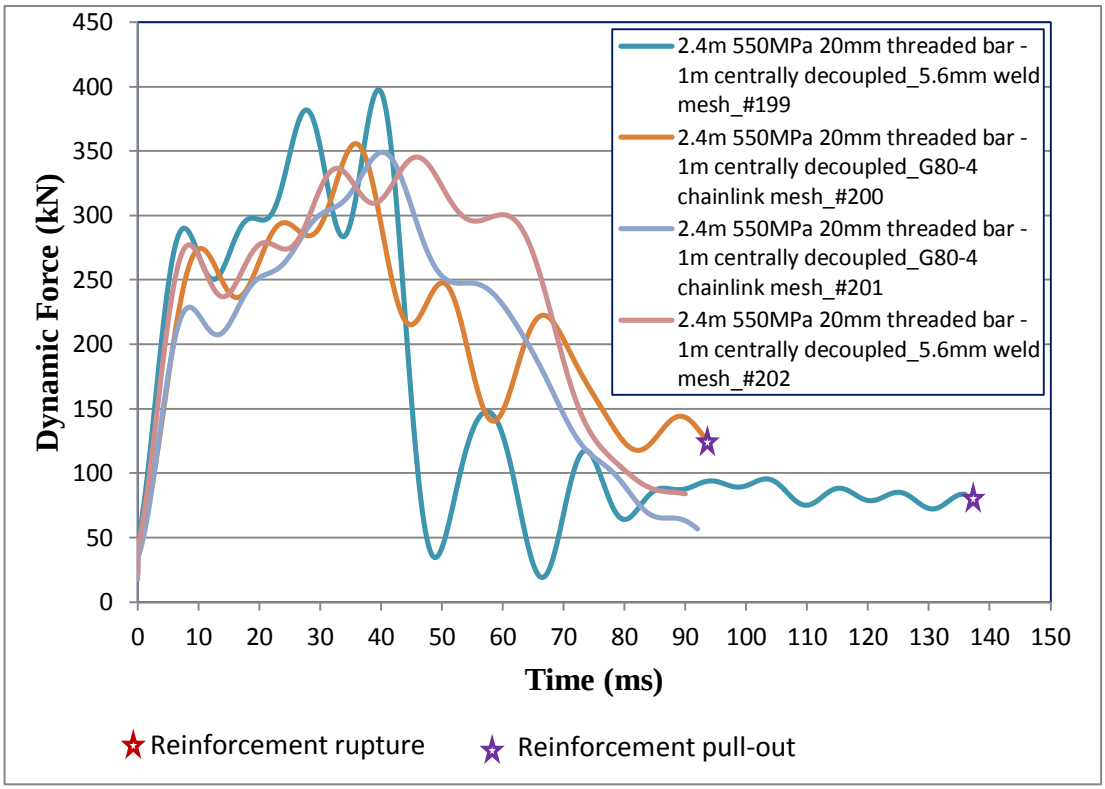

Figure 121: Dynamic Force – Time response of 1m decoupled threaded bars (Program 1).

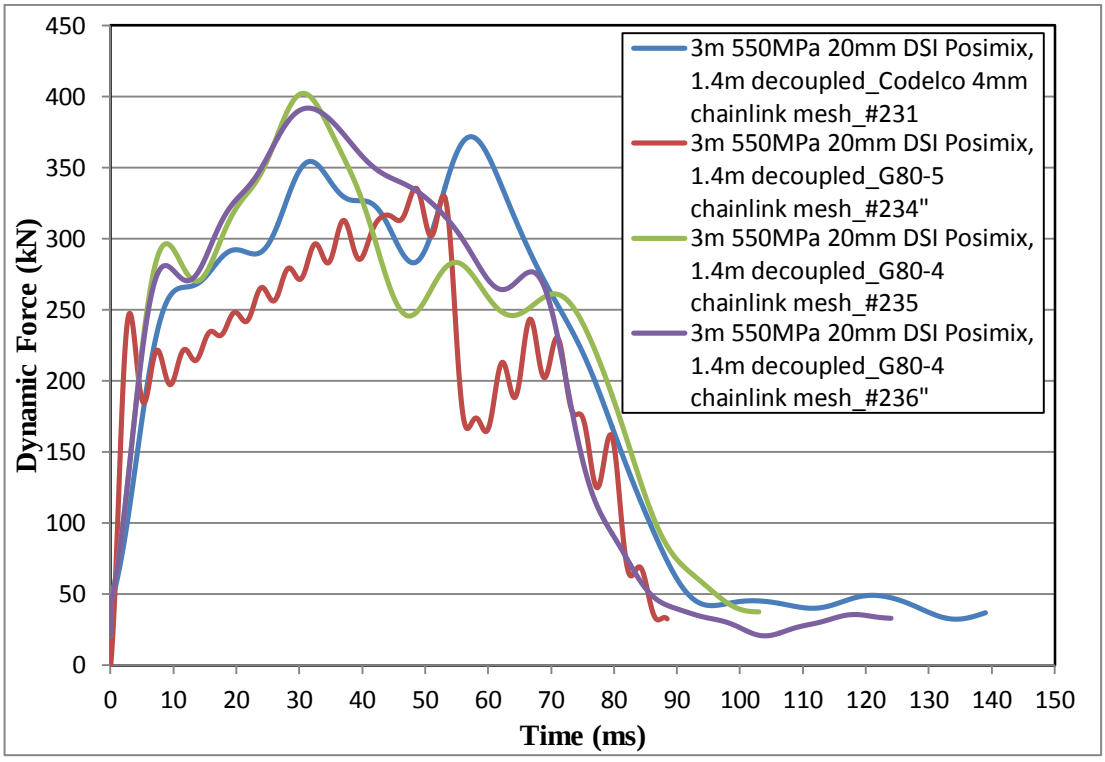

Figure 122: Dynamic Force – Time response of 1.4m decoupled DSI Posimix (Program 2).

7.6 Energy Dissipated by the Reinforcement and Support Systems

Table 10 illustrates the energy dissipated by each of the reinforcement and support systems. Also the table shows the maximum displacement {Smax} and the peak dynamic force of the test.

Table 10: Energy dissipated by the combined scheme

		Reinforcement System				Support system				Total Energy Dissipated by the Combined Scheme
	Test ID	Time (ms)	Displacement (Smax)	Energy Dissipated (kJ)	Peak Dynamic Force (kN)	Time (ms)	Displacement (Smax)	Energy Dissipated (kJ)	Peak Dynamic Force (kN)	
Program 1	195	47.6	77	14.1	265	47.6	115	5.4	210	19.5
	196	52	93	23.5	265.3	43.4	89.6	1.7	265.3	25.2
	197	57	59	14.7	252.2	40.2	67.4	1.3	322	16
	198	68	85.4	19	260	39.4	65.8	6	106.8	25
	199	55.6	>1000	27.7	246	35.7	-	9.3	149.8	37
	200	41.8	174.5	22.1	262.7	52	121	2.7	158.5	24.8
	201	42	136	25.8	261.5	42	113	3.2	74.5	29
	202	64	121	26.3	245.6	35.8	121	8	97	34.3
Program 2	231	57	108	22.8	302.2	45.6	108	4.6	158.5	27.4
	234	68	111	37.1	255.4	55.3	111	4.5	158	41.6
	235	70.7	119.5	25.4	310.6	60.5	119.5	7.6	156.3	33
	236	65	140.4	34.8	300.8	64.5	140.4	8.6	140.7	43.4

Stable Ruptured Pulled out

The ruptured systems are highlighted in red and the systems that survived are in green for clear identification. Reinforcement which failed by pulling out are marked in purple.

Energy dissipated by the combined systems is illustrated in Figure 123. The graph is divided in to regions as low, medium, high and very high according to the typical rock mass demand for ground support design as shown in Table 11 by Villaescusa et al., 2014.

Table 11: Typical Rock Mass Demand for Ground Support Design

Demand Category	**Reaction Pressure (kPa)**	**Surface Displacement (mm)**	**Energy (kJ/m^2)**
Low	<100	<50	<5
Medium	100-150	50-100	5-15
High	150-200	100-200	15-25
Very high	200-400	200-300	25-35
Extremely high	>400	>300	>35

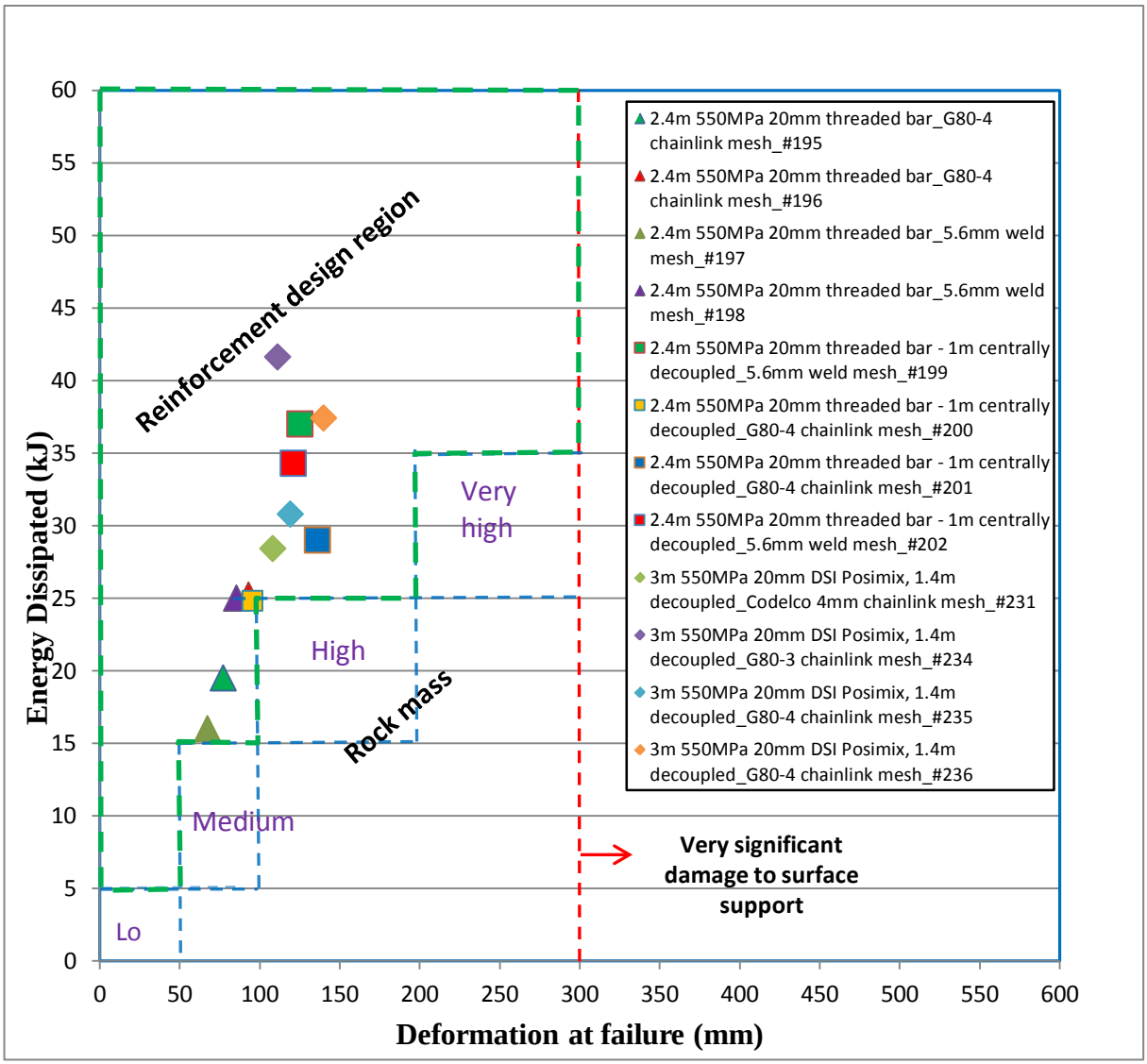

Figure 123: Design of combined scheme under dynamic loading.

CHAPTER 8

CONCLUDING REMARKS

The aim of this thesis was to conduct and analyse the performance of bolt and mesh combined support schemes under dynamic loading conditions at the WASM Dynamic Test Facility.

The WASM Dynamic Test Facility considers the momentum transfer concept to evaluate the energy dissipated by each component of the system and was implemented for a bolt and mesh combined scheme test. Advanced equipment, techniques and instrumentation were used for the complex analyse. The WASM Dynamic Test Facility and its components were discussed in detail.

The investigations involved two combined bolt and mesh scheme test programs. The sample preparation and testing procedures were discussed. It can be concluded that the test programs resulted in improved understanding of bolt and mesh combined schemes. Test results were presented and explained in different formats. Energy dissipated by the combined schemes and contribution of individual elements towards the overall performance were calculated. Higher load bearing capacity of the surface hardware components including plates and long integrated nuts assisted in withstanding higher load transfer.

The project was successfully completed and the results fulfilled the requirement to advance the WASM dynamic test database to the next stage. The facility was enhanced and modified to facilitate testing of a comprehensive range of test specimens during the program. Further studies on combined scheme programs including combined bolts and shotcrete will be conducted at WASM Dynamic Test Facility to strengthen the understanding of combined schemes subjected to dynamic loading conditions.

REFERENCES

Aydan, Ö., Akagi, T. & Kawamoto, T. (1993). The squeezing potential of rocks around tunnels; theory and prediction. Rock Mechanics and Rock Engineering, 26(2), 137-163.

Bieniawski, Z. T. (1984). Rock mechanics design in mining and tunnelling (No. Monograph).

Brown, E.T. (2004). The dynamic environment of ground support and reinforcement. Paper presented at the Ground Support in Mining and Underground Construction: Proceedings of the Fifth International Symposium on Ground Support, Perth, Australia, 28-30 September 2004.

Gaudreau, D., Aubertin, M., & Simon, R. (2004). Performance assessment of tendon support systems submitted to dynamic loading, in Proceeding of Fifth International Symposium of Ground Support and Reinforcement Practice in Mining (eds: E Villaescusa and Y Potvin) pp 299-312.

Hadjigeorgiou, J., & Potvin, Y. (2011). A critical assessment of dynamic rock reinforcement and support testing facilities. Rock mechanics and rock engineering, 44(5), 565-578.

Heal, D., Hudyma, M., & Potvin, Y. (2004). Assesing the in-situ performance of ground support systems subjected to dynamic loading, in proceeding Fifth International Symposium on Ground Support in Mining and Underground Construction, (eds: E.Villaescusa and Y. Potvin) pp 319-326.

Hudson, J. A. (1989). Rock mechanics principles in engineering practice.

Kaiser, P.K., McCreath, D., & Tannant, D. (1996). Canadian Rockburst Support Handbook (Geomechanics Research Centre: Laurentian University)

Morton, E.C., Thompson, A.G., & Villaescusa, E. (2008). Static testing of shotcrete and membranes for mining applications. Paper presented at the Proceedings of the 6th International Conference on Ground Support, Cape Town.

Morton, E.C., Thompson, A.G., & Villaescusa, E. (2009). The performance of mesh, shotcrete and membranes for surface ground support. RockEng09, rock engineering in difficult conditions, CIM, Montreal, Paper, 4022

Morton, E.C., Thompson, A.G, Villaescusa, E. & Roth, A. (2007). Testing and analysis of steel wire mesh for mining applications of rock surface support. Paper presented at the ISRM Congress.

Ortlepp, W.D., & Stacey, T.R. (1997). testing of tunnel support: Dynamic load testing of rock containment systems (eg wire mesh), Safety and in Mines Research Advisory Committee, GAP 221, July, 107p

Ortlepp, W.D.. & Stacey, T.R. (1998). Testing of tunnel support : dynamic load testing of rockbolt elements to provide data for safer support design. Safety in Mines Research Advisory Committee, GAP 423, June, 49p.

Ortlepp, W.D., & Stacey, T.R. (1999). The performance of containment rock support such as wire mesh under simulated rockburst loading, The 6th International Symposium on Ground Support in Mining and Civil Engineering Construction.

Palmstrom, A., & Stille, H. (2007). Ground behaviour and rock engineering tools for underground excavations. Tunnelling and Underground Space Technology,22(4), 363-376.

Player, J., Morton, E., Thompson, A., & Villaescusa, E. (2008). Static and dynamic testing of steel wire mesh for mining applications of rock surface support. Paper presented at the The Sixth International Symposium on Ground Support in Mining and Civil Engineering Construction.

Player, J.R., Thompson, A.G., Villaescusa, E., Stacey, T., & Malan, D. (2008). Dynamic testing of reinforcement systems. Paper presented at the

Player, J.R., A.G. Thompson and E.Villaescusa 2004. Dynamic testing of rock reinforcement using the momentum transfer concept. Ground Support in Mining and Underground Construction, 327-340, Balkema:Leiden.

Player, J.R., Villaescusa, E., & Thompson, A.G. (2005). An examination of dynamic test facilities. Advances Geomechanics in Mines, Australian Centre for Geomechamics

Player, J.R., Villaescusa, E., & Thompson, A.G. (2008). An Examination of Dynamic Test Facilities. Paper presented at the Australian Mining Technology Conference, September 2008, CRC Mining, AusIMM, pp349-379.

Player, J.R., Villaescusa, E., & Thompson, A.G. (2009). Dynamic testing of friction rock stabilisers. RockEng09, Rock Engineering in Difficult Conditions, Toronto, 9-15.

Player, J.R., Villaescusa, E., & Thompson, A.G. (2009). Dynamic testing of threaded bar used for rock reinforcement. RockEng09, Rock Engineering in Difficult Conditions, CIM Montreal, Paper, 4030, 12p.

Plouffe, M., Anderson, T., Judge, K., Stacey, T.R., & Malan, D.F. (2008). Rock bolts testing under dynamic conditions at CANMET-MMSL. Paper presented at

the Proceedings of the 6th International Symposium on Ground Support in Mining and Civil Engineering Construction, Cape Town. Stacey, TR and Malan, DF (eds.). The Southern African Institute of Mining and Metallurgy. Symposium Series S.

Potvin, Y., Wesseloo, J., & Heal, D. (2010). An interpretation of ground support capacity submitted to dynamic loading. Mining Technology, 119(4), 233-245.

Roth, A., Ranta-Korpi, R., Volkwein, A. & Wendeler, C. (2007). Numerical Modelling And Dynamic Simulation of High-tensile Steel Wire Mesh For Ground Support Under Rockburst Loading. Paper presented at the 1st Canada-US Rock Mechanics Symposium.

Stacey, T.R. and Ortlepp, W.D. (1999) Retainment support for dynamic events in mining, Rock Support and Reinforcement Practice in Mining, pp. 329–333.

Stacey, T.R. &Ortlepp, W.D. (2001) Tunnel surface support-capacities of various types of wire mesh and shotcrete under dynamic loading. The Journal of The South African Institute of Mining and Metallurgy, 337-342.

Thompson, A.G., Player, J.R. & Villaescusa, E. (2004). Simulation and analysis of dynamically loaded reinforcement systems. Ground Support in Mining and Underground Construction, 341-358, Balkema:Leiden.

Thompson, A.G., Villaescusa, E., & Windsor, C.R. (2012). Ground support terminology and classification: an update. Geotechnical and Geological Engineering, 30(3), 553-580.

Thompson, A.G. & Windsor, C.R. (1993). Theory and Strategy for Monitoring the Performance of Rock Reinforcement. Proc. Australian Conference on Geotechnical Instrumentation and Monitoring in Open Pit and Underground Mining, Kalgoorlie, 21-23 June, 473-482, Balkema: Rotterdam.

Villaescusa, E. (2014). Geotechnical Design for Sublevel Open Stoping: CRC Press.

Villaescusa, E., Thompson, A.G. & Player, J.R. (2005). Dynamic testing of rock reinforcement systems. In CRCMining Australian Mining Technology Conference-New Technologies to Produce More with Less.

Villaescusa, E., Thompson, A.G. & Player, J.R. (2005). Dynamic testing of ground support systems. Report No. 249 MERIWA Project M349, Phase 1-Final Report and Addendum, 170p.

Villaescusa, E., Thompson, A.G., Player, J..R. & Morton, E.C. (2010). Dynamic testing of ground support systems. Report No. 287 MERIWA Project M349, Phase 2-Final Report, 207p.

Windsor, C.R. & Thompson, A.G.(1993). Rock Reinforcement - Technology, Testing, Design and Evaluation. Comprehensive Rock Engineering (J A Hudson, ed.), Volume 4, Chapter 16, 451-484, Pergamon Press, Oxford.

Yi, X., & Kaiser, P. (1994). Impact testing for rockbolt design in rockburst conditions. Paper presented at the International Journal of Rock Mechanics and Mining Sciences & Geomechanics Abstracts.